Highly charged ions: Optical clocks and applications in fundamental physics

M. G. Kozlov

Petersburg Nuclear Physics Institute of NRC "Kurchatov Institute," Gatchina 188300, Russia and St. Petersburg Electrotechnical University "LETI," Prof. Popov Str. 5, St. Petersburg, 197376, Russia

M. S. Safronova

Department of Physics and Astronomy, University of Delaware, Newark, Delaware 19716, USA and Joint Quantum Institute, National Institute of Standards and Technology and the University of Maryland, Gaithersburg, Maryland 20742, USA

J. R. Crespo López-Urrutia

Max-Planck-Institut für Kernphysik, Saupfercheckweg 1, 69117 Heidelberg, Germany

P. O. Schmidt

Physikalisch-Technische Bundesanstalt Braunschweig, 38116 Braunschweig, Germany and Institut für Quantenoptik, Leibniz Universität Hannover, 30167 Hannover, Germany

(published 4 December 2018)

Recent developments in frequency metrology and optical clocks have been based on electronic transitions in atoms and singly charged ions as references. The control over all relevant degrees of freedom in these atoms has enabled relative frequency uncertainties at a level of 10^{-18}. This accomplishment not only allows for extremely accurate time and frequency measurements, but also to probe our understanding of fundamental physics, such as a possible variation of fundamental constants, a violation of the local Lorentz invariance, and the existence of forces beyond the standard model of physics. In addition, novel clocks are driving the development of sophisticated technical applications. Crucial for applications of clocks in fundamental physics are a high sensitivity to effects beyond the standard model and a small frequency uncertainty of the clock. Highly charged ions offer both. They possess optical transitions which can be extremely narrow and less sensitive to external perturbations compared to current atomic clock species. The large selection of highly charged ions offers narrow transitions that are among the most sensitive ones for the "new physics" effects. Recent experimental advances in trapping and sympathetic cooling of highly charged ions will in the future enable advanced quantum logic techniques for controlling motional and internal degrees of freedom and thus enable high-accuracy optical spectroscopy. Theoretical progress in calculating the properties of selected highly charged ions has allowed the evaluation of systematic shifts and the prediction of the sensitivity to the physics beyond the standard model. New theoretical challenges and opportunities emerge from relativistic, quantum electrodynamics, and nuclear-size contributions that become comparable with interelectronic correlations. This article reviews the current status of the field, addresses specific electronic configurations and systems which show the most promising properties for research, their potential limitations, and the techniques for their study.

DOI: 10.1103/RevModPhys.90.045005

CONTENTS

I. INTRODUCTION

In this review we cover current and new research directions that arise from high-precision spectroscopy and novel optical clocks using trapped highly charged ions (HCI). The recent interest in high-resolution optical spectroscopy of HCI has been triggered by their high sensitivity to a change in the fine-structure constant α (Sec. II). Since the required HCI physics is generally less well known compared to neutral and singly charged atoms, Sec. III recapitulates the current status of theory, including quantum electrodynamics (QED), mostly dealing with few-electron HCI. In Sec. IV we present recent theory on more complicated electronic systems that are particularly interesting for frequency metrology and discuss them in detail.

We present the current status of experimental methods in Sec. V, with a particular emphasis on the field of optical spectroscopy (Sec. V.E). Novel methods needed for high-resolution optical spectroscopy with HCI are introduced in Secs. V.G and VI, and an analysis of clock shift systematics with HCI candidates follows in Sec. VII. Future directions of research are discussed in Sec. VIII.

A. Atomic clocks for exploring old and new physics

Celestial mechanics, based on the (for their time) exceptionally precise measurements of astronomy, became one of the most fruitful disciplines in theoretical physics and was the key for many discoveries in other fields. In the same way, atomic and optical clocks (Ludlow *et al*, 2015) aided by advances in atomic structure theory are evolving into an exceptional driving force for the search for new physics. Frequency measurements of narrow transitions in atoms, with their universal reproducibility that is paradigmatic in science, serve as benchmarks for the most subtle deviations from the theoretical framework of physics, while high-energy physics aims at testing the boundaries of our knowledge in large facilities. These complementary approaches eventually aim at answering the same questions.

In atomic clocks, physics interactions appear as contributions to the electronic binding energies or the transition rates in a hierarchy now stretching over 18 orders of magnitude. Novel clocks are capable of addressing those in more and more depth, and their rapid development in the last decades heralds further advances. Progress in optical clocks is based on an improved control over all degrees of freedom, including the internal state, the motion, and external fields affecting the transition frequency, paired with increased accuracy of electronic structure calculations of atomic properties. This has been accomplished through the rapid development of suitable laser cooling and trapping techniques based on the pioneering work of Hänsch and Schawlow (1975), Ashkin (1978), Neuhauser *et al* (1978), Wineland, Drullinger, and Walls (1978), Wineland and Itano (1979), Bollinger *et al* (1985), Phillips, Prodan, and Metcalf (1985), Aspect *et al* (1986), Stenholm (1986), Lett *et al* (1988), Phillips (1998), and Metcalf and Straten (2007).

However, progress in atoms (such as most HCI) that do not possess the required properties for cooling and trapping could not profit from these advances. This situation has recently changed with the development of quantum logic techniques for spectroscopy in which a cooling ion, trapped together with the spectroscopy ion, provides sympathetic cooling as well as control and readout of the internal state of the spectroscopy ion. This arrangement forms a compound system combining the advantages of both species and makes previously intractable atoms, such as HCI, accessible for high-resolution spectroscopy.

Similarly to the progress in experimental techniques, advances in atomic structure theory are required for exploiting the present and future experimental precision in order to improve our knowledge of the various fundamental

interactions that are intertwined within the electronic shell. For the present status of optical clocks, we refer to the recent review of Ludlow *et al* (2015), and for a general work on atomic physics methods for probing fundamental physics to Safronova *et al* (2018). Within this review we will be concerned with the specific aspects related to the applications of HCI as novel atomic frequency references.

B. Atomic physics at the extremes: Highly charged ions

Since the epoch of reionization—roughly 13×10^9 years ago—atomic matter in the Universe mostly appears as ions (Shull, Smith, and Danforth, 2012). Now the majority of the chemical elements can be found as highly charged ions. Following big-bang nucleosynthesis and 4×10^8 years of expansion, reionization was driven by strong radiation sources, stars coming into being by the gravitational collapse of cold neutral gas. Supernovae later infused space with heavy elements, heating interstellar matter in shocks to very high temperatures (Hitomi Collaboration, 2017). Furthermore, as a consequence of energy virialization in deep gravitational potentials, the translational temperature of the diffuse intergalactic medium containing most of the baryonic matter is also very high (10^5–10^7 K) (Reimers, 2002). Here ions reign absolute, no matter how low the radiation temperature of the medium around them might be. Galaxy clusters, galaxies with their active galactic nuclei, binary x-ray systems, and stars are extremely hot environments; hot winds and relativistic jets expel highly ionized material out of the galactic cores (Hitomi Collaboration, 2016). X-ray astronomy missions such as the present Chandra and XMM-Newton allow us to observe such environments, and they as well as the future XARM (Hitomi Collaboration, 2016) and Athena (Barcons *et al*, 2017) will produce more and more quantitative results.

All this emphasizes the need for laboratory data and advanced atomic structure calculations for their interpretation; therefore, studying HCI is essential for astrophysics diagnostics (Beiersdorfer, 2003). In addition, HCI play a central role in plasma physics (Beiersdorfer, 2015) and in various aspects of fundamental research such as tests of quantum electrodynamics (QED) (Beiersdorfer, 2010), developing relativistic atomic structure theory and other applications (Martinson, 1989; Beyer, Kluge, and Shevelko, 1997; Gillaspy, 2001; Zou *et al*, 2016). In the present review we address novel avenues of research which have recently been proposed and recapitulate about their foundation in the exciting atomic physics properties of HCI.

Because of their fundamental role in atomic structure theory and quantum mechanics, the most investigated isoelectronic sequences have been the hydrogenlike and lithiumlike ones, with one single ns electron being amenable to accurate theoretical calculations of the dominant terms of the energy Hamiltonian. The heliumlike sequence has also seen a wealth of calculations (Drake, 1979, 1988, 2002; Indelicato, Gorveix, and Desclaux, 1987; Chen, Cheng, and Johnson, 1993; Cheng *et al*, 1994; Plante, Johnson, and Sapirstein, 1994; Johnson, Plante, and Sapirstein, 1995; Lindgren, Persson, and Salomonson, 1995; Yan and Drake, 1995; Cheng and Chen, 2000; Andreev *et al*, 2001; Lindgren *et al*, 2001; Artemyev *et al*, 2005), since understanding the two-electron correlations is believed to be the gateway to the study of more complex quantum systems.

Relativistic fine-structure, QED, and nuclear-size effects (see Sec. III) show along any given isoelectronic sequence a much stronger dependence on the nuclear charge than electronic correlations. Advantageously, this tunability of the various terms of the Hamiltonian can be used to tailor studies capable of separating their relative contributions.

Owing to the reduction of the number of bound electrons, electronic structure theory becomes, in principle, less complicated. Nonetheless, in astrophysics and plasma applications [see, e.g., reviews by Beiersdorfer (2003, 2015)], which often deal with ions having more complex electronic structures, an accurate treatment of electronic correlations is as important as that of relativistic effects and QED. This is crucial in order to improve the quantitative understanding of plasmas.

In most cases, the strongest transitions observed in HCI are in the x-ray region. Nonetheless, they also display observable transitions in every spectral range, and, in particular, also in the optical regime around which this review is centered. There are several possibilities for optical transitions arising in HCI (Crespo López-Urrutia, 2008). As a function of increasing charge state, fine- and even hyperfine-structure splittings reach the optical regime. Furthermore, level crossings between different electronic configurations can result in transitions in the optical wavelength range.

Production of HCI in a laboratory environment is a long-standing problem. Few groups could routinely generate those ions, since the techniques were complicated and expensive. For these reasons, there is still an enormous scarcity of data and the majority of possible ions in this "spectral desert" remains unexplored. As for high-accuracy measurements, the best results in the field of HCI spectroscopy lag by more than 10 orders of magnitude behind of what is now possible in atomic physics with neutral atoms or singly charged ions. Compounding the lack of experimental data, theory encounters a rugged terrain when scouting beyond its usual range. Complex electronic configurations with several shell vacancies in the ground-state configuration are still very hard challenges for advanced atomic structure theory.

Further development of both HCI theory and experiment became crucial in the past several years after a completely new avenue of research blossomed following the pioneering work by Berengut, Dzuba, and Flambaum (2010), which identified HCI optical transitions between states with different electronic configurations and proposed their applications for optical metrology and tests of variation of the fine-structure constant. This work and subsequent studies (Berengut, Dzuba, and Flambaum, 2011; Berengut *et al*, 2011, 2012a, 2012b; Derevianko, Dzuba, and Flambaum, 2012; Dzuba, Derevianko, and Flambaum, 2012a, 2012b, 2013; Kozlov, Dzuba, and Flambaum, 2013; Safronova *et al*, 2014a, 2014b, 2014c; Yudin, Taichenachev, and Derevianko, 2014; Dzuba, Flambaum, and Katori, 2015; Dzuba *et al*, 2015) demonstrated that despite very large ionization energies, certain HCI have very narrow transitions that lie in the optical range and can be used for the development of ultrahigh-precision clocks and tests of fundamental physics.

This new dimension in the parameter space of precision atomic physics opens a wide field of research opportunities.

HCI are less sensitive to external perturbations than either neutral atoms or singly charged ions due to their more compact size. Recent studies of systematic uncertainties (Derevianko, Dzuba, and Flambaum, 2012; Dzuba, Derevianko, and Flambaum, 2012a, 2013) have shown that the achievable fractional inaccuracy of the transition frequency in the clocks based on HCI may be smaller than 10^{-19} using shift cancellation schemes. At the same time, the clock transitions in HCI are more sensitive to the variation of α than those of neutral atoms (Berengut, Dzuba, and Flambaum, 2010). Therefore, HCI-based clocks may allow significant improvement of the current experimental limit on α variation on the level $\dot{\alpha}/\alpha \lesssim 10^{-17}$ yr^{-1} (Rosenband *et al*, 2008; Godun *et al*, 2014; Huntemann *et al*, 2014). Moreover, optical clocks are sensitive not only to a linear variation of α, but also to hypothetical oscillations and occasional jumps of this parameter. Such effects can be caused by cosmological fields (Stadnik and Flambaum, 2015, 2016) and topological defects (Derevianko and Pospelov, 2014), which are often considered as candidates for dark matter (Arvanitaki, Huang, and Tilburg, 2015; Derevianko, 2016). In all these cases sensitivity to α variation is given by the same sensitivity coefficients. Therefore, HCI-based clocks are also more sensitive to all these effects than state-of-the-art atomic clocks.

Two major obstacles on the way toward the realization of such proposals in 2010 were the lack of accurate theoretical descriptions of potential clock candidates and, even more importantly, lack of experimental techniques to decelerate, trap, cool, and control HCI to observe such weak transitions and support the development of the frequency standards.

At the present time, theoretical studies have identified a list of HCI candidates for optical clock development and provided extensive calculations of relevant atomic properties. In 2015, crucial experimental steps were achieved with a breakthrough demonstration of sympathetic cooling of Ar^{13+} with a laser-cooled Be^+ Coulomb crystal in a cryogenic Paul trap (Schmöger *et al*, 2015). This experiment heralded the start of a new era in exploration of HCI with the techniques previously reserved for neutral and singly charged systems. Combined with quantum logic spectroscopy in which another ion is used for cooling and readout of the clock transitions, as is done in the Al^+ clock (Schmidt *et al*, 2005), cold trapped HCI suddenly become an experimentally accessible resource for precision fundamental studies. These developments represented a turning point for HCI studies and this review aims to summarize both theoretical and experimental findings and to discuss possible directions of further research.

Both theory and experiment have to be improved in order to achieve the best possible scientific harvest from these investigations. On the other hand, this is a worthwhile endeavor given the plethora of available ground-state configurations with laser-accessible transitions that HCI offer. Furthermore, studies along isoelectronic sequences in HCI afford a large degree of tunability concerning the systematics of the various binding energy contributions, aiding the identification of yet unassigned HCI spectra as shown in Windberger *et al* (2015). New measurements will provide benchmarks of the theoretical predictions and help to further improve the theory.

II. BACKGROUND: VARIATION OF FUNDAMENTAL CONSTANTS

Variation of fundamental constants is predicted by many extensions of the standard model (SM). Experimental searches for α variation allow testing of these models and search for the new physics beyond the SM. Light scalar fields appear very naturally in cosmological models affecting parameters of the SM including α. Space-time variations of these scalar fields are expected because of the evolution of the Universe's composition. Theories unifying gravity and other interactions predict spatial and temporal variation of physical "constants" in the Universe (Marciano, 1984; Dent, Stern, and Wetterich, 2008; Calmet and Keller, 2015). Moreover, all coupling constants and masses of elementary particles in such models can be both space and time dependent and influenced by the local environment (Uzan, 2011).

Searches for variation of fundamental constants are conducted in a very wide range of systems including astrophysical studies of quasar spectra and observation of the 21 cm line in atomic hydrogen, atomic clocks, the Oklo natural nuclear reactor, meteorite dating, stellar physics, cosmic microwave background, and big bang nucleosynthesis [see, e.g., reviews by Chin, Flambaum, and Kozlov (2009), Uzan (2011), and Kozlov and Levshakov (2013)]. Here we only briefly discuss the laboratory limits set on the variation of the fundamental constants by atomic clocks and focus on the HCI proposals.

The transition frequency ν between two electronic energy levels in an atom is dependent on the fine-structure constant:

$$\nu \simeq cR_\infty AF(\alpha), \tag{1}$$

where R_∞ is the Rydberg constant, c is the speed of light in vacuum, A is a numerical factor depending on the atomic number Z, and $F(\alpha)$ is a function which depends upon the particular transition. Based on their respective frequency ranges, current atomic clocks based on such electronic transitions are referred to as optical clocks, while clocks based on hyperfine transitions are referred to as microwave clocks. The frequency of the electromagnetic radiation associated with transitions between the hyperfine levels, such as the Cs transition defining the SI second, may be expressed as

$$\nu_{\rm hfs} \simeq cR_\infty A_{\rm hfs} g_i \frac{m_{\rm e}}{m_{\rm p}} \alpha^2 F_{\rm hfs}(\alpha), \tag{2}$$

where $m_{\rm e}$ and $m_{\rm p}$ are electron and proton masses, respectively, $A_{\rm hfs}$ is a numerical quantity depending on the particular atom, and $F_{\rm hfs}(\alpha)$ is a relativistic correction specific to each hyperfine transition. The dimensionless quantity $g_i = \mu_i/\mu_{\rm N}$ is the g factor associated with the nuclear magnetic moment μ_i, where $\mu_{\rm N} = e\hbar/2m_{\rm p}$ is the nuclear magneton. The potential variation of g factors may be reduced to more fundamental quantities, such as $X_q = m_q/\Lambda_{\rm QCD}$, where m_q is the average light-quark mass and $\Lambda_{\rm QCD}$ is the QCD energy scale. As a result, the hyperfine transition frequencies are sensitive to the variation in α, $\mu = m_{\rm p}/m_{\rm e}$, and X_q.

Measuring the ratios $R = \nu_1/\nu_2$ of optical to hyperfine clocks over time sets limits on the variation of α, the proton-to-electron mass ratio μ, and nuclear g factors, specifically g_{Cs} and g_{Rb}, as these correspond to the two microwave clocks with the smallest uncertainties.

The ratio of frequencies of any two optical clocks depends only upon α since the other constants in Eq. (1) are the same for all transitions between the electronic levels, leaving only the difference in $F(\alpha)$ dependence. The sensitivity of the particular optical atomic clock to α variation depends on the parameter q (Dzuba, Flambaum, and Webb, 1999; Dzuba *et al*, 2002) that links the variation of the transition energy E_0, and hence the atomic frequency $\nu = E_0/h$, to the variation of α

$$\frac{\delta E}{E_0} = \frac{2q}{E_0}\frac{\delta\alpha}{\alpha_0} \equiv K\frac{\delta\alpha}{\alpha_0}, \tag{3}$$

where

$$K = \frac{2q}{E_0} \tag{4}$$

is a dimensionless sensitivity factor. In order to find factor K for the transition $i \to f$ we first calculate parameters q for both levels and then put $q = q_f - q_i$ in Eq. (4).

The relationship between the ratio of two clock frequencies and the variation of α is then given by the difference in their respective K values for each clock transition, i.e., $\Delta K = |K_2 - K_1|$. The larger the value of K, the more sensitive is a particular atomic energy level to the variation of α. Therefore, it is advantageous to select transitions with significantly different values of K, preferably of the opposite sign. These K factors allow comparison of the sensitivity to α variation between transitions with significantly different frequencies.

The K factors are small for most clocks currently in development, Al^+ (0.008), Ca^+ (0.15), Sr^+ (0.4), Sr (0.06), Yb (0.3), and Yb^+ quadrupole transitions (0.88) (Dzuba, Flambaum, and Marchenko, 2003; Dzuba and Flambaum, 2009). The K factors for Hg^+ and Yb^+ octupole clock transitions are -3 and -6, respectively, making them the best candidates for one member of a clock-comparison pair, with the other member taken from the previous group. A particular attraction of HCI is the availability of transitions with much larger K factors.

The most accurate single laboratory test of α variation comes from the Al^+/Hg^+ optical clock comparison (Rosenband *et al*, 2008), setting the limit

$$\frac{\dot\alpha}{\alpha} = (-1.6 \pm 2.3) \times 10^{-17}\ \mathrm{yr}^{-1}. \tag{5}$$

The combined limits to the present day variation of α and μ from all present clock comparisons and dysprosium measurements (Leefer *et al*, 2013) are given by Godun *et al* (2014) and Huntemann *et al* (2014):

$$\frac{\dot\alpha}{\alpha} = (-2.0 \pm 2.0) \times 10^{-17}\ \mathrm{yr}^{-1}, \tag{6}$$

$$\frac{\dot\mu}{\mu} = (0.2 \pm 1.1) \times 10^{-16}\ \mathrm{yr}^{-1}. \tag{7}$$

A number of optical and near-optical transitions in various HCI were shown to be very sensitive to the possible variation of the fine-structure constant (Berengut, Dzuba, and Flambaum, 2010, 2011; Berengut *et al*, 2011, 2012a, 2012b; Derevianko, Dzuba, and Flambaum, 2012; Dzuba, Derevianko, and Flambaum, 2012a, 2012b, 2013; Kozlov, Dzuba, and Flambaum, 2013; Safronova *et al*, 2014a, 2014b, 2014c; Yudin, Taichenachev, and Derevianko, 2014; Dzuba, Flambaum, and Katori, 2015; Dzuba *et al*, 2015). The energy scale for HCI levels is large $[\sim(Q+1)^2\ R_\infty]$, where Q is the ionization charge. Optical transitions arising due to a level crossing take place between states with accidental near degeneracy. Relativistic corrections strongly depend on the orbital angular momentum. For HCI they scale as $\alpha^2 Z^2 (Q+1)^2\ R_\infty$, where Z is the nuclear charge, while optical frequencies are of the order of a fraction of R_∞. If in the optical transition the orbital angular momentum changes by two units or more, the frequency depends on α as (Berengut, Dzuba, and Flambaum, 2010)

$$\frac{\delta\nu}{\nu} \sim \alpha^2 Z^2 (Q+1)^2 \quad \Rightarrow \quad K \sim 2\alpha^2 Z^2 (Q+1)^2.$$

Therefore, the sensitivity of optical transitions in HCI to α variation is enhanced by the factor $(Q+1)^2 \sim 10^2$ compared to similar transitions in neutral atoms.

Calculated sensitivity coefficients of the optical transitions in HCI to α variation are indeed much higher than in neutral atoms or singly charged ions. This opens the possibility to drastically improve present laboratory limits on α variation or find such variation and explore new physics beyond the standard model. Brief reviews of α variation in HCI were recently published by Ong, Berengut, and Flambaum (2014) and Dzuba and Flambaum (2015).

In 2011, a very large analysis of quasar absorption spectra that combined data taken by the Keck telescope in Hawaii and the Very Large Telescope (VLT) in Chile indicated a dipolelike space variation of α on the cosmological distances at the 4σ significance level (Webb *et al*, 2011). A 2015 study of systematic distortions in the wavelengths scales of high-resolution spectrographs (Whitmore and Murphy, 2015) suggested that instrumental error may weaken the spatial variation result, but cannot explain all of the observed α variation. These conclusions were later questioned by Dumont and Webb (2017). At present we are still waiting for new observational data to resolve the "Australian dipole" puzzle.

Up to now, most laboratory searches of α variation were focused on smooth drifts during the whole duration of the experiment (Rosenband *et al*, 2008; Godun *et al*, 2014; Huntemann *et al*, 2014), or on annual variations, which can be linked to the variations of the gravitational potential of the Sun (Blatt *et al*, 2008; Leefer *et al*, 2013). However, some modern models of dark matter predict oscillations of the fundamental constants at the Compton frequency of the cosmological field, or even random jumps when the Earth passes domain walls, or other topological defects, associated with such a field (Derevianko and Pospelov, 2014; Arvanitaki, Huang, and Tilburg, 2015; Stadnik and Flambaum, 2015; Derevianko, 2016).

In the first approximation the sensitivity coefficient of a given optical transition to α variation is the same for gradual

variation and for periodic variation if its frequency is much smaller than the transition frequency. Because of that, HCI can be used to search for such variations and to test predictions of this class of theoretical models of dark matter. Recently, HCI have also been identified as potential candidates for significant improvement for tests of Lorentz symmetry (Shaniv *et al*, 2018). New experimental techniques for HCI described in this review combined with an improved theoretical description will allow for more stringent QED tests.

III. ELECTRONIC STRUCTURE THEORY AND TESTS OF QED

A. Theoretical treatment of QED in HCI

QED laid the foundation of the modern formalism of the standard model as the first relativistic quantum field theory (Bjorken and Drell, 1964; Akhiezer and Berestetskii, 1965; Peskin and Schroeder, 1995). It is arguably the most stringently tested part of the standard model. Highly charged ions are extremely relativistic systems and an accurate prediction of their electronic structure has to include large QED contributions. The understanding of QED contributions is crucial for a number of precision tests of physics beyond the SM, including those described in this review. QED contributions are also needed for determining fundamental constants. Therefore, we start the discussion of HCI electronic structure with the chapter on QED calculations in HCI and briefly review recent bound-state QED (BSQED) tests. We refer the interested reader to reviews by Eides, Grotch, and Shelyuto (2001), Karshenboim (2005), Drake and Yan (2008), Beiersdorfer (2010), Andrey V. Volotka *et al.* (2013), Shabaev *et al* (2015), Indelicato and Mohr (2017), and Sturm *et al* (2017) for detailed discussions of QED calculations and tests of QED. The electronic structure of HCI specific to the metrology applications and searches for the variation of fundamental constants is discussed in Sec. IV.

While in heavy atoms the QED contributions to the binding energy of the inner-shell electrons are equally strong to those in HCI, their investigation is hindered by the presence of filled outer shells. This causes, on the one side, noticeable energy shifts, and, on the other side, reduces the lifetime of excited states through Auger decay coupling the initial state to the ionization continuum (Zimmerer, Grün, and Scheid, 1991). The resulting broadening of the electronic transitions of interest reduces spectral accuracy. In addition, theoretical methods are best developed for few-electron systems, and therefore the research quest was primarily the study of hydrogenlike and lithiumlike heavy HCI, and experimental efforts have also focused on such systems (Beiersdorfer, 2010).

Since the expansion parameter $Z\alpha$ in perturbative theory would approach a value close to 1 for heavy elements, it was not clear how far the usual expansion-based approximations would remain valid, and if contributions from two-loop QED (Yerokhin, Indelicato, and Shabaev, 2003b) could be appropriately accounted for. To address this, nonperturbative, all-order methods have been developed [see, e.g., Lindgren *et al* (2001) and Shabaev (2002)], and two-loop calculations carried out by Yerokhin, Indelicato, and Shabaev (2003b) and Artemyev *et al* (2005).

A consistent QED approach is possible only within $1/Z$ perturbation theory for systems with up to three or four electrons (Yerokhin, Indelicato, and Shabaev, 2003a; Artemyev *et al*, 2005; Yerokhin, Artemyev, and Shabaev, 2007; Sapirstein and Cheng, 2011; Yerokhin and Shabaev, 2015). For many-electron ions, which are of the most interest to this review, the use of mean-field approximations (such as Dirac-Fock approximation) is necessary, and correlations are treated within relativistic quantum mechanics. In this case, QED corrections can be included by means of model potentials (Blundell, 1992; Cheng, Johnson, and Sapirstein, 1993; Flambaum and Ginges, 2005; Roberts, Dzuba, and Flambaum, 2013; Shabaev, Tupitsyn, and Yerokhin, 2013, 2015; Tupitsyn and Berseneva, 2013; Ginges and Berengut, 2016). In such calculations, the electron-electron interaction is usually treated within the Coulomb-Breit approximation (Konovalova and Kozlov, 2015; Schwerdtfeger *et al*, 2015).

Electron-electron correlation effects in many-electron ions can be included with the help of several methods: (i) many-body perturbation theory (MBPT) (Johnson, 2007); (ii) configuration interaction (CI) (Kotochigova and Tupitsyn, 1987; Fritzsche, Froese Fischer, and Gaigalas, 2002; Fischer *et al*, 2007; Yerokhin and Surzhykov, 2012), or multiconfiguration Dirac-Hartree-Fock (Fischer *et al*, 2007); (iii) the coupled-cluster (CC) method (Eliav, Kaldor, and Ishikawa, 1994; Hubac and Neogrady, 1994); (iv) combinations of CI and MBPT (CI + MBPT) (Dzuba, Flambaum, and Kozlov, 1996; Savukov and Johnson, 2002; Kozlov *et al*, 2015), or CI and all-order (CI + AO) methods (Kozlov, 2004; Safronova *et al*, 2009). Recently Tupitsyn *et al* (2016) incorporated four of the most popular effective QED potentials into the CI + AO method and tested them for several HCI. Recent developments of these theoretical methods have considerably improved the accuracy and reliability of newer calculations for HCI and raised the predictive power of theory. We discuss the QED studies in HCI with one to three valence electrons (i.e., H like to Li like) in Sec. III.B and return to the subject of many-electron HCI in Sec. IV.

B. Tests of QED effects in HCI

1. Lamb-shift studies in the x-ray region

In first order, the Lamb shift, understood as the difference between the Dirac binding energy and the actual one, of a hydrogenic ion scales as $(\alpha Z)^4/n^3$, where n is the principle quantum number and rises for the $1s$ electron of U^{91+} to more than 425 eV (Mohr, 1974; Johnson and Soff, 1985). For this reason, soon after the development of experimental methods for the production of HCI (Mokler *et al*, 1985), they were seen as potentially very interesting probes of QED calculations (Mohr, 1985, 1992; Blundell, 1992; Persson *et al*, 1997; Mohr, Plunien, and Soff, 1998; Shabaev, 2002; Johnson, Cheng, and Chen, 2004) and, accordingly, studied in many experiments (Briand, Mossé *et al*, 1983; Briand, Tavernier *et al*, 1983; Deslattes, Beyer, and Folkmann, 1984; Richard *et al*, 1984; Beyer *et al*, 1985, 1991, 1995; Tavernier *et al*, 1985; Marmar *et al*, 1986; Briand *et al*, 1990; Gumberidze *et al*, 2004, 2005). In fact, one of the strongest drives for research with heavy HCI in large facilities such as Bevalac at

Lawrence Berkeley National Laboratory, GSI in Darmstadt, Germany, and GANIL in Caen, France, was testing QED in the nonperturbative regime. The HITRAP facility (Rodríguez *et al*, 2010) at GSI continues pursuing this type of research.

For the ground state of hydrogenlike uranium (U, $Z = 92$), the most recent Lamb-shift measurement by Gumberidze *et al* (2005) has yielded 460.2 ± 4.6 eV to be compared with predicted 463.99(39) eV. Radiative corrections from QED contribute 265.2 eV, and a shift of $-1.26(33)$ eV results from second-order QED (Yerokhin, Indelicato, and Shabaev, 2003b; Beiersdorfer *et al*, 2005). A comparably large correction arises from finite nuclear-size effects (NSE) with a total of 198.54(19) eV (Kozhedub *et al*, 2008). These results confirm QED theory predictions at the 2% level in the strongest stationary electromagnetic fields that nature provides, an extreme regime where the rest mass of the electron is only 4 times larger than its binding energy to the nucleus. Given the high accuracy of theory, hydrogenic systems have been proposed as calculable x-ray standards (Flowers *et al*, 2001).

For two-electron systems, and specifically for heliumlike ions, there is abundant theoretical literature (Indelicato, Gorveix, and Desclaux, 1987; Johnson, Plante, and Sapirstein, 1995; Lindgren, Persson, and Salomonson, 1995; Cheng and Chen, 2000; Andreev *et al*, 2001; Lindgren *et al*, 2001). At medium Z, relativistic configuration interaction and perturbative many-body methods (Chen, Cheng, and Johnson, 1993; Cheng *et al*, 1994; Plante, Johnson, and Sapirstein, 1994; Cheng and Chen, 2000) as well as unified-method calculations (Drake, 1979, 1988, 2002; Yan and Drake, 1995) have yielded reasonably accurate results in close agreement with measurements of the $1s - 2p$ x-ray transitions (Briand *et al*, 1984; Indelicato *et al*, 1986; Widmann *et al*, 1996; Bruhns *et al*, 2007; Amaro *et al*, 2012; Kubiček *et al*, 2012, 2014; Rudolph *et al*, 2013; Beiersdorfer and Brown, 2015; Epp *et al*, 2015; Machado *et al*, 2018).

A controversy arising from a claimed Z-dependent divergence between earlier experimental data and calculations (Chantler *et al*, 2012, 2013; Gillaspy, 2014), soon disputed by Epp (2013), has been settled, with all newer results agreeing very well both with older calculations and advanced theory (Artemyev *et al*, 2005). Nonetheless, better measurements will be needed to test higher-order QED as well as interelectronic contributions to the binding energy in more detail.

In lithiumlike systems, the $2s_{1/2} \rightarrow 2p_{1/2,3/2}$ transition energies display the largest relative QED contributions (up to 15%), and have been studied in detail both experimentally (Schweppe *et al*, 1991; Staude *et al*, 1998; Bosselmann *et al*, 1999; Feili *et al*, 2000; Andreev *et al*, 2001, 2012; Brandau *et al*, 2002, 2003; Epp *et al*, 2007, 2010; Zhang *et al*, 2008) and theoretically among others by Indelicato and Desclaux (1990), Kim *et al* (1991), Artemyev *et al* (1999, 2003), Cheng, Chen, and Sapirstein (2000), Sapirstein and Cheng (2011), and Yerokhin and Surzhykov (2012). A prominent example, the $2s_{1/2} \rightarrow 2p_{1/2}$ transition energy in lithiumlike U^{89+}, 280.645(15) eV, was measured with an 0.005% uncertainty and agrees perfectly with the theoretical value of 280.71(10) eV by Kozhedub *et al* (2008). These results tested second-order (in α) QED effects to 6% (A. V. Volotka *et al*, 2013). Currently, the theoretical accuracy of HCI QED tests is limited by the nuclear-polarization correction.

At this point, there is a general consensus that significant contributions from nuclear-size effects (Johnson and Soff, 1985; Mohr and Soff, 1993; Shabaev, 1993; Beier *et al*, 1998; Shabaev, Artemyev, and Yerokhin, 2000), nuclear-polarization corrections (Plunien *et al*, 1989), and also nuclear-recoil corrections (Shabaev, 1985, 1998; Palmer, 1987; Artemyev, Shabaev, and Yerokhin, 1995a, 1995b; Shabaev *et al*, 1998), which are not sufficiently well known, compromise the ability to extract information on high-order QED contributions. There have been proposals (Shabaev *et al*, 2001) based on the different scaling of the QED and nuclear-size contributions with Z and n that could help solving this conundrum; however, due to the lack of experimental data, their application has been possible only in a few cases until now (Beiersdorfer *et al*, 2005).

2. Fine- and hyperfine-structure transitions

Scaling laws increase the fine- and hyperfine-structure (HFS) energy splittings in HCI by several orders of magnitude. Among other things, this gives rise to intraconfiguration transitions due to changes in total angular momentum J (Crespo López-Urrutia, 2008) at energies well below the x-ray and soft x-ray regions that have already been mentioned. Rearrangements of configurations giving rise to level crossings are another possibility for optical transitions (Berengut, Dzuba, and Flambaum, 2010; Ong, Berengut, and Flambaum, 2014; Windberger *et al*, 2015).

Experimentally, the accuracy that can be obtained is much higher in the optical range than in the x-ray region: e.g., an uncertainty of only 0.6 ppm was achieved for $1s^2 2s^2 2p\,^2P_{3/2}$-$^2P_{1/2}$ transition in boronlike Ar^{13+} ions at 441.255 68(26) nm (Draganič *et al*, 2003; Mäckel *et al*, 2011). Theory is 2 orders of magnitude less accurate (Tupitsyn *et al*, 2003; Artemyev *et al*, 2007). Since the nonrelativistic energies of $p_{1/2}$ and $p_{3/2}$ states are the same, this line and many other intraconfiguration electric-dipole ($E1$) forbidden transitions in a large number of isoelectronic sequences that contain similarly large relativistic and QED contributions are excellent candidates for future precision tests of many-body BSQED, in particular, by means of sympathetically cooled HCI (Schmöger *et al*, 2015).

The first direct observation of a HFS in the optical range was achieved by resonant laser excitation of the $M1$ transition coupling the two hyperfine levels of the ground state of hydrogenlike $^{209}Bi^{82+}$ ions circulating at relativistic velocities in the GSI heavy-ion storage ring ESR (Klaft *et al*, 1994), followed by spontaneous-emission measurements of $^{187}Ho^{66+}$ (holmium, $Z = 67$) (Crespo López-Urrutia *et al*, 1996), $^{185,187}Re^{74+}$ (rhenium, $Z = 75$) (Crespo López-Urrutia, Beiersdorfer, Savin, and Widmann, 1998), and $^{203,205}Tl^{80+}$ (thallium, $Z = 81$) (Beiersdorfer *et al*, 2001) ions trapped in an electron-beam ion trap (EBIT), and a further experiment on $^{207}Pb^{81+}$ (Seelig *et al*, 1998) at ESR. In all those experiments systematic effects, low resolution, and statistics limited the relative wavelength accuracies to about 1×10^{-4}.

On the theoretical side, the one-loop self-energy correction to the first-order hyperfine interaction in hydrogenic ions for

various nuclear charges was theoretically studied by Persson *et al* (1996). Vacuum-polarization corrections to the HFS of Bi HCI were analyzed by Labzowsky *et al* (1997), and leading nonrecoil radiative corrections to the HFS including effects of extended nuclear magnetization calculated by Sunnergren *et al* (1998). As for the nuclear-recoil effect, Shabaev (1998), Shabaev *et al* (1998, 2001), and Shabaev, Artemyev, and Yerokhin (2000) performed a sophisticated analysis of its influence on the various transitions.

3. Nuclear-size effects: Charge radius and magnetization distribution

The uncertainty of the leading radiative terms in all previously mentioned calculations seems to be small compared with that of finite NSE appearing at the few percent level in the HFS splitting (Shabaev *et al*, 1997). Since the finite charge radius can be independently measured in scattering experiments, its contribution (at the 10% level of the transition energy) to the HFS could be reasonably inferred. However, the nuclear magnetization distribution, or Bohr-Weisskopf (BW) effect (at the level of 1% of the total HFS), is extremely difficult to determine independently. Basically, the only other method that can measure this quantity is γ spectroscopy, and more recently also laser spectroscopy on muonic atoms. Therefore, in most cases the BW effect is accounted for based on uncertain models of the nuclear magnetic structure. The situation in the BSQED tests with HCI is akin to that of the laser spectroscopy of hydrogen and the proton-size puzzle (Pohl *et al*, 2010, 2013, 2016; Pohl, 2016; Beyer *et al*, 2017): our limited knowledge of the nucleus is the frontier for the most stringent tests of QED.

In order to suppress the uncertainties stemming from finite NSE, Shabaev *et al* (2001) introduced the concept of the specific isonuclear difference between the ground-state HFS of the Li-like ion $\Delta E(2s)$ and the H-like ion $\Delta E(1s)$:

$$\Delta' E = \Delta E(2s) - \xi \Delta E(1s), \tag{8}$$

where the parameter ξ is theoretically chosen to cancel the NSE in this difference.

By scaling with $1/n^3$ and applying relativistic corrections, ξ can be calculated with high precision. For Bi (bismuth, $Z = 83$) ions, the method now achieves a relative uncertainty of $\approx 10^{-4}$ following better calculations (Volotka *et al*, 2012) of the two-photon exchange corrections. If HFS were measured at the 10^{-6} level, many-body QED effects could be benchmarked at a few percent level (A. V. Volotka *et al*, 2013). Experiments are already approaching this level of accuracy, e.g., for the $2s_{1/2} \rightarrow 2p_{1/2}$ extreme ultraviolet (EUV) hyperfine transitions in Li-like and Be-like ions of ^{141}Pr (Beiersdorfer *et al*, 2014).

Karpeshin and Trzhaskovskaya (2015) proposed the opposite approach, namely, to investigate the nuclear magnetization distribution based on the HFS experimental data for various isoelectronic sequences as had been demonstrated by Crespo López-Urrutia, Beiersdorfer, Savin, and Widmann (1998) and Beiersdorfer *et al* (2001) for the cases of Re and Tl HCI.

In order to solve some open questions, Lochmann *et al* (2014) repeated the HFS measurements in hydrogenlike and lithiumlike Bi and obtained values in disagreement with earlier experimental work by Klaft *et al* (1994). Recently, Ullmann *et al* (2017) remeasured the HFS transitions in $^{209}Bi^{82+}$ and $^{209}Bi^{80+}$ and obtained ξ with more than an order of magnitude improvement in precision. Its theoretical value of $\xi = 0.168\,86$ allows one to cancel the BW correction for ^{209}Bi (Shabaev *et al*, 2001). However, the experimental result $\Delta' E = -61.012(5)(21)$ meV (statistical and systematic uncertainties given in parentheses) disagreed by 7σ with the predicted value of $-61.320(4)(5)$ meV (Volotka *et al*, 2012) (uncertainties in first and second parentheses arise from uncalculated higher-order terms and the uncertainty of the complete cancellation of all nuclear effects, respectively). This result was considered a challenge to bound-state strong-field QED theory (Ullmann *et al*, 2017). However, the explanation which was found soon after was rather mundane: the value of the nuclear magnetic moment for ^{209}Bi that was used to analyze the data was simply wrong as recently found out by Skripnikov *et al* (2018). Chemical shifts which are difficult to be taken into account have now been properly included. This was a suspicion that Gustavsson and Mårtensson-Pendrill (1998) and Gustavsson (1999) had expressed in their analyses of the results of Klaft *et al* (1994).

In this context, it is important to mention that the ubiquitous atomic diamagnetism modifies the magnetic field experienced by the nucleus in every determination of the nuclear gyromagnetic ratio. This intrinsic effect is always present when bound electrons surround the nucleus. Calculations of the diamagnetic shielding factors that result from this effect have theoretical uncertainties. Even more problematic are chemical shifts that appear in molecules imbedded in chemical samples. Therefore, the accuracy of the derived "corrected" nuclear magnetic moments is reduced, and the interpretation of experiments becomes problematic. As an example, the nuclear magnetic shielding factors by the single bound electron in hydrogenic systems (Yerokhin *et al*, 2011) have to be calculated to all orders of QED expansion in the nuclear binding strength parameter. In principle, solving these issues is a prerequisite for the intended high-level QED tests, as pointed out by Gustavsson and Mårtensson-Pendrill (1998) and Gustavsson (1999).

4. Microwave studies of the bound-electron g factor

Hitherto, the most stringent benchmark of QED calculations, and thus of the standard model, comes from the good agreement of the measurements of the fine-structure constant α (a parameter of the model that cannot be calculated from the first principles) by strictly different methods. In the first method, the experimental value of the free-electron magnetic-moment anomaly a_e (Mohr, Taylor, and Newell, 2012; Mohr, Newell, and Taylor, 2016) is measured in a Penning trap (Hanneke, Fogwell, and Gabrielse, 2008) and combined with exact QED calculations that include electroweak and hadronic contributions using expansions in a power series of α/π with calculable coefficients. The second approach is based on the measured Rydberg constant R_∞ (Wicht *et al*, 2002; Cadoret

et al, 2008; Bouchendira *et al*, 2011) obtained by atom interferometry of recoiling atoms upon photon absorption.

For BSQED, the steep scaling laws governing the spin-orbit interaction make trapped HCI extremely sensitive probes. The g factor of the bound electron [for a theory review see Shabaev *et al* (2015)] is determined to a very high precision also in Penning traps (Sturm, Werth, and Blaum, 2013; Sturm *et al*, 2017), to ten significant digits in the case of H-like $^{28}Si^{13+}$ as demonstrated by Sturm *et al* (2011, 2013) and Schabinger *et al* (2012). Here the experimental relative uncertainty is only 4×10^{-11}, leaving theoretical, uncalculated two-loop QED corrections of order $\alpha^2(\alpha Z)^5$ and higher (Pachucki *et al*, 2005) as the largest source of uncertainty. These results could be further improved by combining theoretical and experimental values for two different H-like ions (Sturm *et al*, 2014). This idea of combining precise g-factor measurements and QED calculations (Sturm *et al*, 2013; Yerokhin and Harman, 2013; Czarnecki and Szafron, 2016) has recently yielded a 13-fold improvement on the electron mass determination (Sturm *et al*, 2014; Köhler *et al*, 2015; Zatorski *et al*, 2017).

The most stringent BSQED experimental test of the g factor for a three-electron system was carried out for Li-like $^{28}Si^{11+}$ (silicon, $Z = 14$) by Wagner *et al* (2013) and Volotka *et al* (2014) and is in excellent agreement with theory that rigorously treats two-photon exchange corrections (Volotka *et al*, 2014). With the works by Wagner *et al* (2013), relativistic interelectronic interactions, one-electron BSQED in magnetic fields, and screened bound-state QED are tested at a level of precision corresponding to 0.001%, 0.7%, and 3%, respectively.

Using cancellations of BSQED contributions between different isotopes, e.g., for $^{40}Ca^{17+}$ and $^{48}Ca^{17+}$ ions, nuclear effects can be tested (Köhler *et al*, 2016). This is a complementary approach to the specific difference scheme [Eq. (8)] used to eliminate the nuclear effects in the g-factor calculations (Shabaev *et al*, 2002; Volotka and Plunien, 2014). This methodology can be extended (Shabaev *et al*, 2006; Andrey V. Volotka *et al.*, 2013) to α determinations using specific differences of the g factors of B-like and H-like ions with zero nuclear spin. Future experiments with a Penning trap, ALPHATRAP (Sturm, Werth, and Blaum, 2013; Sturm *et al*, 2017), coupled to an EBIT, and ARTEMIS (von Lindenfels *et al*, 2013) at the HITRAP (Kluge *et al*, 2008) facility at GSI, will explore the application of these methods to HCI in very high charge states.

IV. HCI ELECTRONIC STRUCTURE AND FREQUENCY METROLOGY

As discussed in the previous section, BSQED tests and the corresponding measurements of fundamental constants have to be carried out in HCI with a very few valence electrons. In contrast, the metrology applications and the search for the variation of fundamental constants discussed in Sec. II requires HCI with rather complicated electronic structures, with the special exception of the HFS in H-like ions. In this section, we discuss the electronic structure of HCI relevant to these new applications. At first glance, the idea to use HCI for optical clocks may appear strange. The energy scale for HCI electronic levels is about $(Q+1)^2 R_\infty$, where Q is the ion charge. Therefore, one would expect optical transitions in HCI taking place only between highly excited Rydberg states being broadened by competing x-ray transition branches. Certainly, electric-dipole ($E1$) transitions from the ground state lie in the extreme UV or x-ray wavelength regime. Nonetheless, optical transitions of interest to metrology in HCI occur within the ground-state configuration due to fine structure, HFS, and also near level crossings, when the ions in the isoelectronic sequence change ground-state configurations. We will now consider this latter case.

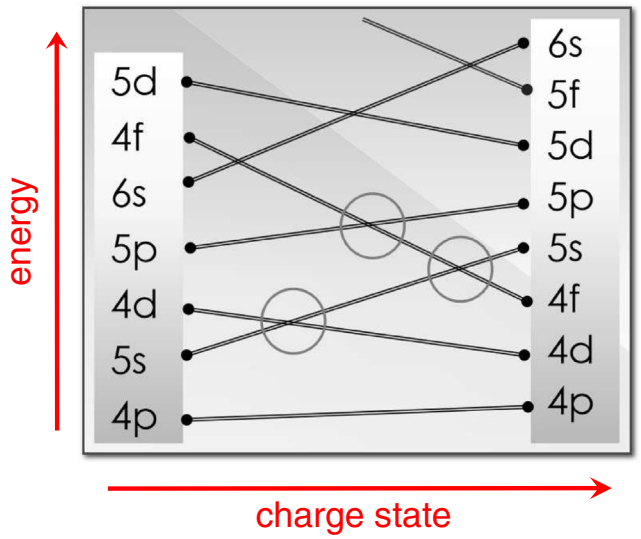

FIG. 1. Schematic of the shell order in neutral atoms (left) and in hydrogenlike ions (right) (Berengut *et al*, 2012b). One can see that the "diving" of $4d$ and $4f$ shells results in level crossings in the areas marked by circles.

The first calculations of HCI systems which display such level crossings were done by Berengut, Dzuba, and Flambaum (2010). The general idea of that paper is as follows: the order of shells in neutral atoms follows the $n+l$ rule[1] and is different from that of the hydrogenlike ions (see Fig. 1). For example, in hydrogen the $4f$ shell immediately follows $4s$, $4p$, and $4d$ shells, while in the periodic table it starts to fill after the $6s$ shell at $Z = 58$ (cerium). The energy of the $4f$ levels decreases much faster than energies of other levels if we move along isoelectronic sequences. As a result, we can expect a reordering of electron configurations (level crossings) near some value of Z. When such crossings involve the ground state of an ion, we get low energy transitions, which may lie in the optical range. If these transitions are of $p-f$ or $s-f$ type (i.e., high-order multipole transitions), they are very narrow and suitable for high-precision metrology. Note that the $s-d$ crossing may also lead to narrow optical transitions, but such crossings happen at a relatively low ionization stage. For example, the $6s-5d$ crossing takes place in a Tm-like

[1]The $n+l$ rule, or Madelung rule, says that in neutral atoms the orbitals with lower values of $n+l$ are filled first. For equal $n+l$, the orbitals with smaller n are filled. This rule predicts the following filling order: $1s, 2s, 2p, 3s, 3p, 4s, 3d, 4p, 5s, 4d, 5p, 6s, 4f, 5d, 6p, 7s, 5f, 6d, 7p, 8s, \ldots$.

sequence between Ta^{4+} and W^{5+} (Berengut, Dzuba, and Flambaum, 2011).

The level crossings discussed above unavoidably take place along certain isoelectronic sequences. However, the exact position of the crossing and details of the level structure near it are difficult to predict. It requires calculations with very high accuracy as the energy scale of the spectrum is defined by the binding energy of the outermost electrons, which is of the order of $(Q+1)^2R_\infty$. Thus, any quantitative predictions can be made only on the sophisticated level of the theory when relativistic, QED, and correlation effects are treated with the highest possible level of precision.

Alternatively, one can consider transitions between the levels of the ground-state multiplet of an HCI. Such transition energies are of the order of $(Z\alpha)^2(Q+1)^2R_\infty$. For moderately heavy HCI these $M1$ transitions may lie in the visible range. This is the case, for example, for Al-like ions $V^{10+}-Cu^{16+}$ (Yu and Sahoo, 2016). Nandy and Sahoo (2016) studied the fine-structure transition $^2F_{7/2}\rightarrow{}^2F_{5/2}$ in the configuration $4f^{13}5s^2$ of the ions W^{13+}, Ir^{16+}, and Pt^{17+}. Windberger *et al* (2016) studied $M1$ optical transitions between fine-structure levels in Sn^{11+}–Sn^{14+} ions. All these fine-structure transitions are of $M1$ type. For optical clocks we want to have weaker transitions to allow for significantly narrower lines. Schiller (2007) and Yudin, Taichenachev, and Derevianko (2014) considered $M1$ transitions between hyperfine levels in heavier H-like HCI, such as $^{171}Yb^{69+}$ or $^{207}Pb^{81+}$, where these transitions lie in the optical range.

Next we will focus mostly on level crossings, where transitions are of quadrupole or even octupole type and the lines are extremely narrow. Calculations of the ion properties in the vicinity of the level crossing are technically difficult. Interesting crossings happen for degrees of ionization higher than 10 ($Q\gtrsim 10$), when binding energies are of the order of 1 keV. That means that we need atomic calculations with very high accuracy to identify optical transitions, which correspond to energy differences of the order of 1 eV. In order to get transition energies with 10% accuracy, one needs fractional accuracy of the theory on the order of 10^{-4} or better. This is challenging for existing theoretical methods. As a result, the first theoretical paper (Berengut, Dzuba, and Flambaum, 2010) was followed by intensive further research (Berengut, Dzuba, and Flambaum, 2011; Berengut *et al*, 2011, 2012a, 2012b; Derevianko, Dzuba, and Flambaum, 2012; Dzuba, Derevianko, and Flambaum, 2012a, 2012b, 2013; Kozlov, Dzuba, and Flambaum, 2013; Yudin, Taichenachev, and Derevianko, 2014; Dzuba, Flambaum, and Katori, 2015). The most accurate calculations were done using a state-of-the-art hybrid approach that combines coupled-cluster and configuration interaction methods (Safronova *et al*, 2014a, 2014b, 2014c; Dzuba *et al*, 2015). The last three works specifically considered all HCI which satisfied the following criteria:

- the existence of long-lived metastable states with transition frequencies to the ground states in the range $(0.1-1.8)\times 10^{15}$ Hz,
- high sensitivity to α variation,
- the existence of stable isotopes, and
- relatively simple electronic structure with one to four valence electrons.

Safronova *et al* (2014a, 2014b, 2014c) found that only four isoelectronic sequences satisfy all four criteria: Ag like, Cd like, In like, and Sn like, which include ions with 46-electron core $[1s^2\cdots 4d^{10}]$. Berengut *et al* (2012b) and Dzuba *et al* (2015) considered heavier actinide ions which satisfy all criteria above with the exception of the existence of stable isotopes.

A suitable transition for laser cooling and internal state readout is not required for the HCI when using quantum logic spectroscopy in which a cotrapped singly charged ion provides for these features as described in more detail in Sec. VII.C. The dependence of the clock transition on external fields and their gradients causes systematic effects in atomic clocks. The size of HCI scales as $1/(Q+1)$ and their dipole and quadrupole moments and polarizabilities, both static and dynamic, are suppressed by an order of magnitude and up to several orders for level-crossing and hyperfine optical transitions, respectively. A number of papers provided detailed investigation of systematic effects in optical clocks based on HCI, reaching the conclusion that the next order of magnitude improvement in the accuracy of frequency standards to 10^{-19} uncertainty may also be achievable with HCI (Derevianko, Dzuba, and Flambaum, 2012; Dzuba, Derevianko, and Flambaum, 2012a, 2013; Yudin, Taichenachev, and Derevianko, 2014; Dzuba, Flambaum, and Katori, 2015). The systematic effects in HCI clocks are discussed in more detail in Sec. VII.D.

In the remaining part of this section we discuss calculations of the spectra, lifetimes, and sensitivity to α variation for particular systems. The accuracy of theoretical predictions strongly depends on the number of valence electrons, as the valence-valence correlations are very strong and cannot be accurately treated perturbatively. As a result, CI represents the best strategy to include valence-valence correlations. However, the number of configurations that has to be included into the CI calculations grows exponentially with the number of valence electrons, limiting accurate calculations to a few valence electrons. Systems with more valence electrons usually also have a much denser spectrum, leading to experimental difficulties in spectra identification, exacerbated by large uncertainties in the theoretical predictions.

We start with the discussion of the proposals with H-like ions, which are based on the narrow $M1$ hyperfine transitions. All other HCI optical clock proposals are grouped by the number of valence electrons, starting with the systems with one electron above the closed shells and then discussing systems with two, three, and four electrons. Finally, we discuss systems with one or more holes in almost filled shells and a case with a midfilled $4f$ shell.

A. HFS of hydrogenlike ions

As mentioned in Sec. III.B.2, in heavy H-like HCI with nuclear spin $1/2$ the hyperfine transitions may lie in the optical and near-optical range. These transitions are of the $M1$ type and are very weak because they require a nuclear spin flip. Schiller (2007) analyzed systematic effects for the cases of $^{61}Ni^{27+}$ and $^{207}Pb^{81+}$. Yudin, Taichenachev, and Derevianko (2014) discussed hyperfine transitions in H-like Yb, Pt, Hg, Tl, and Pb ions with clock wavelengths below 3 μm and nuclear spin $I=1/2$, listed in Table I. For these ions, the

TABLE I. Clock transition wavelengths λ (in μm) and natural linewidth $\gamma/2\pi$ (in Hz) for hyperfine transitions in H-like ions. The values are from Yudin, Taichenachev, and Derevianko (2014).

Ion	λ (μm)	$\gamma/2\pi$
$^{171}Yb^{69+}$	2.16	0.43
$^{195}Pt^{77+}$	1.08	3.4
$^{199}Hg^{79+}$	1.15	2.8
$^{203}Tl^{80+}$	0.338	111.2
$^{205}Tl^{80+}$	0.335	114.2
$^{207}Pb^{81+}$	0.886	6.2

ground-state hyperfine structure consists of only $F = 0$ and 1 levels, simplifying experimental realization since the $F = 0$ level does not have Zeeman components. They evaluated systematic effects due to quadrupole shifts in inhomogeneous electric fields, Zeeman shifts, blackbody radiation (BBR) shifts, and ac Stark shifts induced by the clock laser. As a result, Yudin, Taichenachev, and Derevianko (2014) concluded that systematic effects can be controlled at a level below 10^{-20} fractional accuracy. However, the achievable instability even for $^{171}Yb^{69+}$, which has the longest upper clock state lifetime of 0.37 s, is $\sigma_y(\tau) \approx 5 \times 10^{-15}/\sqrt{t/\mathrm{s}}$, requiring 9.5 months to reach 10^{-18} fractional accuracy for a single HCI (see Sec. VII.E.1).

Hyperfine transitions are particularly interesting for the search for a variation of fundamental constants because, like the Cs clock transition, they depend on α, the proton-to-electron mass ratio μ, and nuclear g factors, which can be interpreted in terms of the variation of $X_q = m_q/\Lambda_{\mathrm{QCD}}$, according to Eq. (2) (Oreshkina *et al*, 2017). All other optical atomic clocks are sensitive only to the variation of α. This means that by comparing such a HCI hyperfine clock with any other optical clock one can significantly improve the laboratory limit on $\dot{\mu}/\mu$, which is constrained according to Eq. (7) at the level of 10^{-16} yr^{-1}.

The present constraint is limited by the Cs clock accuracy and the long averaging times to reach low statistical uncertainties. Both limitations may be overcome using optical hyperfine transitions in HCI. Availability of different nuclei may also allow the setting of further constraints on the variation of X_q. Moreover, the sensitivity coefficients to α-variation K for heavy H-like HCI monotonically grow with Z and significantly exceed the sensitivity of the Cs clock $K_{\mathrm{Cs}} = 2.83$ for all ions listed in Table I. Recently an accurate calculation of the sensitivity coefficients was done by Oreshkina *et al* (2017), who also considered other H-like and Li-like ions (note that they use relativistic units, and their sensitivity coefficients to α variation differ from ours by 2).

B. HCI with one valence electron

1. Ag-like ions

The single-valent systems are simplest from the theoretical point of view. Berengut, Dzuba, and Flambaum (2010) already pointed out that the $5s - 4f$ crossing in the Ag-like isoelectronic sequence ($N = 47$) takes place near Pm^{14+}. The ions Nd^{13+} ($Z = 60$) and Pm^{14+} have the ground-state configuration $[1s^2 \cdots 4d^{10}]5s$ and the closely lying first excited state configuration $[1s^2 \cdots 4d^{10}]4f$. These configurations exchange places in Sm^{15+}. Energies and α-variation sensitivity coefficients q [Eq. (3)] relative to the ground state for Nd^{13+} and Sm^{15+} are listed in Table II. Energies and parameters q are given in cm^{-1}. K is dimensionless. The table also lists the enhancement factors $K = 2q/E$ [Eq. (4)], wavelengths λ (in nm) for transitions from the ground states, and total radiative lifetimes τ (in s). The experimental wavelengths from Sugar and Kaufman (1981) are given; the remaining values are from the CI + AO calculation (Safronova *et al*, 2014c). Theoretical energy values are listed for consistency with the q values. The Ag-like ions are among the very few HCI with near-optical transitions for which experimental measurements are available.

TABLE II. Energies and α-variation sensitivity coefficients q relative to the ground state for HCI with one and two valence electrons. $K = 2q/E$ is the enhancement factor. Energies and parameters q are given in cm^{-1}. K is dimensionless. Wavelengths λ (in nm) for transitions from the ground states and total radiative lifetimes τ (in s) are listed. Nd^{13+}, Sm^{15+}, Nd^{12+}, Sm^{14+}, and Es^{17+} values are from the CI + AO calculation (Safronova *et al*, 2014c; Dzuba *et al*, 2015). Nd^{13+} and Sm^{15+} wavelengths are experimental values from Sugar and Kaufman (1981). Cf^{17+} results are CI + MBPT calculations from Berengut *et al* (2012b). The * indicates cases with no stable isotopes.

Ion	Level	Energy	q	K	λ	τ
Nd^{13+}	$5s_{1/2}$	0				
	$4f_{5/2}$	55 706	104 229	3.7	179	1.3×10^{6}[a]
	$4f_{7/2}$	60 134	108 243	3.6	166	0.996
Sm^{15+}	$4f_{5/2}$	0				
	$4f_{7/2}$	6 444	5 910	1.8	1526	0.308
	$5s_{1/2}$	60 517	−134 148	−4.4	166	3.1×10^{5}
$*Cf^{17+}$	$5f_{5/2}$	0				
	$6p_{1/2}$	18 686	−449 750	−48	535	
	$5f_{7/2}$	21 848	17 900	1.6	458	
Nd^{12+}	$5s^2\ ^1S_0$	0				
	$5s4f\ ^3F_2$	79 469	101 461	2.6	126	8.5×10^{10}
	$5s4f\ ^3F_3$	80 769	102 325	2.4	124	19.7
Sm^{14+}	$4f^2\ ^3H_4$	0				
	$5s4f\ ^3F_2$	2 172	−127 720	−118	4600	5.6×10^{13}[b]
	$5s4f\ ^3F_3$	3 826	−126 746	−66	2614	8.51
$*Es^{17+}$	$5f^2\ ^3H_4$	0				
	$5f6p\ ^3F_2$	7 445	−46 600	−13	1343	11 000

[a]This value includes $E3$ and $M2$ transitions. Inclusion of the hyperfine-induced $E1$ transition for $^{143}Nd^{13+}$ decreases the lifetime to $(1.1\text{–}1.2) \times 10^6$ s, depending on the hyperfine component of the transition (Dzuba and Flambaum, 2016).

[b]The hyperfine quenching reduces this lifetime in $^{147}Sm^{14+}$ to $5 \times 10^7 - 2 \times 10^9$ s (Dzuba and Flambaum, 2016).

Comparison of the theoretical and experimental energies relative to the ground state for Nd^{13+}, Sm^{15+}, and Ce^{9+} is given in Table III, adapted from Safronova *et al* (2014c). The experimental values are from Sugar and Kaufman (1981) and Joshi, Ryabtsev, and Churilov (2001). Ce^{9+} has a $5s^2$ closed shell, so it can be considered as a system with either one or

TABLE III. Comparison of the energies of Ag-like Nd^{13+}, Sm^{15+}, and In-like Ce^{9+} ions relative to the ground state with experiment (Sugar and Kaufman, 1981; Joshi, Ryabtsev, and Churilov, 2001). Differences with experiment are given in cm^{-1} and % in columns "Diff.," Adapted from Safronova *et al* (2014c).

Ion	Level	Expt.	CI + AO	Diff.	Diff. %
Nd^{13+}	$5s_{1/2}$	0	0	0	
	$4f_{5/2}$	55 870	55 706	164	0.29
	$4f_{7/2}$	60 300	60 134	166	0.28
	$5p_{1/2}$	185 066	185 028	38	0.02
	$5p_{3/2}$	234 864	234 887	−23	−0.01
Sm^{15+}	$4f_{5/2}$	0	0	0	
	$4f_{7/2}$	6 555	6 444	111	1.69
	$5s_{1/2}$	60 384	60 517	−133	−0.22
	$5p_{1/2}$	268 488	268 604	−116	−0.04
	$5p_{3/2}$	333 203	333 385	−182	−0.05
Ce^{9+}	$5p_{1/2}$	0	0	0	
	$5p_{3/2}$	33 427	33 450	−23	−0.07
	$4f_{5/2}$	54 947	54 683	264	0.48
	$4f_{7/2}$	57 520	57 235	285	0.50

three valence electrons as discussed later. Excellent agreement with experiment is observed for all levels. A detailed calculation of the Ag-like ion properties is given by Safronova *et al* (2014b).

The Pm^{14+} ion has no stable isotopes and while the CI + MBPT calculation predicted that the $5s$ and $4f_{5/2}$ states are separated by 3973 cm^{-1} (Berengut, Dzuba, and Flambaum, 2010), the CI + AO calculations predicted only about 300 cm separation (Safronova *et al*, 2014b).

Nd^{13+} represents a particularly attractive case since the strongest transition from the metastable $4f_{5/2}$ level of this ion is $E3$, resulting in the extremely long lifetime of more than 15 days (see Fig. 2). The wavelength of the $5s - 4f$ transition in Nd^{13+} is in the vacuum-ultraviolet (VUV). The amplitudes of such strongly forbidden transitions may depend on the nuclear spin and can be significantly enhanced for odd isotopes. Dzuba and Flambaum (2016) calculated such hyperfine-induced transitions for $^{143}Nd^{13+}$, $^{149}Pm^{14+}$, $^{147}Sm^{14+}$, and $^{147}Sm^{15+}$. The $^{143}Nd^{13+}$ lowest excited state value in Table II includes $E3$ and $M2$ transitions. Inclusion of the hyperfine-induced $E1$ transition for $^{143}Nd^{13+}$ decreases the lifetime to $(1.1–1.2) \times 10^6$ s, depending on the hyperfine component of the transition (Dzuba and Flambaum, 2016). The contribution of the hyperfine-induced $E1$ transition to the lowest excited state lifetime of the $^{147}Sm^{15+}$ is only 1%.

Dzuba, Derevianko, and Flambaum (2012b) carried out a detailed assessment of the systematic uncertainties for Nd^{13+} and Sm^{15+}, including BBR shifts, Zeeman shifts, electric-quadrupole shifts, and other perturbations, concluding that the fractional accuracy of the clocks based on these systems may reach 10^{-19} if efficient shift cancellation schemes are applied (see Sec. VII).

2. Tl-like californium

Berengut *et al* (2012b) considered the $5f - 6p$ crossings which occur for the actinide ions. The CI + MBPT results for the Cf^{17+} ion are listed in Table II. Cf^{17+} has a $6s^2$ closed shell, so it may be considered as a system with a single valence electron. The sensitivity to α variation of the excited $6p_{1/2}$ state with respect to the ground state is extremely large, $q = -450\,000$ cm^{-1} with $K = 48$. Neither californium nor einsteinium, considered later, have stable isotopes. However, they have very long-lived isotopes, such as ^{249}Cf with half-life of 351 yr and ^{252}Es with half-life of 1.3 yr. There are many facilities, including Berkeley, Dubna, Darmstadt, RIKEN, etc., which produce and study unstable isotopes (Meierfrankenfeld, Bury, and Thoennessen, 2011; Runke *et al*, 2014).

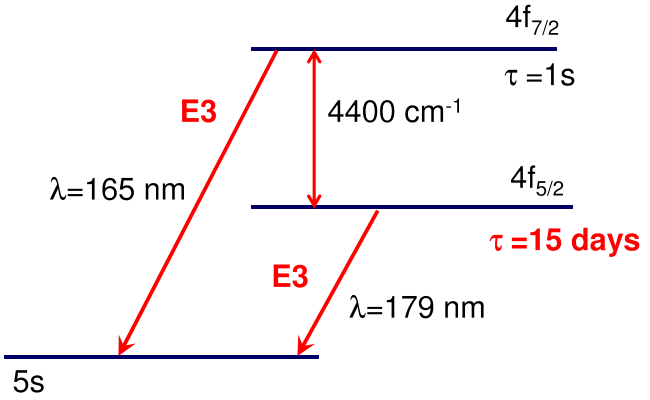

FIG. 2. Energy levels and radiative lifetimes of low-lying levels of Ag-like Nd^{13+}. Vertical intervals are not to scale. The lowest state lifetime includes $E3$ and $M2$ transitions. Inclusion of the hyperfine-induced $E1$ transition for $^{143}Nd^{13+}$ decreases the lifetime to 12.5–14 days, depending on the hyperfine component of the transition (Dzuba and Flambaum, 2016). From Safronova *et al*, 2014b.

C. HCI with two valence electrons

1. Cd-like ions

Cd-like ions Nd^{12+} and Sm^{14+} have two valence electrons and ground configurations $5s^2$ and $4f^2$, respectively. In both cases the first excited configuration is $4f5s$. The lowest multiplet of this configuration is $^3F_{2,3,4}$. In Nd^{12+} the levels of this multiplet lie at approximately 79 500, 80 800, and 83 700 cm^{-1} above the ground state, while for Sm^{14+} they are much lower, at 2200, 3800, and 8800 cm^{-1}, respectively, as illustrated in Table II. Therefore neither of the ions have transitions in the visible range and Pm has no stable isotopes. The lowest level $^3F_2$ is connected to the ground state by an $M2$ transition and has an extremely long lifetime, while the other levels of this multiplet have lifetimes of the order of seconds. The $M2$ lifetimes are strongly quenched by hyperfine-induced $E1$ transitions, by 4–6 orders of magnitude in $^{147}Sm^{14+}$, depending on the hyperfine component of the transition (Dzuba and Flambaum, 2016). Other details can be found in Safronova *et al* (2014a) and Dzuba and Flambaum (2016).

2. Pb-like californium and einsteinium

Cf^{16+} has a very dense and complex spectrum with three closely lying configurations $5f^2$, $5f6p$, and $6p^2$. According to

the CI + MBPT calculation by Berengut *et al* (2012b), the ground state is $J = 3[5f6p]$, with the first excited state $J = 0[6p^2]$ at about 5000 cm^{-1} and $J = 4[5f^2]$ at roughly 10 000 cm^{-1}. QED and high-order correlation corrections may shift levels enough to even change their order. Therefore, new studies are necessary to predict this spectrum more reliably. Note that the sensitivity coefficients q are very large and have opposite signs: $q(J = 3) \approx -371\,000$ cm^{-1} and $q(J = 0) = +415\,000$ cm^{-1}. Es^{17+} was considered by Dzuba *et al* (2015) using the CI + AO method; the clock transition data are listed in Table II.

D. HCI with three valence electrons

1. In-like ions

There are two level crossings in the In-like isoelectronic sequence ($N = 49$). There is a crossing of the $5p$ and $4f$ shells near $Z = 59$ as well as a crossing of the $5s$ and $4f$ shells near $Z = 63$. The ground configuration at the first crossing is $5s^2nl$, where $nl = 5p$ or $4f$. Near the second crossing the $5s^24f$ and $4f^25s$ configurations have similar energies. Both crossings can be adequately studied using a three-electron model with the closed core $[1s^2 \cdots 4d^{10}]$.

At the first crossing the order of levels changes from $5p_{1/2}$, $5p_{3/2}$, $4f_{5/2}$, and $4f_{7/2}$ for Ce^{9+}, to $5p_{1/2}$, $4f_{5/2}$, $4f_{7/2}$, and $5p_{3/2}$ for Pr^{10+}, and, finally, to $4f_{5/2}$, $4f_{7/2}$, $5p_{1/2}$, and $5p_{3/2}$ for Nd^{11+}. The all-order results from Safronova *et al* (2014b, 2014c) are compiled in Table IV. The theoretical spectrum of the Pr^{10+} ion is shown in Fig. 3. The energies of the $4f$ levels of Pr^{10+} are difficult to calculate accurately as they are very close to the ground state $5p_{1/2}$. The one-electron binding energies of the $5p_{1/2}$ and $4f_{5/2}$ states are 1.3×10^6 cm^{-1}, and these values cancel to 99.7% when two energies are subtracted to obtain a theoretical prediction for a transition energy 3700(200) cm^{-1} (Safronova *et al*, 2014b).

Theory predicts that a second crossing takes place between Sm^{13+} and Eu^{14+}. Calculated energy levels are listed in Table IV. For the Sm^{13+} ion, the closest configuration to the ground fine-structure multiplet $^2F_J[5s^24f]$ is $5s4f^2$. This leads to an interesting level structure with a metastable $J = 7/2[5s4f^2]$ level in the optical transition range from both levels of the ground multiplet $^2F_{5/2,7/2}[5s^24f]$. For Eu^{14+} the ground state belongs to the configuration $5s4f^2$ and the first excited level belongs to the configuration $4f^3$. These levels are very close and their theoretical uncertainty is comparable to the energy interval. For example, QED corrections for the configuration $4f^3$ exceed 1000 cm^{-1} (Tupitsyn *et al*, 2016) and corrections from the effective three-electron interactions are of similar size (Kozlov *et al*, 2016). It is possible that missing correlation corrections can change the ground state to $J = 9/2[4f^3]$. An experimental measurement of the spectrum of Eu^{14+} would allow testing of the theory for such difficult cases.

2. Bi-like californium and einsteinium

Cf^{15+} and Es^{16+} were studied using the CI + AO method by Dzuba *et al* (2015). Theoretical spectra of these ions are shown in Figs. 4 and 5. In both ions the first excited state is metastable and linked to the ground state by an $E2$ transition. For the Cf^{15+} ion, this transition has a large sensitivity to α variation, $q = +380\,000$ cm^{-1}. For the Es^{16+} ion both levels belong to the same $5f^26p$ configuration and the q factor is smaller, $q = -184\,000$ cm^{-1}. CI + AO results are listed in Table IV.

TABLE IV. Energies and α-variation sensitivity coefficients q relative to the ground state in cm^{-1}; enhancement factor $K = 2q/E$, wavelengths λ (in nm) for transitions to the ground state, and lifetimes τ (in s) for HCI with three and four valence electron configurations. All values are obtained using the CI + AO method. Cf^{15+} and Es^{16+} values are from Dzuba *et al* (2015); the other data are from Safronova *et al* (2014c). Eu^{14+} and Cf^{15+} values include QED and three-electron corrections from Kozlov *et al* (2016) and Tupitsyn *et al* (2016). The * indicates cases with no stable isotopes.

Ion	Level	Energy	q	K	λ	τ
Ce^{9+}	$5s^25p_{1/2}$	0				
	$5s^25p_{3/2}$	33 450	37 544	2.2	299	0.0030
	$5s^24f_{5/2}$	54 683	62 873	2.3	182	0.0812
	$5s^24f_{7/2}$	57 235	65 150	2.3	174	2.18
Pr^{10+}	$5s^25p_{1/2}$	0				
	$5s^24f_{5/2}$	3 702	73 849	40	2700	8.5×10^4
	$5s^24f_{7/2}$	7 031	76 833	22	1422	2.35
	$5s^25p_{3/2}$	39 141	44 098	2.3	256	0.0018
Nd^{11+}	$5s^24f_{5/2}$	0				
	$5s^24f_{7/2}$	4 180	3 785	1.8	2392	1.19
	$5s^25p_{1/2}$	53 684	−85 692	−3.2	186	0.061
Sm^{13+}	$5s^24f\,^2F_{5/2}$	0				
	$5s^24f\,^2F_{7/2}$	6 203	5 654	1.8	1612	0.367
	$4f^25s\,^4H_{7/2}$	20 254	123 621	12	494	0.133
Eu^{14+}	$4f^25s\ J = 7/2$	0				
	$4f^3\ J = 9/2$	1 262	137 437	218	7924	
	$4f^25s\ J = 9/2$	2 594	1 942	1.5	3855	
	$4f^3\ J = 11/2$	5 388	141 771	53	1856	
$*Cf^{15+}$	$5f6p^2\,^2F_{5/2}$	0				
	$5f^26p\,^4I_{9/2}$	12 898	380 000	59	775	6900
	$5f6p^2\,^2F_{7/2}$	22 018			454	0.012
$*Es^{16+}$	$5f^26p\,^4I_{9/2}$	0				
	$5f^26p\,^2F_{5/2}$	6 994	−184 000	−53	1430	16 000
	$5f^3\,^2H_{9/2}$	10 591			944	3.4
Pr^{9+}	$5s^25p^2\,^3P_0$	0				
	$5s^25p4f\,^3G_3$	20 216	42 721	4.2	475	6.6×10^{14}
	$5s^25p4f\,^3F_2$	22 772	42 865	3.8	426	59.0
	$5s^25p4f\,^3F_3$	25 362	47 076	3.7	382	5.33
Nd^{10+}	$5s^24f^2\ J = 4$	0				
	$5s^25p4f\ J = 3$	1 564	−81 052	−104		16 000
	$5s^24f^2\ J = 5$	3 059	3 113	2.0		1.4
	$5s^25p4f\ J = 2$	5 060	−60 350	−24	2200	25

E. Sn-like ions with four valence electrons

Pr^{9+} and Nd^{10+} are the ions of interest in the Sn-like isoelectronic sequence. Pr^{9+} is particularly interesting,

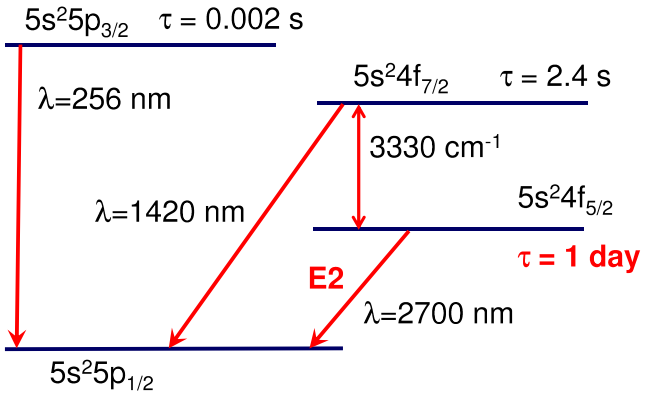

FIG. 3. Energy levels and radiative lifetimes of low-lying levels of In-like Pr^{10+}. From Safronova *et al*, 2014c.

because the lowest metastable state $J = 3[5p4f]$ is extremely long lived, with a 495 nm transition to the ground state in the optical range; see Fig. 6. The strongest allowed transition for even isotopes is $M3$, making this ion a unique system. We expect that in odd isotopes the lifetime of that level will be strongly quenched due to the hyperfine admixture of $E1$ transition. The next two levels also have optical transitions to the ground state and lifetimes of 59 and 5.3 s, respectively. In addition, there is a strong $M1$ transition to the ground state from the $^3P_1[5p^2]$ level at 351 nm that may be useful for cooling and probing. The first excited state of Nd^{10+} is so close to the ground state that the theoretical uncertainty is on the order of the transition energy. The atomic parameters are listed in Table IV. Further details are given by Safronova *et al* (2014a, 2014c).

F. Ions with holes in almost filled 4*f* shells

Berengut *et al* (2011) considered Ir^{16+} and W^{7+} ions with one hole in the $4f$ shell. The energies of the $4f^{13}5s^2$ and $4f^{14}5s$ configurations in Ir^{16+} were predicted to be sufficiently close for an optical transition. According to the CI

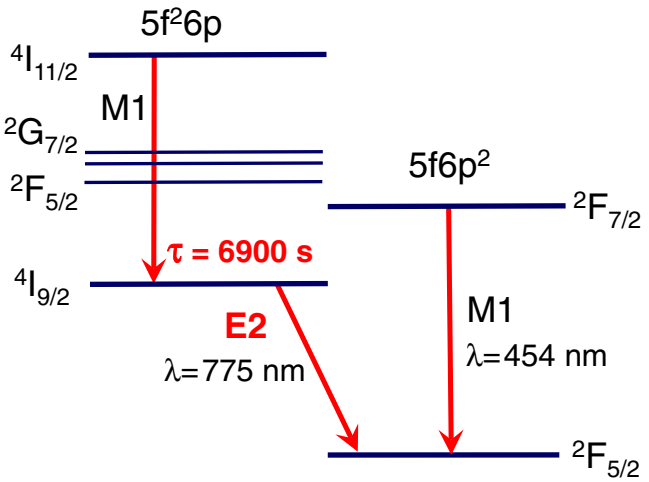

FIG. 4. Low-lying energy levels of Cf^{15+}. Leading configurations are shown on the top. $E2$ clock transitions are between the ground and first excited states.

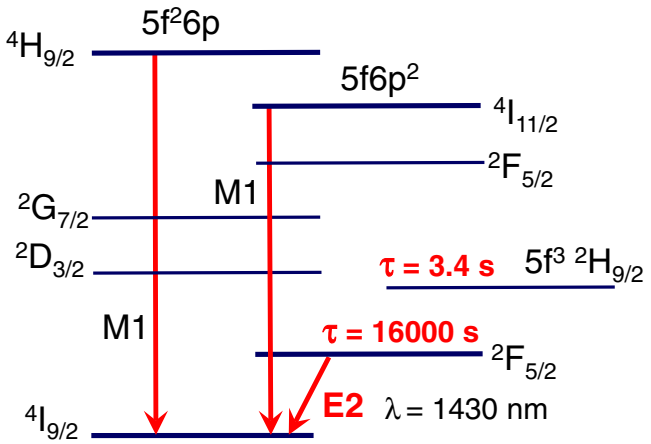

FIG. 5. Low-lying energy levels of Es^{16+}. Leading configurations are shown on the top.

calculation the Ir^{16+} ion has ground multiplet $^2F_{7/2,5/2}[4f^{13}5s^2]$ with large fine-structure splitting $\Delta_{FS} \approx 25\,900$ cm^{-1} and excited state $^2S_{1/2}[4f^{14}5s]$ roughly at 37 000 cm^{-1} (see Table V). Later these levels were recalculated within the MBPT method by Safronova, Flambaum, and Safronova (2015) and Nandy and Sahoo (2016) using the CC approach. Both calculations gave the same ground doublet and the level $^2S_{1/2}[4f^{14}5s]$ approximately at 28 000 and 38 000 cm^{-1}, respectively. All three calculations gave close values of the fine-structure splitting between 25 000 and 26 000 cm^{-1}.

A similar crossing between the one-hole configurations $4f^{13}5p^6$ and $4f^{14}5p^5$ takes place for W^{7+} (Draganič *et al*, 2003; Berengut *et al*, 2011). Theory predicts the following order of levels: $^2F_{7/2}[4f^{13}5p^6]$, $^2P_{3/2}[4f^{14}5p^5]$, $^2F_{5/2}[4f^{13}5p^6]$, and $^2P_{1/2}[4f^{14}5p^5]$. The fine splittings for two multiplets are about 18 000 and 90 000 cm^{-1}, respectively. At present only CI calculations are available and the accuracy of the theory is not sufficient to reliably predict the distance between the multiplets.

In addition to one-hole ions, Berengut *et al* (2011) also considered the two-hole systems Ir^{17+} and W^{8+}. The Ir^{17+} ion has low-lying levels of the $4f^{12}5s^2$, $4f^{13}5s$, and $4f^{14}$

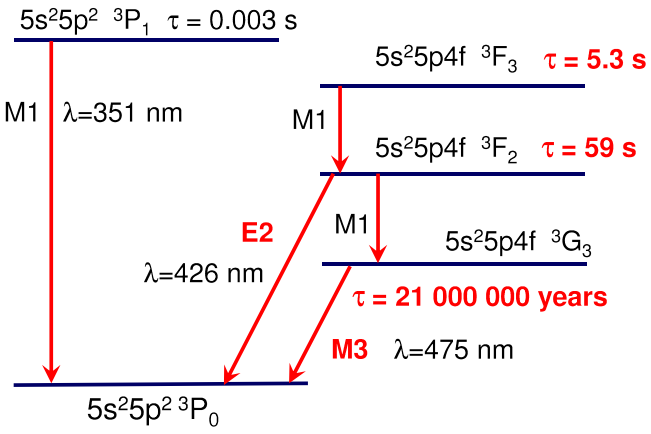

FIG. 6. Energy levels and radiative lifetimes of low-lying levels of Sn-like Pr^{9+}. From Safronova *et al*, 2014b.

configurations. Spectra of these ions are much denser and, according to the calculation, include many optical lines. However, the present theory may be rather unreliable for predicting the energy difference between different configurations. One needs to include more correlations to reduce the theoretical uncertainty. On the other hand, all such ions are particularly interesting because of the very large q factors, which determine sensitivity to α variation. For Ir^{17+} ions, spectra were recently studied by Windberger *et al* (2015), along with the isoelectronic, Nd-like sequence ions of W, Re, Os, and Pt.

Other systems with two-hole $4f^{12}$ configuration were discussed by Derevianko, Dzuba, and Flambaum (2012) and Dzuba, Derevianko, and Flambaum (2012a). They pointed out that there are always optical transitions between levels of this configuration independently on the degree of ionization, and the first excited state is always metastable. For the HCI the two holes form the relativistic configuration $4f_{7/2}^2$. The allowed total angular momenta for this configuration are $J = 6$, 4, 2, and 0. According to Hund's rules, the $J = 6$ state is the ground state and the $J = 4$ state is the first excited state. These states are connected by an electric-quadrupole transition. The configuration $5s^24f^{12}$ is the ground-state configuration for Ce-like ions ($Z = 58$) beginning from Re^{17+}. There are many ions of this type starting from Re^{17+} to U^{34+}. An analysis of the systematic shifts of transitions within this configuration by Derevianko, Dzuba, and Flambaum (2012) showed that the largest ones are caused by magnetic fields and the zero-point-energy motion of the trapped ion. The former effect can be suppressed by averaging two transitions with different signs of the projections M_J. An estimate of the latter effect is based on the observation that trapping parameters are similar to those in the Al^+/Be^+ clock, but that HCI are about 10 times heavier than Al. This mass difference leads to a suppression of the time-dilation effects for heavy HCI, assuming a similarly efficient sympathetic cooling (see Sec. VII.B). Derevianko, Dzuba, and Flambaum (2012) concluded that all investigated systematic effects may be suppressed to a fractional level of 10^{-19} by applying efficient shift-suppression schemes. We note that the transitions between the fine-structure states are generally not sensitive to α, since all such transitions have similar K factors. Deviations from the LS coupling scheme lead to small differences in sensitivity $\Delta K \ll 1$ (Kozlov, Tupitsyn, and Reimers, 2009).

The more complex Ho^{14+} ion was proposed for metrology applications by Dzuba, Flambaum, and Katori (2015). This ion has as its ground-state configuration $4f^65s$, a first excited configuration $4f^55s^2$, and a very rich optical spectrum, which includes a potential hyperfine-induced clock transition at approximately 400 nm and a strong cooling and detection transition at 260 nm. The paper includes estimates of the transition rates and lifetimes. The values are listed in Table V. However, the clock state prediction has a very large uncertainty, probably as high as 10 000 cm^{-1}. Sympathetic cooling of Ho^{14+} is discussed by Okada, Ichikawa, and Wada (2015). Their simulations show that at least ten such ions can be cooled to sub-milli-kelvin temperatures by sympathetic cooling with a single laser-cooled Be^+ ion.

TABLE V. Energies and α-variation sensitivity coefficients q relative to the ground state in cm^{-1}; $K = 2q/E$ is the enhancement factor. Wavelengths λ (in nm) for transitions to the ground states are listed. All values are from the CI calculations and are expected to have large uncertainties; see the text. Ir^{16+} and Ir^{17+} values are from Berengut *et al* (2011) and Ho^{14+} values are from Dzuba, Flambaum, and Katori (2015).

Ion	Level		Energy	q	K	λ
Ir^{16+}	$4f^{13}5s^2$	$^2F_{7/2}$	0			
	$4f^{13}5s^2$	$^2F_{5/2}$	25 898	23 652	1.8	386
	$4f^{14}5s$	$^2S_{1/2}$	37 460	367 315	20	267
Ir^{17+}	$4f^{13}5s$	$^3F_4$	0			
	$4f^{13}5s$	$^3F_3$	4 838	2 065	0.9	2067
	$4f^{13}5s$	$^3F_2$	26 272	24 183	1.8	381
	$4f^{14}$	$^1S_0$	5 055	367 161	145	1978
	$4f^{12}5s^2$	$^3H_6$	35 285	−385 367	−22	283
	$4f^{12}5s^2$	$^3F_4$	45 214	−387 086	−17	221
Ho^{14+}	$4f^65s$	$^8F_{1/2}$				
	$4f^55s^2$	$^6H_{5/2}$	23 823	−186 000	−16	420

V. EXPERIMENTAL METHODS FOR HCI STUDIES

A. Early spectral observations

Experimental observations of forbidden optical transitions in HCI have a surprisingly long history. Actually, the first detections of forbidden lines were reported in the year 1869 by Harkness and Young, who saw during a total eclipse how the solar corona emitted green light at 530 nm from an unknown and extremely light element, as it was believed. Grotrian (1939) and Edlén (1943, 1947) hypothesized the presence of highly ionized atoms in the corona having fine-structure transitions that would explain the observed lines. This implied coronal temperatures in the range of 1 MK, in contradiction with the then prevailing understanding of the Sun, and gave a first insight into the very hot universe of modern astrophysics. Diagnostics of hot astrophysical plasmas was therefore the first application of forbidden optical transitions in HCI. The first laboratory experiments had to wait until the production of such ions became feasible in a controlled way.

B. First laboratory methods

After decades of research with large devices such as theta pinches that used powerful pulsed electrical discharges to generate ions in high charge states, the sliding spark method (Feldman, Swartz, and Cohen, 1967) provided a source of comparatively small size and achieving ionization stages as high as Fe XVIII. In the 1970s, the beam-foil method (Bashkin, 1968; Berry, 1977) was introduced. It starts with moderately charged ions that are accelerated to energies in the range 100 keV–10 MeV per unit of charge and sent through a submicrometer thin foil which strips further electrons and generates HCI in highly excited states (Berry, 1977). Spectroscopic investigations were carried out by observing the trail of excited ions exiting the foil in a mostly perpendicular direction. However, with HCI moving at speeds of a few mm/ns, allowed transitions with ps and ns range

upper level lifetimes are predominantly detected, while the forbidden optical transitions with ms lifetimes do not produce sufficiently strong signals due to finite detector size. A severe handicap for precision measurements was the geometry-dependent Doppler shift, which in spite of various corrections could not be completely canceled. Another problem was the simultaneous presence of several charge states in a manifold of multiply excited configurations at the exiting channel. This hindered line identification and the assignment of electronic levels. Given those difficulties, the field achieved what was possible at that time and produced pioneering systematic spectroscopic data.

Magnetic-fusion research devices such as tokamaks provided for the first time a limited number of forbidden optical observations (Suckewer *et al*, 1982; Kaufman *et al*, 1983; Edlén, 1984; Finkenthal, Bell, and Moos, 1984). Calculations were made for identification and plasma diagnostic purposes (Feldman, Seely, and Bhatia, 1985). Again, the Doppler width and the difficult control of the plasma composition and conditions hindered dedicated high-resolution studies. More recently, the analysis of Zeeman splitting and polarization of visible transitions has also been reported (Iwamae *et al*, 2007). Spectroscopy in general, and forbidden transitions, in particular, offer opportunities for temperature and density diagnostics in magnetic-fusion plasmas (Beiersdorfer, 2015).

C. Early laboratory sources of HCI

The development of stationary HCI sources solved most of those problems and made HCI more easily accessible to experimentalists. Among those, electron-cyclotron resonance ion sources (ECRIS) (Geller, 1970; Briand *et al*, 1975; Bechtold *et al*, 1980) based on the electron heating of a thin plasma by powerful microwaves in a magnetic bottle yielded microampere beams of HCI in moderate charge states, typically used to load accelerators. Optical access to the plasma volume was constrained by the bulky and complicated magnetic structures surrounding it. As for the charge states of HCI produced in ECRIS, they have typically been limited to $q < 28+$ by the plasma conditions. Nonetheless, it was a flexible source and this was soon recognized. One of the first examples of optical spectroscopy was the observation by Prior (1987) of fine-structure transitions in ions with open p and d subshells by using beams from an ECRIS at the Lawrence Berkeley Laboratory. The very intense currents of HCI available there (tens of microamperes) made it possible to observe the decay of a small fraction of the metastable ions passing in front of a spectrometer equipped with a position-sensitive microchannel plate detector. In this way, intraconfiguration fine-structure transitions from F-like ions (Ar^{9+}, K^{10+}, and Ca^{11+}), O-like ions (K^{11+} and Ca^{12+}), and B-like ions (Ar^{13+} and K^{14+}) were measured. The transitions $3d^9\,{}^2D_{5/2\to3/2}$ in Nb^{14+}, $3d\,{}^3D_{4\to3}$ as well as the $3d^8\,{}^3F_{2\to3}$ in Nb^{15+}, and the $3d^7\,{}^4F_{9/2\to7/2}$ in Nb^{16+} were also investigated. Spectral resolution and wavelength accuracy were both instrumentally and methodologically limited to a level of 0.1%.

Another step in the direction of higher charge states and better control was the introduction of electron-beam ion sources (EBIS) by Arianer *et al* (1975), Arianer and Goldstein (1976), Donets (1967, 1985, 1990), and Donets and Pikin (1975). An intense, narrow electron beam was generated through magnetic compression that compensated the mutual repulsion of the electrons in the beam. This development owed much to radar technology, which had made use of such beams to generate microwaves. Accumulation of multiply charged ions inside the electron-beam space-charge distribution was recognized as a factor for the beam neutralization. Unfortunately, due to technical difficulties, spectroscopy on EBIS devices was not strongly pursued although a few cases of in-source x-ray spectroscopy (Ali *et al*, 1990, 1991) were reported.

D. Production of HCI with electron-beam ion traps

It was recognized that ion heating by electron-beam instabilities was hindering the production of the highest charge states in EBIS devices (Levine, Marrs, and Schmieder, 1985). Correcting this problem, the decisive invention of the EBIT by Levine *et al* (1988, 1989), Penetrante *et al* (1992), and Marrs, Beiersdorfer, and Schneider (1994) at the Lawrence Livermore National Laboratory (LLNL) prepared the field for many long ranging developments. To mention some examples, see investigations of QED effects in x-ray emission spectra (Beiersdorfer *et al*, 1993, 1995, 1998, 2005), studies of the dielectronic-recombination process (Knapp *et al*, 1989; Beiersdorfer *et al*, 1992; Watanabe *et al*, 2007) and quantum interference in photorecombination processes (Knapp *et al*, 1995; González Martínez *et al*, 2005; Nakamura *et al*, 2009), nuclear-size determinations (Elliott, Beiersdorfer, and Chen, 1996), lifetime measurements of forbidden transitions (Wargelin, Beiersdorfer, and Kahn, 1993; Crespo López-Urrutia, Beiersdorfer, Savin, and Widmann, 1998; Crespo López-Urrutia, Beiersdorfer, and Widmann, 2006), laser spectroscopy of the $2s - 2p$ He-like transitions (Hosaka *et al*, 2004), charge exchange (Beiersdorfer *et al*, 2000, 2003; Wargelin *et al*, 2005; Otranto, Olson, and Beiersdorfer, 2006; Allen *et al*, 2007), plasma-polarization spectroscopy (Beiersdorfer, Crespo López-Urrutia *et al*, 1997; Shlyaptseva *et al*, 1997, 1998; Nakamura *et al*, 2001; Amaro *et al*, 2017; Shah *et al*, 2018), effects of Breit interaction in x-ray emission (Hu *et al*, 2012), soft x-ray laser spectroscopy (Epp *et al*, 2007; Bernitt *et al*, 2012), photoionization of HCI with soft x rays (Simon *et al*, 2010a), and mass spectroscopy (Ettenauer *et al*, 2011), as well as in-trap nuclear spectroscopy of radioactive isotopes (Lennarz *et al*, 2014).

Differences between EBIS and EBIT are small, but in some aspects decisive. In an EBIT, the interaction region with maximum magnetic field is generally shorter than in an EBIS. This seems to reduce in an EBIT the growth of electron-beam instabilities and also allow for higher electron-beam compression and, thus, charge density. Both effects, high current density and beam stability, speed up the ionization process. Furthermore, evaporative cooling from the trap region is easier to realize in short traps than in an EBIS, with its long interaction region. The most visible difference is the presence of viewing ports giving optical access to the center of the trap in EBITs, which were designed as spectroscopic sources.

Application of spectroscopic diagnostics to the trap paved the way to a detailed understanding of the time-dependent processes inside the trap, and, consequently, to the physics of HCI. EBIS, in contrast, were primarily conceived as ion sources for accelerators. Diagnostics are typically based on the ion yield after extraction for the accelerators essential figure of merit. However, the approach to studying the ionization process without photon information misses an important part of the information that spectroscopy can provide.

EBITs, for reasons we will see, became true spectroscopy workhorses and produced an enormous scientific harvest. Experimentally, production of HCI in more or less arbitrary charge states is now routinely performed with EBITs, and therefore several groups worldwide started utilizing such devices (Silver *et al*, 1994; Gillaspy *et al*, 1995; Currell *et al*, 1996; Biedermann *et al*, 1997; Nakamura *et al*, 1997; Crespo López-Urrutia *et al*, 1999; Ovsyannikov and Zschornack, 1999; Watanabe and Currell, 2004; Dilling *et al*, 2006; Böhm *et al*, 2007; Fu *et al*, 2010; Xiao *et al*, 2012; Takacs *et al*, 2015). In view of their apparent advantages and of the large body of experimental results, in the following we will focus on the uses of the versatile EBITs.

1. Ionization and trapping mechanism

The principle of operation in both EBIS and EBIT is the interaction of an intense (mA to A), strongly focused electron beam with atoms and their ions [for more details see, e.g., Beyer, Kluge, and Shevelko (1997), Gillaspy (2001), and Currell and Fussmann (2005)], as sketched in Fig. 7.

Ionization of neutral atoms injected as dilute atomic or molecular beams crossing it yields first singly charged positive ions which stay trapped by, and mostly within, the negative space-charge potential of the beam. This parameter has its strongest gradient at the beam edge. Between that point and the beam central axis at tens of micrometers from it a potential difference of tens of volts appears. From the point of view of a neutral injected from a room-temperature atomic beam with a kinetic energy of 25 meV, ionization to the first charge state within the beam means the sudden appearance of 1000 times stronger trapping potential. This results in instantaneous trapping of the ions produced. Subsequent beam-ion interactions raise the charge state until the physical limit is reached, namely, when the binding energy of the remaining bound electrons is higher than the electron-beam energy. Electron-beam energies in the range 40 eV to 200 keV have been used for preparing and studying ions ranging from N^{3+} (Simon *et al*, 2010b) up to U^{92+} (Marrs, Elliott, and Knapp, 1994) with EBITs. Recombination of the HCI is reduced by having an excellent vacuum, suppressing charge exchange with residual gas. Efficient ionization takes place at energies well above the pertinent thresholds, but the long trapping times (seconds to hours) allow compensation for the small electron-impact ionization cross sections close to threshold.

2. Photorecombination and charge-exchange processes

Acting in the opposite direction, photorecombination of free beam electrons with the HCI under emission of a photon [the so-called radiative recombination (RR)] is rather weak for ions in relatively low charge states, but becomes intrinsically strong for ions with open L and K shells, in particular, if the charge state is also very high. This process, RR, is akin to time-reversed photoionization. Another one is dielectronic photorecombination involving the resonant excitation of an inner-shell electron during the capture process and the subsequent relaxation of this intermediate state through photon emission. It is extremely effective at certain discrete energies with several orders of magnitude larger cross sections. While it affects typically only one charge state at each beam energy, its total contribution can be several times larger than that of RR with thermal electron distribution functions. Charge exchange is the process by which HCI capture electrons from residual gas neutrals by overcoming their ionization potential in collisions at the range of several atomic units. The cross sections for this are rather large (on the order of 10^{-14} cm^2) and therefore an excellent ultrahigh vacuum (UHV) is typically needed to store HCI. The charge-state distribution found in an EBIT is, in general, ruled by a set of coupled rate equations (Penetrante, Bardsley, DeWitt *et al*, 1991; Penetrante *et al*, 1992) containing all those ionizing and recombining terms. Under normal conditions it is comprised of only a few charge states, and it can be optimized to contain a rather dominant ionic species.

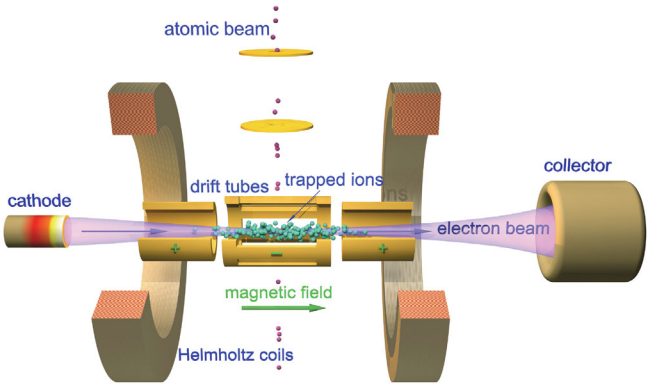

FIG. 7. Schematic depiction of an EBIT (Levine *et al*, 1988, 1989). A zone of high electron density (with values up to $10^{13} e^-/\text{cm}^3$ and a diameter of less than 0.1 mm) is formed in the central region of the ultrahigh vacuum device by the interaction of a magnetic field of typically a few T with an electron beam (up to 1 A) emitted from a cathode of a few mm diameter. The negative space-charge potential of this charge distribution is capable of radially trapping positive ions. Axial confinement along the beam propagation direction is achieved by an ensemble of adequately biased, hollow cylindrical electrodes (drift tubes) arranged along the beam axis. Production of positive ions is driven by electron-impact ionization resulting from the beam interaction with injected atomic species (e.g., an atomic beam). A rather narrow distribution of charge states can be reached of which the highest value depends on the electron-beam energy. Because of their high ionization rate, strong electrostatic confinement as well as am efficiently suppressed ion-recombination rate, EBITs can quickly generate and trap ions in charge states up to U^{92+} (Marrs, Elliott, and Knapp, 1994) and retain them for periods of time on the order of hours.

3. Electron-impact excitation of transitions

An invaluable advantage of an EBIT is the fact that the electron beam also copiously excites the trapped HCI. This together with the convenient geometry giving radial optical access to the trap region at a few-centimeters distance allows for spectroscopic observations in all spectral ranges. The space-charge potential forms a narrow (50 to 500 μm), few-centimeters long cylindrical ion cloud which can readily be imaged onto the entrance slit of a spectrograph. In some experiments, the narrow ion cloud acts as the entrance slit of the spectrograph. The radiation emitted by the ions is then collimated, dispersed by a grating or crystal, and focused onto the spectrograph focal plane. In this type of configuration the intensity of the spectral line on the focal plane is higher than in the cases where an intermediate image on a real entrance slit is used for two reasons, since less lossy optical components are needed. However, the absence of a real entrance slit imposes a lower limit on the experimentally observable line width, and therefore also in the achievable spectral resolution.

Within the ion cloud, the density of HCI grows in time (Blessenohl *et al*, 2018; Micke *et al*, 2018) due to electron-impact ionization up to values that typically compensate a sizable fraction (10% to 90%) of the total negative space charge generated by the electron beam. This final ion density is dependent on the applied axial trapping potential and the ion-evaporative cooling regime that is used for the trap. Taking into account the range of possible charge states, this implies HCI densities from 10^9 to $10^{12}/\mathrm{cm}^3$, surrounding or immersed in a negative space charge of up to $10^{13}/\mathrm{cm}^3$ electrons. Since, depending on their translational temperature and charge state, the HCI may follow orbits with maximum distances from the trap axis up to 0.3 mm, their time-integrated overlap with the electron beam can be substantially reduced. This lowers the effective electron density governing the excitation rate. Thereby, the effective electron density can become 100 times lower than the actual electron density of the beam (Liang *et al*, 2009).

The total HCI count in charge states of interest can be from only a few (e.g., for the "ultimate" U^{92+}) to hundreds of millions, with experiments covering the whole range. Appropriately designed experiments have been running with count rates of only tens of counts per hour for both visible or x-ray photons, but under favorable conditions tens of thousands of counts per second have been achieved.

Because of the stability of normal EBIT operations, the more time-consuming measurements can be run for days and weeks with little intervention needed.

4. Preparation of neutrals for ionization and trapping

In practical terms, the ions from a certain chemical element to be studied have to be generated starting from atoms or molecules containing them. Several methods are available for the initial loading of the trap. This choice of method somewhat determines the charge-state distribution, as described next.

The ionization processes that govern the time evolution of the system can be described by coupled differential rate equations including ionization and recombination terms. An additional source term has to be considered if a steady-state atomic beam is used. This is normally the case if light elements have to investigated, since their losses are higher than for heavy elements. This results from the lower maximal charge state they can naturally reach, as given by their Z, and by the much stronger trapping experienced by heavy elements. In particular, barium ($Z = 56$), that emanates from the heated cathode, shows a tendency to accumulate in the trap axis within a time scale of typically 30 s, thereby expelling lighter ions. This contamination imposes the application of a regular trap-dumping step on a similar time scale when light ions are to be studied. Every time the HCI inventory of the trap is dumped, the filling and ionization starts anew.

If neutral atoms are not constantly injected but introduced in a pulsed mode, the charge-state evolution is more homogeneous than in the first case and yields a narrower charge-state distribution. This is for instance the case if one chooses a starting population of singly charged ions injected along the magnetic field axis.

Heavy elements are more easily accumulated than light ones, and evaporative cooling makes longer trapping times possible with them. Therefore, the injection rate can be very low, since ion losses are very small. In principle, this would favor the appearance of a narrow charge-state distribution. On the other side, very high charge states in heavy ions show an enhanced radiative recombination rate ($\propto Z^4$), which counteracts the ionization term and broadens the distribution. In the case of a very heavy HCI such as U^{92+}, the charge-state distribution reached at 190 keV may encompass U^{86+} to U^{92+} with its maximum at $q = 88$ (Marrs, Elliott, and Knapp, 1994), a small fraction in the hydrogenlike state, and a very small one in the bare state. In moderate charge states, recombination processes are weaker and the charge-state distribution becomes narrower than in the aforementioned case and can easily be made to peak at the charge state of interest. This is the case for most of the ions in the context of the present review.

Concerning the choice of chemical elements, there is no limitation in sight. EBIT operation has been reported for basically all types of gaseous and solid stable elements, and radioactive isotopes have also been studied with them. A common and convenient approach is the use of gases or volatile compounds containing heavier elements. Very low vapor pressure, such as organometallic substances at the rate of micrograms per day, have been extensively used to produce molecular beams for injection into the EBIT (Watanabe *et al*, 2001). External ion injection from laser-ion sources (Niles *et al*, 2006; Trinczek *et al*, 2006), oven-based Knudsen cells (Yamada *et al*, 2007), and vacuum-discharge sources (Brown *et al*, 1986) has also been reported.

Quantities of atoms needed to feed an EBIT are truly microscopic: operation with nanogram (and even picogram) probes electrochemically coated on needles positioned close to the electron beam was reported for HCI such as $^{233,235}U^{88+}$ and $^{248}Cf^{96+}$ (Elliott and Marrs, 1995; Elliott, Beiersdorfer, and Chen, 1996; Beiersdorfer, Elliott *et al*, 1997).

More recently, direct injection of radioactive isotopes produced online by accelerators, and with lifetimes in the millisecond range, has also been reported. The experimental cycle lasting only a fraction of a second involved the extraction of the isotope from the target, generation of a beam of singly

charged ions, transfer into an EBIT, and ionizing it (so-called "charge breeding" in the accelerator community) there to an HCI state, extraction from the EBIT, and transfer to a Penning trap (Dilling *et al*, 2006). There precision atomic mass measurements were carried out taking advantage of the increased precision that can be afforded by the linear scaling of the cyclotron frequency with the HCI charge. At higher charge values, the same experimental accuracy in the determination of the cyclotron frequency and thus of the ion mass can be achieved in a shorter time. This is particularly important if the radioactive decay of the species of interest is very fast. Other experiments involved fundamental studies of β decay and bound-internal conversion processes (Ettenauer *et al*, 2011; Lennarz *et al*, 2014) in charge states relevant for nucleosynthesis in stellar and supernova environments. In general, these methods have considerably expanded the range of isotopes which can be made available for future optical clocks and precision atomic physics experiments.

5. Techniques for HCI delivery

Since HCI production in general relies on energetic interactions between neutral atoms and electrons inside a trap or source, the kinetic energy distribution of the ions, as parametrized by their translational temperature, is rather inappropriate for precision laser-spectroscopic measurements. Therefore, if HCI are needed for this type of experiments, a cooling method capable of lowering the HCI temperature from the MK range down to at least the mK and μK regime of modern laser spectroscopy.

To achieve this, methods for their transfer to, and retrapping in, Penning or radio-frequency Paul traps for their further cooling and study had to be developed. As with other sources of ions, HCI are delivered to other experiments by means of vacuum beam lines using electrostatic and magnetic guiding fields generated by appropriate electrodes and magnets. The key limitation is the very small production rate, resulting from the combined effect of minute ionization cross sections and the need to stepwise pass through many successive charge states. Typical HCI currents from EBITs are therefore in the range from pA to fA for individual charge states in a steady-extraction mode; bunches of 10^2 to 10^7 HCI are standard in the pulsed mode (Gillaspy, 2001; Currell, 2003; Blessenohl *et al*, 2018; Micke *et al*, 2018).

One example of the use of extracted HCI was the investigation of their collisions with surfaces. The mechanisms for the fast HCI-charge neutralization upon surface impact, with the possible formation of "hollow atoms" (Winter and Aumayr, 1999) in which the inner shells were not fully occupied, attracted considerable interest and were the subject of detailed studies. McDonald *et al* (1992) and Aumayr *et al* (1993) investigated the electron yields caused by the impact of slow HCI on clean surfaces (of up to 280 electrons per ion) using EBIT-extracted $^{136}Xe^{21+\cdots51+}$ and $^{232}Th^{51+\cdots80+}$ ions. Recently, similar experiments using graphene targets have identified the essential contribution of interatomic Coulomb decay (Wilhelm *et al*, 2017) to the femtosecond-scale neutralization and deexcitation of HCI in such collisions.

Collisions of HCI with neutral atoms at energies in the keV regime are dominated by the transfer of electrons from the neutral target to the HCI. This electronic charge-exchange process was also studied using HCI beams extracted from EBITs for ions ranging from $Ar^{16+\cdots18+}$ to U^{88+} (Schneider *et al*, 1994; Otranto, Olson, and Beiersdorfer, 2006; Allen *et al*, 2007; Xue *et al*, 2014). Furthermore, charge exchange with residual gas within an ion source leads to HCI losses, and thus ultrahigh vacuum levels ($< 10^{-9}$ mbar) are required both within the whole apparatus and beam line.

Because of the fact that translational temperature and spatial distribution of the ions at the source (usually parametrized in accelerator physics using the so-called emittance in units of mm mrad) can severely reduce the efficiency of the beam line transmission, ion transport is usually performed by applying accelerating potentials on the order of tens of kilovolts. And ion optics elements such as einzel lenses as well as electrostatic or magnetic quadrupoles are introduced at several places in order to refocus the divergent ion beam and keep it from hitting the guiding elements and vacuum chamber.

Buffer-gas precooling of ions, sometimes applied to improve the emittance of ion sources, is prohibited with HCI due to charge-exchange induced losses. However, in spite of the high temperature of the HCI at the beginning (on the order of MK), EBIS and EBIT show rather good emittance parameters (a few mm mrad), since the ions are produced in a small volume with a well-defined, strong magnetic field. A small source volume in ion optics allows for the formation of well-collimated ion beams. After extraction from the source, the magnetic field adiabatically drops to much lower values, and this transforms most of the radial component of the thermal motion inside the ion source into longitudinal momentum. This is favorable for the ion transport through long beam lines.

Since the yield available from HCI sources is small by comparison with that of other atomic species, various techniques were proposed in order to optimize the production of cold HCI, e.g., mixing HCI with cold electrons (Poth *et al*, 1991; Quint *et al*, 2001; Beier *et al*, 2005; Kluge *et al*, 2008) or evaporative cooling from a bunch of HCI oscillating inside a Penning trap (Hobein *et al*, 2011).

One method successfully applied to HCI is pulsed extraction from an EBIT followed by phase-space cooling of the formed ion bunch by application of a position-dependent, sudden electric pulse (Schmöger, Schwarz *et al*, 2015) to the HCI bunch as it moves through a hollow electrode in which a linearly growing potential is established. Under typical conditions, the HCI bunch extracted from a +700 V potential shows an energy spread of 11 to 25 eV per unit of charge Q. A single charge state is selected based on the time of flight to the pulsed buncher, which is on the order of 10 μs and shows a spread of roughly 150 ns. Hence, faster ions reach farther and higher into this positive-potential ramp than slow ones. When the bunch resides within the electrode, the potential ramp is switched off within tens of ns. In this way, more kinetic energy is removed from the faster ions than the slower ones, and an additional time-focusing effect can be conveniently achieved. The HCI leave the pulsed buncher with a kinetic energy of approximately $130 \times q$ eV and a reduced energy spread of $\leq 7 \times q$ eV. With this procedure, the loading efficiency into the rf trap is increased by a factor of 50 (Schmöger, Schwarz *et al*, 2015).

Then, the by now shorter and more velocity-homogeneous bunches overcome a dc potential barrier of nearly 130 V that removes most of their kinetic energy, before entering through a switchable ring electrode to the rf quadrupole electrode structure of the trap. This guides the HCI over a length of several cm toward a second ring electrode acting as an electrostatic mirror at the rear end of the quadrupole structure. Given that the HCI bunch now moves more slowly, the entrance electrode of the rf quadrupole can be readily switched to a high positive potential before HCI reflected from the mirror electrode on the other end of the trap return. Therefore, the bunch cannot leave the rf quadrupole and performs a linear oscillatory motion back and forth along its axis.

These steps are complemented with a dissipative process that removes kinetic energy from the oscillating HCI. For this purpose, a continuously laser-cooled ensemble of other ions is prepared within the rf quadrupole (Schmöger, Schwarz *et al*, 2015), thereby providing stopping power at the beginning, and sympathetic cooling at the end of the procedure as discussed in more detail in Sec. VI.B.

E. Optical spectroscopy of HCI

1. Measurements of the HFS of hydrogenic ions

As mentioned, an important boost to the field of optical spectroscopy with HCI occurred as both ion storage rings (Klaft *et al*, 1994; Seelig *et al*, 1998) and EBITs (Crespo López-Urrutia *et al*, 1996; Crespo López-Urrutia, Beiersdorfer, Widmann *et al*, 1998; Beiersdorfer *et al*, 2001) reported HFS measurements in hydrogenlike ions of heavy elements. It was clear that scaling laws would shift the 21 cm microwave transition of atomic hydrogen into the optical region and reduce its enormous 11×10^6 yr lifetime to milliseconds. At the same time, relativistic, QED (Persson *et al*, 1996), and nuclear-size effects were boosted to the level of 50%, 10%, and 0.5% of the total ground-state hyperfine transition energy (Shabaev, 1993, 1994), respectively. As detailed in Sec. III.B, tests of QED in strong fields were the main interest of the community, and theoretical work aimed at separating and distinguishing the various contributions from two-loop QED, nuclear-recoil effects, and nuclear magnetization distribution in the measured transitions from each other.

Lacking sufficient accuracy, models of nuclear magnetization were deemed far more uncertain than the dominant first-order QED contributions, thus leading to the application of the HFS data to determining nuclear magnetic radii (Crespo López-Urrutia, Beiersdorfer, Widmann *et al*, 1998; Beiersdorfer *et al*, 2001).

2. Other optical spectroscopic observations

A parallel development was the study of specific transitions in Ti-like ions [starting with Ba^{34+} using optical spectrometers in the work of the NIST EBIT group (Morgan *et al*, 1995; Porto, Kink, and Gillaspy, 2000)] that showed an interesting behavior, namely, a slowly varying wavelength as a function of the nuclear charge along that isoelectronic sequence. This was later also studied by other groups (Utter, Beiersdorfer, and Brown, 2000; Watanabe *et al*, 2001), namely, the very weak dependence of their wavelengths on the atomic number Z and thus the charge state of the ion. The reason for this is a competition of relativistic and correlation effects that results in a near cancellation of the otherwise very strong scaling of forbidden transitions to high photon energies with Z.

Further exploratory experiments showed the existence of many forbidden optical transitions which could be observed in emission with an EBIT (Bieber *et al*, 1997; Serpa, Bell *et al*, 1997).

With increased wavelength resolution resulting from reduced slit widths, lower HCI temperatures, and concomitantly smaller Doppler broadening, and larger spectral dispersion instrumentation, optical measurements in the EBIT at Freiburg University in Germany (later moved to MPIK in Heidelberg) became sensitive to QED contributions, relativistic nuclear-recoil effects, and the Zeeman structure of forbidden lines (Draganič *et al*, 2003; Soria Orts *et al*, 2006, 2007).

In order to exploit these results, more and more sophisticated calculations were produced (Tupitsyn *et al*, 2003; Artemyev *et al*, 2007). Lifetimes of the metastable levels from which the optical transitions arise were measured (Serpa, Morgan *et al*, 1997; Träbert, 2002, 2008), reaching accuracies at the 1% level (Brenner *et al*, 2007, 2009) and beyond, whereas QED contributions from the electron anomalous magnetic moment could be resolved (Lapierre *et al*, 2005, 2006).

F. Electronic structure determination in HCI

Since most of the ions of interest have never been investigated, thorough theoretical and experimental studies of their electronic structure will be required for clarifying the actual electronic structure and identifying the transitions of interest. Ritz-Rydberg analysis of optical transitions has been used for the ground-state configuration of HCI in a few cases (Windberger *et al*, 2016; Torretti *et al*, 2017) and has helped in clarifying the physics of EUV radiation sources for nanolithography, which are based on laser-produced plasmas containing tin HCI (Harilal *et al*, 2006; O'Sullivan *et al*, 2015).

Typically, optical measurements in an EBIT are carried out with the help of grating spectrometers, since the high temperature of trapped HCI does not support a spectroscopic resolving power $E/\Delta E \geq 30\,000$. One example of such a measurement is shown in Fig. 8. A few measurements have been carried out by means of laser spectroscopy both in storage rings and, as proposed initially by Back *et al* (1998), in EBITs by Mäckel *et al* (2011) and Schnorr *et al* (2013). Both types of experiments suffer from the wide velocity distribution of the storage ring (at the level of $E/\Delta E \leq 10\,000$) and the aforementioned translational temperature inside EBITs ($E/\Delta E \leq 30\,000$). There have also been experiments using free-electron lasers and synchrotrons in combination with EBITs. These studies have progressively expanded the field of laser spectroscopy into the EUV and soft x-ray (Epp *et al*, 2007; Bernitt *et al*, 2012) and x-ray regions (Rudolph *et al*, 2013, Epp *et al*, 2015), however with the aforementioned limitations in spectral resolution.

G. Compact EBITs for novel spectroscopic applications

Laser spectroscopy, metrology, and quantum computational studies with trapped ions are most frequently based on the

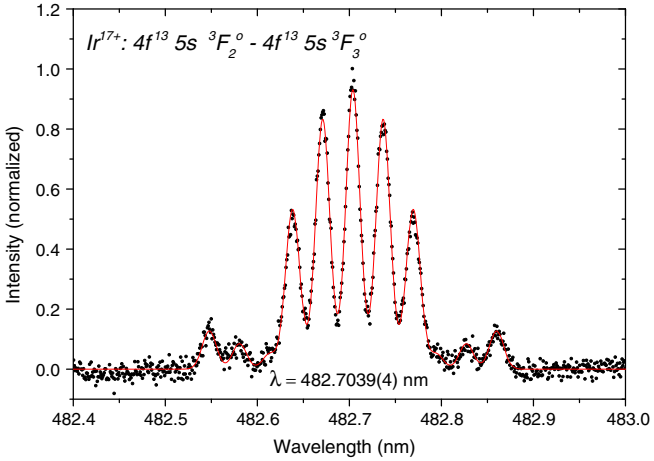

FIG. 8. Line profile of an optical transition within the $4f^{13}5s$ configuration of Ir^{17+} ion obtained at the Heidelberg EBIT. The Zeeman splitting due to the 8-T magnetic field of the trap is clearly visible. From Bekker, 2017.

in-trap production of the ions using electron-impact ionization or photoionization of atoms. Less often, ions are brought into the system from an external source by means of an ion transfer beam line. The first approach offers a more compact setup but can cause certain problems of electrode contamination which may constitute a hindrance for long-term stability in metrological work. The second option, the generation of ions in a separate setup, is more complex but has advantages: more versatility in terms of the types of ions available and lesser contamination of trap electrodes and optics by the atomic sources. In principle, HCI would be more amenable to this latter approach, although one could conceive both electron-beam ionization [as in, e.g., Schabinger *et al* (2012)] and pulsed-laser based production schemes for moderately charged ions working within the trap chamber. The most convenient approach, however, is to separate production and spectroscopy while maintaining an overall compact envelope for the whole apparatus.

In general, easy availability of HCI is a prerequisite for their investigation. Production of HCI in accelerator facilities will still remain restricted to a few groups worldwide. A widespread application of HCI to atomic physics research and metrology calls for small and compact sources with minimal setup and maintenance costs and simple and reliable operation. There exist already a number of publications on small HCI sources which can be set up with moderate resources and effort within a student project or purchased from a commercial provider.

Most of the spectroscopic and HCI-interaction experiments mentioned were based on rather powerful cryogenic EBITs using superconducting magnets. Although far smaller than accelerator-based HCI research devices, they still need a dedicated laboratory room and a scientific team for operation. During the last decades several groups have been working on the development of more compact, and economic, systems.

The first EBIS based on permanent magnets (Khodja and Briand, 1997) were followed by other "warm-type" instruments not requiring superconducting magnets at cryogenic temperatures. The Tokyo group built an EBIT based on permanent magnets (Motohashi *et al*, 2000) for spectroscopic studies. Others followed (Kentsch *et al*, 2002; Nakamura *et al*, 2004, 2008; Sakaue *et al*, 2009; Xiao *et al*, 2012; Takacs *et al*, 2015). They can generate and trap ions having ionization potentials of a few keV that will allow one to reach charge states up to 60+ for heavy elements. Currently, such devices have typically a total footprint of one square meter and operate unattended for extended periods of time both as sources of ions or for spectroscopic observation.

At NIST, HCI have been extracted from the EBIT and injected into compact Penning traps (Brewer, Guise, and Tan, 2013) of a small footprint, where Rydberg states of the HCI shall be prepared for laser spectroscopy. These experiments start with mass selected HCI pulses from the EBIT, extracted at energies of up to $4 \times 10^3 \times q$ eV, with q being the charge of the HCI. The Penning trap captured a significant fraction (up to several thousand) of those ions in a potential well of $(4–12) \times q$ eV by opening and closing the axial trapping potential. This captured fraction has a selected, narrower kinetic energy distribution (FWHM $\approx 5.5 \times$ q eV) than the HCI both inside the EBIT and in the extracted bunch. Other experiments performed there with extracted ions have aimed at measuring the lifetime of the Kr XVIII $3d\ ^2D_{5/2}$ metastable state (Guise *et al*, 2014). A compact EBIT under construction will be used as a HCI source (Hoogerheide and Tan, 2015) in combination with the compact Penning trap.

Other compact devices based on the electron-beam ionization and trapping by the negative space charge have recently appeared. A strong pointlike magnetic focus generates HCI in charge states as high as Ir^{55+} in a compact and simple device developed by Ovsyannikov and Nefiodov (2016a, 2016b) with an overall dimension of less than $0.2 \times 0.2 \times 0.2$ m^3 volume, for which HCI extraction in the radial direction was also demonstrated.

For the operation of electron beams at lower energies of less than 1 keV suitable for the production of HCI predominantly

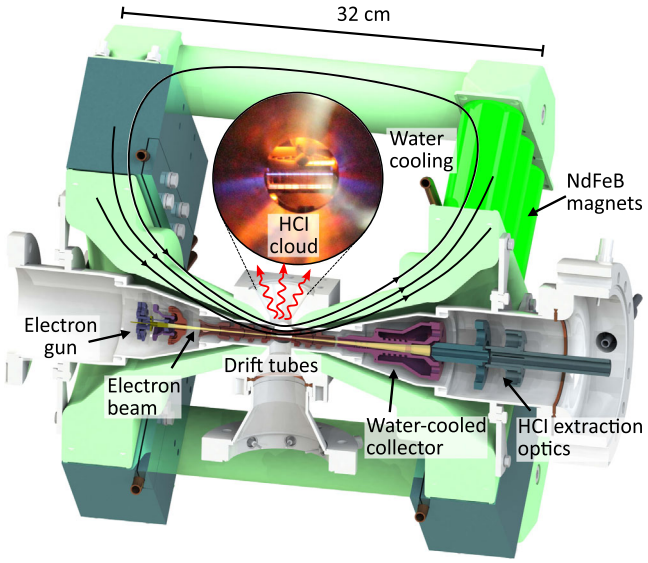

FIG. 9. Design of the compact EBIT operating at PTB for the dedicated production of HCI in an optical clock experiment. The inset shows light emission induced by electron-impact excitation of the trapped ions. From Micke *et al*, 2018.

in charge states with many optical transitions, and moreover offering good ion beam properties, special care has to be taken in the field design. Recently, novel EBITs using permanent magnets, schematically shown in Fig. 9, have reached magnetic field strengths of 0.86 T and demonstrated excellent electron-beam energy resolution for x-ray studies, ion extraction, and optical spectroscopy (Micke *et al*, 2018). One of these devices was recently installed at the German metrology institute Physikalisch-Technische Bundesanstalt (PTB) to operate an optical clock based on HCI. The magnetic cage of the EBIT has dimensions of $0.3 \times 0.3 \times 0.3$ m^3. It surrounds a vacuum system that is attached to a transport and deceleration beam line and has an overall area of approximately 1 m^2. It operates at UHV conditions suitable for its connection with a cryogenic rf trap, CryPTEx-PTB (Peter Micke *et al*, 2018) based on the CryPTEx design (Schwarz *et al*, 2012) in which very long HCI storage times will be required for optical clock applications.

One can expect that the rapid development in this field will probably bring even smaller EBIS and EBITs to the market and substantially reduce the barrier for the use of HCI in the laser spectroscopy community.

VI. PREPARATION OF COLD HIGHLY CHARGED IONS

A. Evaporative cooling of HCI

A key element for the success of spectroscopy experiments in EBITs was the very early introduction of evaporative cooling to their operation. The first proposal, modeling, and realization of this technique by Penetrante at LLNL in 1990 (Penetrante, Bardsley, DeWitt *et al*, 1991; Penetrante, Bardsley, Levine *et al*, 1991; Schneider *et al*, 1991; Marrs, Elliott, and Knapp, 1994; Marrs, 1999) preceded its application to Bose-Einstein condensates. There was an understanding that electron-ion collisions in the deep potential well caused by the negative space charge would lead to heating of the HCI and to their eventual loss. Therefore, a cooling mechanism would be needed to keep the ions inside the trap for a long time. This was found in taking advantage of the fact that HCI from lighter elements could not reach the high charge states of cotrapped heavier elements. Ion-ion collision rates are extremely enhanced between HCI as the product of the squares of the individual colliding charges. Efficient thermalization across ion species thus redistributes energy from the heavier ions, subject to the strongest electron-impact heating, and the lighter ones.

The relevant trapping parameter is the product of the charge state Q (on the order of $Q \sim 20$) times the potential difference between the trap center and its edge ($\Delta V \approx 50$ V). This gives a trap depth of $\Delta V \times Q \approx 1000$ eV, corresponding to a "temperature" of 12 MK. Therefore, light HCI with lower absolute charge states (say, Ne^{10+}) experience a shallow potential well (here of about 200 eV), while sharing a common temperature with the much more deeply trapped heavier ones reaching far higher charge states under the same electron-beam energy conditions (for example, Ba^{46+} would experience a trapping potential of 920 eV in the present example). As a consequence, lighter ions in the hot tail of the thermal distribution preferably escape from the trap. Thereby, each evaporating ion in charge state Q removes from the thermal ensemble left behind an energy equivalent to the individual trapping potential, i.e., $\Delta V \times Q$. A rough estimate of a typical heating rate for a single heavy HCI (Ba^{46+}) yields that the EBIT electron beam transfers a thermal energy of the order of 100 eV/s through collisions. This heating rate can easily be compensated by the evaporation of a light HCI from the ion ensemble every couple of seconds. A steady supply of light atoms, e.g., from an atomic beam to the trap center, will result successively in their ionization, thermalization, and evaporation, accomplishing an efficient removal of the heat constantly generated by the elastic collisions of electrons from the beam with trapped HCI.

Evaporative cooling was the key to achieve in principle unlimited trapping times for HCI from heavy elements, which are at the same time those really needing long storage times for reaching the highest charge states. In principle, evaporative cooling also works without the need of a mixture of elements. Regulation of evaporative cooling is rather unproblematic: The potential barrier which has to be overcome can be tuned by varying the electrostatic potential applied to one of the cylinder-shaped electrodes or drift tubes in the EBIT. The use of the magnetic trapping mode (Beiersdorfer, Schweikhard *et al*, 1996), in which the electron beam is turned off but the HCI remain trapped in the resulting Penning trap, was also combined with evaporative cooling for in-trap laser-spectroscopic measurements (Mäckel *et al*, 2011; Schnorr *et al*, 2013). However, trapping-field inhomogeneities, space-charge effects, and voltage noise on the electrodes have until now limited the reach of the method to temperatures of a few eV $\times q$, while in principle lower values should be achievable.

Furthermore, compared with other ion traps operating in the mK and μK regime by means of laser cooling, actual HCI temperatures after evaporative cooling only go down to the level of 0.2 MK (Beiersdorfer, Osterheld *et al*, 1996; Mäckel *et al*, 2011; Schnorr *et al*, 2013). The insufficient cooling causes Doppler broadening and relativistic Doppler shifts and is the main reason for the lack of data on HCI with a precision better than a few parts per million (ppm), an astounding gap of 12 orders of magnitude to the 10^{-18} accuracy of the best optical clock data. Unfortunately, all other HCI sources are also limited in similar ways. In some cases, as in accelerators, storage rings, and beam-foil methods, the ion beam temperature results from its momentum distribution. In plasmas, both high ion temperatures and electron-density effects broaden transitions to the same level. For these reasons, the highest-resolution spectroscopy is carried out nowadays in traps under application of laser cooling and related techniques. This calls for transferring the HCI from their source to another type of trap more amenable to those methods.

B. Sympathetic cooling of HCI

Overcoming the difficulty of the high HCI temperatures borne by the violent HCI production processes has been a long-standing goal. Laser cooling, the tool of choice with atoms and singly charged ions, is impossible with HCI due to the lack of the necessary fast-cycling optical transitions. While HCI are rich on forbidden lines, electric-dipole ($E1$)

transitions take place in them at much higher energies, typically in the soft x-ray and x-ray domains.

Attempts to solve this shortcoming using sympathetic cooling in Penning traps were already proposed in the 1990s, and two groups, LLNL and GSI, started working on them with the aim of achieving enhanced spectroscopic measurements. At LLNL, resistive cooling schemes (Church *et al*, 1999; Gruber *et al*, 2001) for HCI retrapped in a Penning trap after extraction from an EBIT were implemented, and sympathetic cooling was achieved (Gruber *et al*, 2001). The team at GSI worked on the development of sophisticated deceleration and cooling schemes (Poth *et al*, 1991; Quint *et al*, 2001; Beier *et al*, 2005; Winters *et al*, 2005; Kluge *et al*, 2008; Rodríguez *et al*, 2010) needed to bring HCI produced with a relativistic heavy-ion accelerator to a standstill in order to load precision ion traps.

Recently, a combination of HCI production in an EBIT and sympathetic cooling inside of a Coulomb crystal of laser-cooled Be^+ ions contained in a linear rf trap (Schwarz *et al*, 2012; Versolato *et al*, 2013) demonstrated how to bring the temperature of HCI by 8 orders of magnitude down to the mK regime, and opened the possibilities afforded by rf traps to the study of HCI. An artist's impression and schematic are shown in Figs. 10 and 11, respectively. The different components of the system are an EBIT for the ion production, a transfer beam line for mass selection and deceleration, and a cryogenic rf trap. Figure 12 shows the Doppler cooling scheme applied for preparation of the Coulomb crystals. Within the work reported by Schmöger, Schwarz *et al* (2015) and Schmöger *et al* (2015), the HCI transferred to the rf quadrupole were finally embedded in a Coulomb crystal. Because of the high charge state, HCI easily reach Q/m values greater than that of the cooling ions and therefore tend to occupy the positions along the rf trap axis, where micromotion is minimized. The laser-cooled Be^+ ions are displaced from those positions and arrange themselves surrounding the HCI as well as sympathetically cooling them.

In order to theoretically explore other possible Coulomb crystal configurations, the full Coulomb interaction and cooling with a thermal bath and laser interaction molecular dynamics simulations were carried out by Pedregosa (2017) using a velocity-Verlet algorithm implemented in FORTRAN90. Three phases were analyzed: in the first, no cooling was applied; in the second, a thermal bath was added; and in the third, laser cooling by two lasers counterpropagating in the axial direction was turned on. The simulations probed parameters such as q/m, the absolute as well as relative number of cooling ions and sympathetically cooled HCI and the role of the thermal bath temperature. An example in which Ar^{5+} ions are cooled by 300 Be^+ ions is displayed in Fig. 13. Further simulations were performed for Ar^{13+} ions using the parameters shown in Table VI. The results indicate for the cotrapped HCI higher radial and axial trap frequencies than those of the cooling Be^+ ions, arising from the much steeper potential gradients experienced by the HCI. This could benefit reaching appropriate Lamb-Dicke parameters for the HCI.

These simulations imply that in a very large trap stable configurations containing 300 Be^+ ions and up to nearly 20 000 Ar^{13+} sympathetically cooled to 100 mK are possible. However, the resulting ensembles would also become rather long and wide (several mm) and thus would suffer from micromotion, which is included in the simulations.

Experimental temperature determinations by Schmöger (2017) yielded values of 10 mK and below for the HCI. For faster capture of the HCI in the Coulomb crystals, it was expeditive to use large ensembles of several hundred Be^+ ions. Expelling most of them by means of changes in the trapping parameters leads to the ideal configuration for high-resolution quantum logic spectroscopy: a single Be^+ cooling a single Ar^{13+}, as shown in Figs. 14(a) and 14(b), respectively. An effect which has not yet been fully quantified is the partial shielding of the rf field at the HCI positions by the Be^+ ions surrounding them.

In Fig. 14(a) a Be^+ Coulomb crystal containing implanted Ar^{13+} is shown. Schmöger (2017) used these in a first attempt to detect fluorescence from those HCI upon excitation with a low-drift laser system (Leopold *et al*, 2016) developed for this

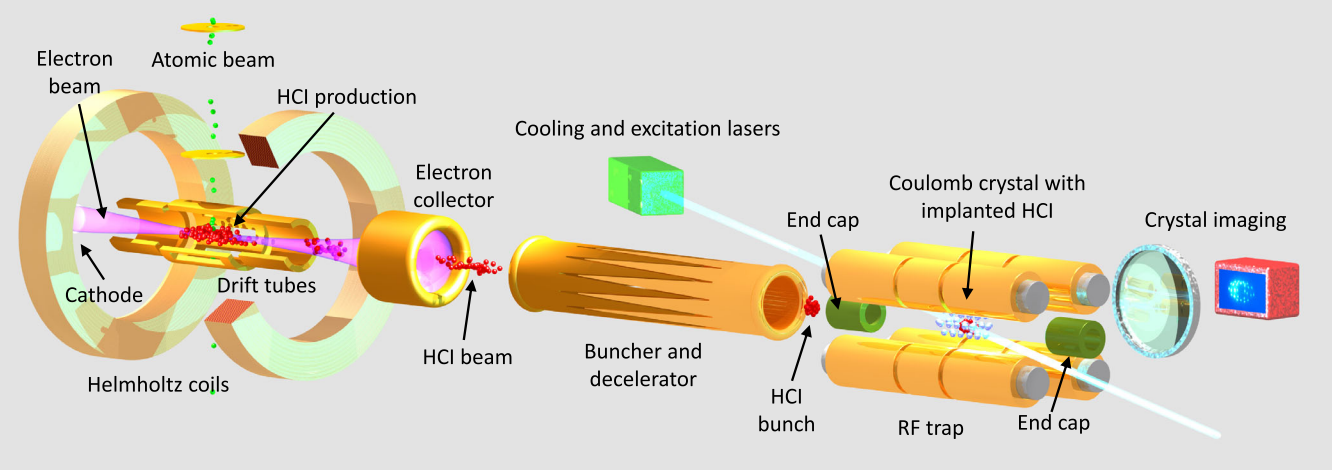

FIG. 10. Schematic representation of an experiment using sympathetic cooling of HCI for optical clock applications (Schmöger, Schwarz *et al*, 2015; Schmöger *et al*, 2015). HCI are produced in an electron-beam ion trap (left), extracted from it, decelerated and bunched, and implanted into a Coulomb crystal of singly carged ions at mK temperatures. The implanted HCI strongly repel their fluorescing, laser-cooled Be^+ neighbors. This provides information about the location and charge of the implanted ions.

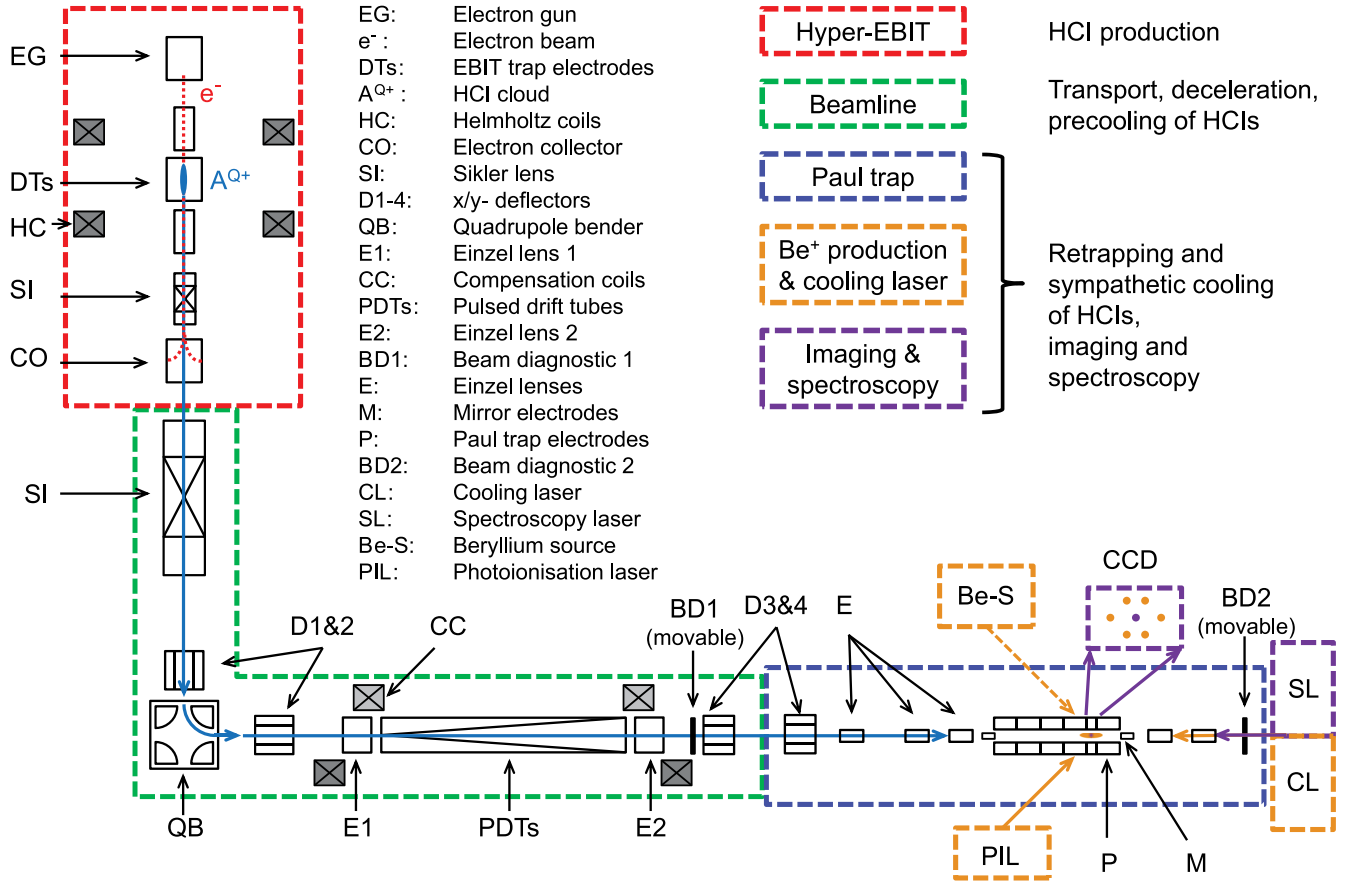

FIG. 11. Scheme of the experiment in which Ar^{13+} ions were sympathetically cooled by laser-cooled Be^+ ions using a laser at $\lambda = 313$ nm. From Schmöger *et al*, 2015.

purpose. Because of insufficient knowledge of the exact frequency of the $2p_{3/2} \rightarrow 2p_{1/2}$ transition at approximately 441.255 nm, and the faintness of the expected signal in comparison with technical background noise, the experiment has not yet been successful. In the near future, an enlarged detection solid angle, noise reduction, and better prior knowledge of the scanning range for the transitions of interests should enable this type of fluorescence studies that can support electronic structure determinations. Searches for highly forbidden transitions benefit from better knowledge

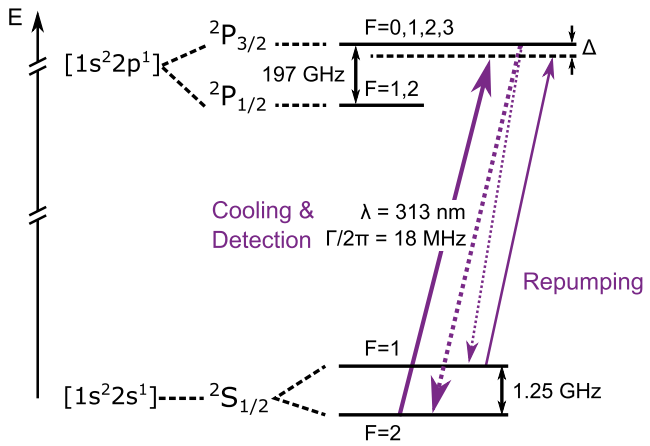

FIG. 12. Doppler cooling of Be^+ ions as applied by Schmöger, Schwarz *et al* (2015), Schmöger *et al* (2015), and Schmöger (2017). The cooling radiation at $\lambda = 313$ nm and the repumper are produced using the technique proposed by Wilson *et al* (2011).

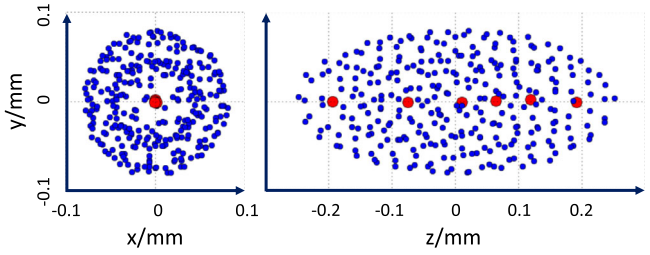

FIG. 13. Simulation of a Coulomb crystal containing 300 laser-cooled Be^+ ions cooling six Ar^{5+} with a very close charge-to-mass ratio Q/m equal to 0.111 and 0.125, respectively. The thermalization in this case is very good, and the radial and transversal temperatures of all components are about 4 mK. However, the crystalline order is less apparent due to the close similarity of the Q/m for the two ion species. This leads to very close trap frequencies ($2\pi\omega_{xy} = 273$ vs 309 kHz, $2\pi\omega_{xy} = 139$ vs 147 kHz) in both the axial and the radial direction, and to intermixing as well as easy interchangeability of the positions for the Be^+ and the Ar^{5+} ions. For larger differences in Q/m, the different species arrange themselves in a well-separated manner. From Pedregosa, 2017.

TABLE VI. Parameters for a molecular dynamics simulation of a Coulomb crystal containing sympathetically cooled HCI: Dimension r_0, frequency of rf drive $2\pi\Omega_{rf}$, dc, respectively, ac operation potentials V_{dc} and V_{rf}, simulation time step dt, trap-stability parameters a and q, trap axial half length z_0, trap geometric correction factor κ, and radial or axial trap frequencies $2\pi\omega_{x,y/z}$ for the cotrapped Be^+ and Ar^{13+}. From Pedregosa, 2017.

Parameter	Value	Unit
r_0	3.5	mm
$2\pi\Omega_{rf}$	3.96	MHz
V_{dc}	5.0	V
V_{rf}	36.25	V
dt	2.52	ns
z_0	2.7	mm
κ	0.259	
$q_{Ar^{13+}}$	0.047	
q_{Be^+}	0.21	
a	0	
$2\pi\omega_{x,yAr^{13+}}$	760	kHz
$2\pi\omega_{zAr^{13+}}$	531	kHz
$2\pi\omega_{x,yBe^+}$	189	kHz
$2\pi\omega_{zBe^+}$	310	kHz

of the intraconfiguration transitions of $M1$ type, as shown by Windberger *et al* (2015).

For one single Ar^{13+}, the fluorescence rate at saturation for this $M1$ transition is approximately 100/s (Lapierre *et al*, 2005, 2006). With a detection solid angle of the order of 1%, and including the photomultiplier detection efficiency and other losses, a few ions should provide a signal rate of 0.1/s, which in principle could be measured against a photomultiplier tube dark count rate of 4/s. These limitations in the signal-to-noise ratio can be overcome by more elaborate quantum state detection systems, e.g., based on quantum logic (Schmidt *et al*, 2005; Hempel *et al*, 2013; Wan *et al*, 2014) as discussed in Sec. VII.C. These techniques are crucial for addressing even more-forbidden transition types ($E2$, $M2$, $E2M3$) for optical clocks.

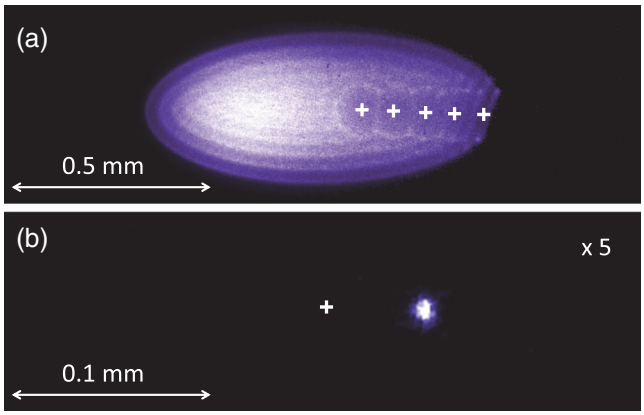

FIG. 14. Images of Be^+ Coulomb crystals with implanted HCI. (a) Ellipsoidal crystal containing five Ar^{13+} ions. Unbalanced light pressure due to one-sided laser cooling caused the cocrystalized HCI to preferentially accumulate in one side. HCIs close to the crystal edge occupied nonequidistant equilibrium positions. (b) Single Ar^{13+} ion cooled by a single Be^+ ion (Schmöger *et al*, 2015) under modified trapping parameters (note the change of scale in the images). This latter configuration allows for the best sympathetic cooling conditions and eventually for ground-state cooling, which enables quantum logic detection (Schmidt *et al*, 2005).

Since, as previously mentioned, trapping of a single HCI together with a single sympathetically cooling Be^+ ion has now been demonstrated (Schmöger *et al*, 2015), the possibility of sideband cooling to the ground state of motion as discussed in Sec. VII.B will in the near future allow for the application of advanced detection schemes such as quantum logic spectroscopy (Schmidt *et al*, 2005) for addressing very slow clock transitions in HCI. Sympathetic cooling overcomes the main difficulty for high-resolution laser spectroscopy and frequency metrology with HCI. In this way, the plethora of quantum manipulation techniques available in the atomic physics community gains a wide class of experimental target beyond the much-studied alkalilike ions. In essence, a working technique combining the HCI source and the rf trap as needed for these studies is now within reach for high-precision frequency-metrology groups. Optical clocks based on trapped singly charged ions (Rosenband *et al*, 2008; Chou *et al*, 2010; Dubé *et al*, 2014; Huntemann *et al*, 2016; Huang *et al*, 2017) have achieved accuracies which in science have only that of optical lattice clocks as peers (Ludlow *et al*, 2015). The introduction of HCI as pacemakers will open up new opportunities for further enhancement of accuracy and sensitivity for fundamental physics searches.

VII. TOWARD HIGH-RESOLUTION SPECTROSCOPY

Several challenges need to be addressed to make HCI accessible for high-precision spectroscopy and optical clocks. The main goal of an atomic frequency standard is the realization of the unperturbed frequency of the reference or clock transition. In this context, two types of uncertainties are important: the statistical uncertainty (sometimes also called instability or uncertainty type A) and the systematic uncertainty (sometimes also called inaccuracy or uncertainty type B). While the systematic uncertainty quantifies how well we believe we are able to reproduce the unperturbed transition frequency, statistical uncertainty tells us for how long we need to average frequency measurements to achieve a certain resolution. Systematic uncertainties of clocks beyond the current accuracy of a few parts in 10^{16} of the best Cs frequency standards (Guéna *et al*, 2017) can be estimated only by considering all possible shifts to the measured frequency. This includes changes to the atomic structure due to interaction with external fields, but also relativistic effects from motion and gravity. The instability of a frequency standard in which N uncorrelated atoms are probed simultaneously is ultimately limited by quantum projection noise (Itano *et al*, 1993). In the simple case of Ramsey interrogation (Ramsey, 1985) of a transition with frequency ν_0 using perfect pulses and a probe time T_R, we get a fractional frequency uncertainty expressed in the form of an Allan deviation (Allan, 1966; Riehle, 2004; Riley, 2008) of

$$\sigma_y(t) = \frac{1}{2\pi\nu_0\sqrt{NT_R t}}. \tag{9}$$

From Eq. (9) it becomes clear that a high transition frequency, many atoms, and a long probe time reduce the averaging time t to achieve a certain resolution. The probe time is a special case, since it can be limited either by the lifetime of the excited clock state or by the coherence time of the probe laser (Riis and Sinclair, 2004; Peik, Schneider, and Tamm, 2006; Leroux *et al*, 2017). The currently best lasers achieve a flicker noise floor-limited instability of 4×10^{-17} (Matei *et al*, 2017) and support probe times of several seconds. For a single atom, the best possible statistical uncertainty is achieved for a probe time equal to the excited state lifetime τ of the clock transition. It is given by (Peik, Schneider, and Tamm, 2006)

$$\sigma_y(t) = \frac{0.412}{\nu_0\sqrt{\tau t}}. \tag{10}$$

In the remainder of this section, we discuss the technical issues and systematic frequency shifts, their measurement, and suppression, specific to HCI. Frequency shifts arise from motion and from external fields causing a differential shift of the two clock levels. For evaluating the performance as a frequency reference, we need to know the atomic parameters (from theoretical atomic structure calculations or measurements) and the strength of the external field. In some cases suppression techniques exist to reduce the influence of external perturbations on the clock transition. While recent reviews have addressed these issues for single-ion clocks (Poli *et al*, 2013; Ludlow *et al*, 2015), we will provide the scaling of these effects to HCI. Some effects such as electric and magnetic field shifts will be reduced, while others (collisional shift, motion-induced shifts) may be enhanced. The section ends with an assessment of potential HCI optical clock candidates and their expected performance.

A. Trapping

Radio-frequency Paul traps have been the workhorse in all areas of ion-based research that require isolation from external fields, such as ion optical clocks, quantum-information processing, quantum simulation, and quantum metrology (Wineland *et al*, 1998; Major, Gheorghe, and Werth, 2006). In spherical Paul traps, a 3D oscillating quadrupole field provides confinement in all directions. At the center of the quadrupole, a single ion can be stored almost perturbation free. To trap more ions, linear Paul traps have been invented in which an oscillating 2D radial electric field combined with a static axial field provides trapping. In both cases harmonic trapping at secular frequencies between 100 kHz up to a few MHz can be achieved with rf drive frequencies Ω_{rf} oscillating typically at least 1 order of magnitude higher. A large variety of electrode geometries and material choices exist for ion traps, ranging from microfabricated surface traps providing a scalable approach with multiple segments (Chiaverini *et al*, 2005; Britton *et al*, 2006; Seidelin *et al*, 2006) sometimes even in a cryogenic environment (Labaziewicz *et al*, 2008) to macroscopic traps for optical clocks with ion-electrode distances on the order of 1 mm (Doležal *et al*, 2015). The latter provide large optical access for efficient detection and probing the ion from various directions. They feature deep trapping potentials on the order of a few eV for storage times of many hours up to a few months. They offer moderately large motional frequencies of up to several MHz to allow recoil-free spectroscopy in the Lamb-Dicke regime while maintaining potentially low motional heating rates of only a few motional quanta per second (Brownnutt *et al*, 2015). Recently even linear multi-ion traps for precision spectroscopy and optical clocks have been developed (Herschbach *et al*, 2012; Pyka *et al*, 2014; Doležal *et al*, 2015; Keller *et al*, 2015, 2016), with trap-induced shifts below 10^{-19} fractional frequency uncertainty (Keller *et al*, 2017). While most single-ion frequency standards in the past are room-temperature systems, with the notable exception of the Hg^+ clock (Rosenband *et al*, 2008), cryogenic Paul traps are mandatory for HCI to achieve a sufficiently long lifetime through excellent vacuum conditions (Schwarz *et al*, 2012). Conveniently, at the same time the BBR shift (see Sec. VII.D.2) becomes negligible. One typically distinguishes two types of motion of an ion in a Paul trap: fast micromotion at frequency Ω_{rf} and so-called secular motion at lower oscillation frequencies. Paul traps support only stable trajectories for certain charge-to-mass ratios for a given geometry and a rf trapping field (Drakoudis, Söllner, and Werth, 2006; Major, Gheorghe, and Werth, 2006). In the simplest case, stable trapping in linear Paul traps is achieved if the radial secular frequency ω_r is significantly smaller than the trap drive frequency Ω_{rf}, or $q \approx 2^{3/2}\omega_r/\Omega_{\mathrm{rf}} < 0.908$ (Ghosh, 1996). This has to be taken into account when trapping HCI, in particular, when trapping them simultaneously with singly charged atomic ions as discussed in the next section. Since the stability criterium scales with the charge-to-mass ratio, Be^+ is a suitable cooling ion species for many medium-charged HCI. As an example, Fig. 15 shows the stability parameter for two of the radial modes of a $^9Be^+ - {}^{40}Ar^{Q+}$ ion crystal. For sufficiently small q, secular motion decouples from micromotion and it can be assumed to be harmonic in all three directions (Dehmelt, 1968), which is what we assume from

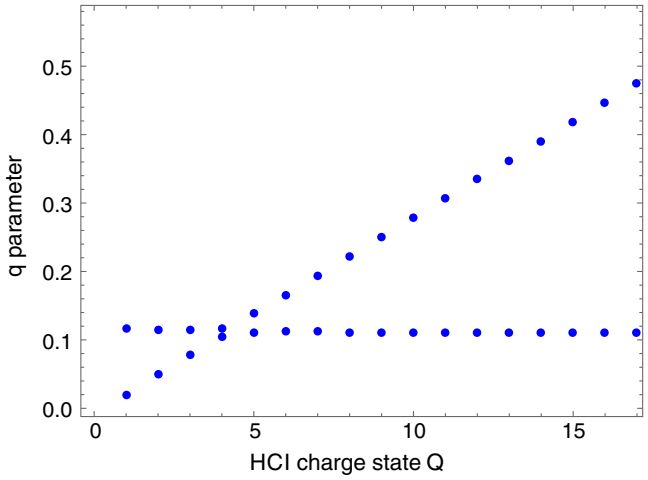

FIG. 15. Stability parameter for a HCI in a linear Paul trap. The stability parameter q is plotted for the radial modes of a two-ion crystal consisting of a singly charged $^9Be^+$ and an $^{40}Ar^{Q+}$ ion as a function of the Ar-ion's charge Q for a single Be^+ radial trapping frequency of $\omega_r = 2\pi \times 2.2$ MHz and $\Omega_{\mathrm{rf}} = 2\pi \times 50$ MHz. All charge states satisfy the stability criterion $q < 0.908$.

now on. Residual effects of micromotion have to be included separately as discussed in Sec. VII.D.4.

B. Sympathetic cooling

One of the key ingredients for the success of atomic systems over the past 25 years is the control of their motion through Doppler laser cooling and other advanced cooling techniques (Chu, 1998; Cohen-Tannoudji, 1998; Phillips, 1998). The first laser-cooling concepts were in fact developed and experimentally demonstrated for trapped ions (Wineland and Itano, 1979; Drullinger, Wineland, and Bergquist, 1980). Since then, laser cooling has become mandatory for all optical ion clocks, since it allows localization of the ion to well below the wavelength of the spectroscopy light, which is equivalent to the condition of recoil-free absorption in the Lamb-Dicke regime (Dicke, 1953). For HCI optical clock candidates that do not have a sufficiently fast (MHz linewidth) and closed transition suitable for laser cooling, sympathetic cooling can be provided by another atomic species that is laser coolable. This is implemented by trapping the HCI together with the cooling ion into the same trapping potential and taking advantage of their mutual Coulomb repulsion (Larson *et al*, 1986; Barrett *et al*, 2003; Wan *et al*, 2015). While initial stopping and Doppler cooling of HCI is performed in clouds of laser-cooled atomic ions (Schmöger *et al*, 2015) as described in Sec. VI.B, precision spectroscopy demands smaller ion crystals, consisting of the simplest case of two ions.

The strong Coulomb repulsion between two cold ions with charges $Q_{1,2}$ in a linear Paul trap results in equilibrium positions $d_{1,2}$ away from the center of the trap according to

$$d_{1,2} = Q_{2,1}/[4\pi\epsilon_0 u_0 (Q_1 + Q_2)^2]^{1/3}. \tag{11}$$

Here $u_0 = m\omega_z^2/Q$ quantifies the strength of the axial trapping potential in terms of a single reference ion with mass m, charge Q, and secular frequency ω_z.

The ions perform a coupled motion around these equilibrium positions appropriately described in a normal mode framework. For two ions, we have two modes in each direction, the in- and out-of-phase mode (indices i, o) with mode frequencies $\omega_{i,o}$. We can thus write the oscillation $z_{1,2}(t)$ of the two ions along a selected direction as a superposition of the contributions from the two modes along this direction (James, 1998; Kielpinski *et al*, 2000; Morigi and Walther, 2001; Wübbena *et al*, 2012)

$$z_1(t) = [\hat{z}_i b_{1,i} \sin(\omega_i t + \phi_i) + \hat{z}_o b_{1,o} \cos(\omega_o t + \phi_o)]/\sqrt{m_1},$$
$$z_2(t) = [\hat{z}_i b_{2,i} \sin(\omega_i t + \phi_i) + \hat{z}_o b_{2,o} \cos(\omega_o t + \phi_o)]/\sqrt{m_2}.$$

Here $\hat{z}_{i,o}/\sqrt{m_{1,2}} = \sqrt{2E_{i,o}}/\omega_{i,o}$ is an excitation amplitude that depends on the kinetic energy $E_{i,o}$ in each mode, and $b_{k,\alpha}$ are mode amplitudes normalized to $b_{2,o} = -b_{1,i}$ and $b_{2,i} = b_{1,o}$ with $b_{1,i}^2 + b_{1,o}^2 = 1$. The modes have phases $\phi_{i,o}$ that depend on the initial conditions. While identical ions have (anti)symmetric mode amplitudes for the in-phase (out-of-phase) mode in each direction, a difference in mass and/or charge results in one ion having a large mode amplitude, while the other has a small amplitude for one mode and vice versa for the other mode along the same direction.

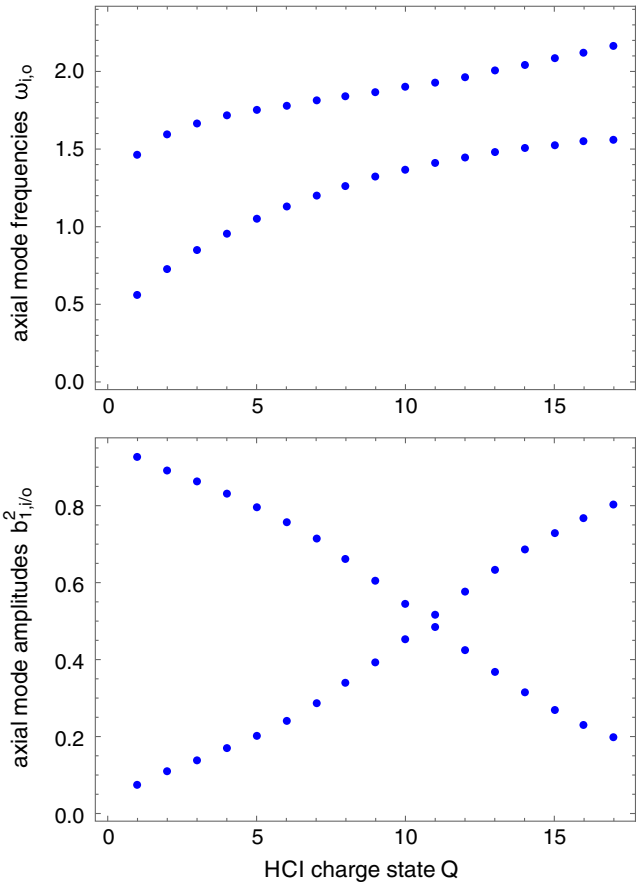

FIG. 16. Coupled axial mode parameters for an Ar^{Q+}/Be^+ two-ion crystal in a linear Paul trap as a function of the HCI charge Q. Top: mode frequencies; bottom: mode amplitudes. The position of the mode amplitude crossing point is determined. For details see text.

Figure 16 shows the axial mode frequency and Fig. 17 shows one set of radial mode frequencies $\omega_{i,o}$ and the square of the amplitudes $b_{1,i}^2$, $b_{1,o}^2$ of a two-ion crystal consisting of a singly charged $^9Be^+$ and an $^{40}Ar^{Q+}$ ion as a function of the Ar-ion's charge Q. A single Be^+ ion would have an axial (radial) mode frequency of $\omega_z = 2\pi \times 1$ MHz ($\omega_r = 2\pi \times 2.2$ MHz). While the axial modes remain strongly coupled for all charge states, this is not the case for the radial modes. The radial mode frequency corresponding closely to the single Be^+ ion mode remains almost constant for all charge states, while the other mode frequency increases as a function of the HCI charge state. Similarly, one mode amplitude remains almost constant near a value of 1, while the other one is close to 0. An exception is $Q = 4$, for which the charge-to-mass ratios of $^9Be^+$ and $^{40}Ar^{4+}$ are almost equal. Thus, away from this "resonance" in the coupling the ions are radially only weakly coupled. A similar, but less pronounced effect is observed for singly charged ions with different masses (Wübbena *et al*, 2012). The mode decoupling is more pronounced for HCI, since (in contrast to singly charged ions with different masses) their distance $(d_1 + d_2)$ increases with their charges according to Eq. (11). However, the resonances in the radial mode

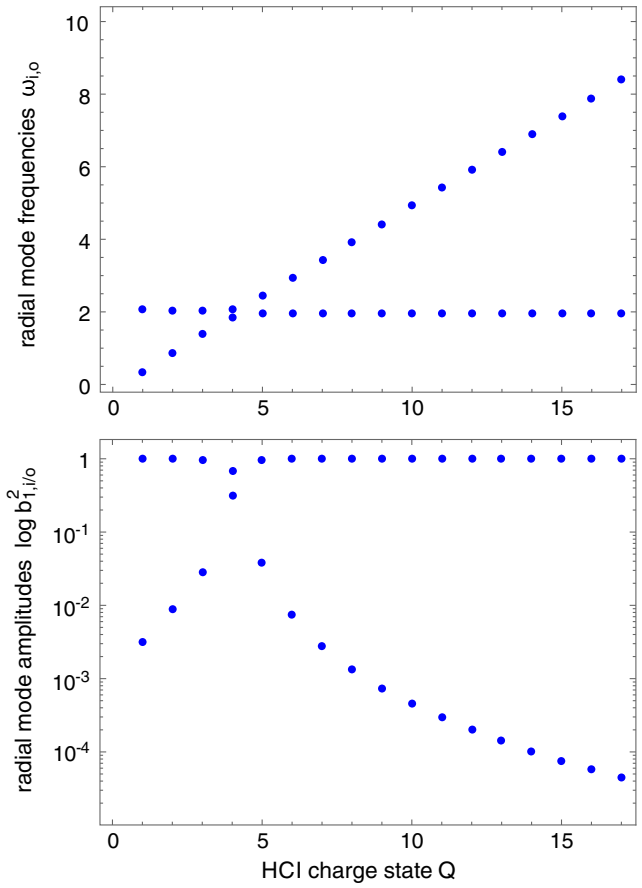

FIG. 17. Coupled radial mode parameters for an Ar^{Q+}/Be^+ two-ion crystal in a linear Paul trap as a function of the HCI charge Q. Top: mode frequencies; bottom: mode amplitudes. The position of the mode amplitude crossing point is determined. For details see text.

coupling can be exploited if a HCI with a suitable cooling transition and matching Q/m can be found. The axial mode amplitudes become equal at a charge state that is larger compared to the radial modes, since they depend not only on the individual ion confinement, but also the distance between the ions.

The reduction in coupling has two consequences for the two radial modes for which the Doppler cooling ion has only a small mode amplitude b_r. First, the Doppler cooling rate scales with the square of the mode amplitude. Together with typical time scales to reach Doppler cooling temperature after a background gas collision on the order of milliseconds for a single ion (Wübbena *et al*, 2012), cooling a mode with $b^2 \sim 10^{-4}$ (see Fig. 17) would take up to 10 s, which is unacceptably long. However, cooling these radial modes can be made more efficient by tilting the ion crystal out of the axial alignment through application of a static electric field. This enhances the mode coupling and has already been successfully demonstrated in the Al^+/Be^+ quantum logic optical clock (Rosenband *et al*, 2008, supplementary information).

Second, in the presence of motional heating mechanisms (in addition to photon scattering), the steady-state temperature will be larger than the Doppler cooling temperature (Wübbena *et al*, 2012). Anomalous motional heating from fluctuating electric fields is the most common heating mechanism in ion traps and HCI will be particularly sensitive to it owing to their high charge state. Although the exact origin of anomalous heating remains elusive, for most traps the heating rate is significantly reduced at cryogenic temperatures and for large ion-electrode distances (Hite *et al*, 2012; Brownnutt *et al*, 2015). Since for HCI macroscopic traps at cryogenic temperatures will be employed, it can be expected that the anomalous heating rate is sufficiently small to allow efficient sympathetic cooling. Assuming a typical heating rate of 1 phonon/s for a trap with around 0.7 mm ion-electrode separation (Keller *et al*, 2016), the temperature of the weakly coupled modes for the Be^+/Ar^{13+} example already discussed would be elevated by less than 10% above the Doppler cooling limit. The reduction of cooling rates for modes with a small amplitude of the cooling ion also hold for all other cooling techniques, such as sideband or electromagnetically induced transparency cooling (Roos *et al*, 2000; Lin *et al*, 2013; Lechner *et al*, 2016; Scharnhorst *et al*, 2017) that allow reaching the motional ground state.

C. Quantum logic spectroscopy

In addition to providing sympathetic cooling, the singly charged atomic ion ("logic ion") can also be employed for preparation and read-out of the internal state of the HCI during the spectroscopy sequence using quantum logic spectroscopy (Schmidt *et al*, 2005; Rosenband *et al*, 2008). Following the original implementation, state detection would be accomplished by applying a series of laser pulses to the HCI and atomic ion in the motional ground state that implement so-called sideband pulses changing the internal state while adding or removing a quantum of motion (Wineland *et al*, 1998). This way, a SWAP operation exchanging the amplitudes between the internal state of the HCI and the motion would be implemented, followed by another SWAP between the motion and the internal state of the atomic ion. Such a sequence maps the internal state of the HCI faithfully onto the internal state of the atomic ion, where it can be detected with high fidelity (Schmidt *et al*, 2005; Hume, Rosenband, and Wineland, 2007). Similarly, internal state preparation could be accomplished by applying sideband pulses to the HCI to drive the HCI into the target state. Dissipation is provided through ground-state cooling on the singly charged atomic ion, which makes the sideband pulses irreversible (Schmidt *et al*, 2005; Chou *et al*, 2017). A parallel quantum readout algorithm for multiple clock ions using as few logic ions as possible has also been developed (Schulte *et al*, 2016). Other forms of quantum logic spectroscopy are more suitable for fast transitions. For example, in photon recoil spectroscopy (Hempel *et al*, 2013; Clos *et al*, 2014; Wan *et al*, 2014), recoil upon photon absorption by the spectroscopy ion changes the motional state, which can be detected with high efficiency on the logic ion. In species with many levels, incoherent photon scattering can lead to state diffusion, thus losing the ion to unobserved metastable states. By employing a state-dependent optical dipole force (ODF), incoherent photon scattering can be significantly suppressed, which enables spectroscopy of species with nonclosed broad transitions, such as molecules (Wolf *et al*, 2016). The same technique could be employed for an efficient search and identification of previously unknown

lines in HCI. In one possible implementation, an oscillating ODF would be scanned over a wide range of optical frequencies. The optical force exerted on the HCI near an atomic resonance can be detected via the logic ion. The polarization dependence of the ODF could be used to determine the involved angular momentum states.

In summary, using a cotrapped singly charged atomic ion for sympathetic cooling and quantum logic spectroscopy, any HCI can be spectroscopically investigated as long as sideband transitions can be driven with high fidelity on either the transition of interest or any another suitable transition. Therefore, the choice of HCI for an optical clock is entirely dictated by its atomic properties.

D. Systematic frequency shifts

The evaluation of systematic frequency shifts is one of the most important tasks when developing a frequency standard. The most common shifts arise from external fields coupling differentially to the two clock levels. The shift is characterized by its magnitude and associated uncertainty. Its magnitude is given by the properties of the external field (ac or dc, strength, orientation, polarization, gradient, etc.) and the atomic properties of the clock levels. The field can either be measured externally or through the atoms, or by using a combination of measurements and simulation, as is the case, e.g., for modeling the thermal environment of the ion to evaluate the blackbody radiation shift (Dubé *et al*, 2013; Doležal *et al*, 2015). Similarly, the atomic parameters can either be measured or one can rely on accurate atomic structure calculations. The uncertainty of a shift is given by the combined uncertainty of all individual contributions, i.e., the uncertainty in the atomic properties and the uncertainty in the properties of the external field. In some cases, shifts can be suppressed by taking advantage of symmetries in the shift. Averaging frequency measurements involving different levels of the Zeeman substructure of the atomic energy levels eliminates the linear Zeeman shift and the electric-quadrupole shift (Dubé *et al*, 2005). In these cases the uncertainty in the shift is determined by its variation during the averaging process, which has to be determined experimentally. Choosing a clock ion species with advantageous atomic properties can be simpler to implement and may eventually result in smaller systematic uncertainties compared to an atom for which cancellation schemes are required. Following Itano (2000), Ludlow *et al* (2015), and Schmidt and Leroux (2015) we discuss the dominant shifts and possible cancellation schemes in trapped ion frequency standards applied to HCI.

1. Magnetic field shifts

External magnetic fields couple to the magnetic moment of the electron μ_B (order of magnitude 14 MHz/mT/h shifts) and the nucleus μ_N (7.6 kHz/mT/h shifts). The coupling with the external field required to define a quantization axis for cooling is in competition with the internal coupling between the magnetic moments. This results in nonlinear shifts of the corresponding Zeeman levels as a function of the magnetic field strength. Of interest for clocks is the differential frequency shift Δf_B between a selected ground and excited state, which can be expressed as a Taylor expansion according to

$$\Delta f_B = C_{M1}B + C_{M2}B^2 + C_{M3}B^3 + \cdots.$$

It is usually sufficient to consider only the first two terms for typical magnetic fields of a few 100 μT that are applied to provide a quantization axis for laser cooling and optical pumping. Electronic states with a total angular momentum quantum number $J = 0$ exhibit only the small nuclear Zeeman effect, whereas states with $J > 0$ have the much larger electronic Zeeman shift. In both cases, the C_{M1} term of Δf_B scales linearly with the magnetic quantum number m. The linear Zeeman effect vanishes for transitions $m = 0 \rightarrow m' = 0$, where the (un)primed magnetic quantum number denotes the (ground) excited state. In all other cases, averaging two (or more) transitions with shifts of equal magnitude, but opposite sign, allows recovering the unshifted transition frequency. In fact, by averaging transitions involving all Zeeman components of a state eliminates linear Zeeman shifts, as well as the electric-quadrupole shift discussed in the next section (Dubé *et al*, 2013). The quadratic Zeeman effect is the next largest contribution. It arises from the decoupling of nuclear and electronic magnetic moments as a function of the external magnetic field strength. For atoms with $J > 0$ and hyperfine structure, the external field mixes states of different hyperfine quantum numbers F. The corresponding quadratic shift can be derived from first-order perturbation theory to be $C_{M2} \sim (g_J\mu_B - g_I\mu_N)^2/h^2A$, where g_J and g_I are the electronic and nuclear g factors, respectively, and A is the hyperfine constant, characterizing the splitting between F states. For singly charged ions, typical values for C_{M2} range from a few to a few ten kHz/mT^2. Since the hyperfine splitting scales in HCI as $ZZ_a/(Q+1)$, where Z_a is the effective charge seen by the outer electrons (Berengut *et al*, 2012a), stronger external field perturbations are required to compete with the internal coupling. This results in a small quadratic Zeemann shift. In case the clock transition is a hyperfine transition, the expression for the shift coefficient simplifies to $C_{M2} = 2\mu_B^2/(h^2\nu_0)$ (Yudin, Taichenachev, and Derevianko, 2014).

In the case of $J = 0$ levels, a quadratic Zeeman effect arises through external field-mediated mixing of fine-structure components. The shift is then again proportional to the difference of the involved magnetic moments, divided by the fine-structure splitting. In singly charged ions the C_{M2} coefficient is on the order of a few ten Hz/mT^2. Since the fine-structure splitting in HCI scales with $Z^2Z_a^2/(Q+1)$ (even more strongly than the hyperfine splitting), the quadratic Zeeman shift is further suppressed (Berengut *et al*, 2012a). To evaluate the shift precisely, the magnetic field and its variation needs to be determined with high accuracy. Where available, transitions with large and calibrated C_{M1} coefficients can be employed for this task. Alternatively, from the difference of the two transitions averaged to eliminate the linear Zeeman shift, the magnetic field can be derived.

The previous discussion applies to dc magnetic fields. For ac magnetic fields, the linear Zeeman shift averages to zero. However, the quadratic term $\Delta f_{M2} = C_{M2}\langle(B - B_0)^2\rangle$ remains and may be significant. In ion traps ac magnetic fields can arise from the trap rf drive or from power line noise.

In both cases, the shift needs to be calibrated either by sideband spectroscopy or by extrapolation to zero field.

2. Electric field shifts

a. ac Stark shift

Ions are located at the position of a vanishing dc electric field in the absence of other forces. Therefore, the dominant electric-field shifts arise from field gradients and oscillating electric fields. Oscillating electric fields couple to the polarizability of the atom's states via the ac Stark effect, while field gradients couple to electric-quadrupole moments a state might have. The quadratic Stark effect of state $|\gamma J\rangle$, characterized by a set of quantum numbers γ, can be treated as a small perturbation to the linear Zeeman effect, resulting in a scalar shift of

$$h\Delta f_S(\gamma, J, \vec{E}) = -\alpha_S(\gamma, J)|\vec{E}|^2/2. \tag{12}$$

The scalar polarizability α_S depends on the atomic state and, in general, on the frequency of the oscillating electric field $\vec{E}$. Atomic states with $J > 1/2$ and $F > 1/2$ have an additional tensor component of the polarizability $\alpha_T(\gamma, J)$. The tensorial part depends on the quantum numbers F, m_F and on the polarization of the electric field with respect to the quantization axis of the atom. Sources of ac electric fields are the trap rf drive field, thermal blackbody radiation, the clock interrogation laser, or the cooling laser for the atomic ion applied during interrogation. They all couple the clock states off resonantly to other levels, resulting in a differential shift. For example, the root mean square (rms) electric field associated with BBR near room temperature is given by $\langle E^2(T)\rangle = (831.9\ \mathrm{V/m})^2[T(\mathrm{K})/300]^4$. While in singly charged ions the shift from BBR of the ion's environment can be significant, it is negligible for HCI. This has two reasons. First, HCI traps are operated at cryogenic temperatures near $T = 4$ K where the BBR shift is suppressed by more than 7 orders of magnitude compared to room-temperature operation owing to the T^4 scaling of the shift. Second, the size of the electron orbitals $\sqrt{\langle r^2\rangle}$ scales as $1/Z_a$, where Z_a is the effective charge state of the ion, while the energy spacing ΔE between levels connected by strong $E1$ transitions scales as Z_a^2. Thus the polarizability behaves as $\alpha \approx \langle r^2\rangle/\Delta E \propto 1/Z_a^4$ (Berengut *et al.*, 2012b), contributing to a further suppression of polarizability shifts. ac Stark shifts arising from the rf trapping field of the Paul trap will be discussed in Sec. VII.D.4.

b. Electric-quadrupole shift

Atomic states with $J, F > 1/2$ are no longer spherically symmetric, but exhibit higher-order electric multipole moments that couple to the corresponding electric-field components. The largest contribution is the quadrupole moment which interacts with electric-field gradients according to the Hamiltonian (Itano, 2000)

$$H_Q = \boldsymbol{\nabla E}^{(2)} \cdot \boldsymbol{\Theta}^{(2)}, \tag{13}$$

where $\boldsymbol{\Theta}^{(2)}$ is the electric-quadrupole operator for the atom and $\nabla \boldsymbol{E}^{(2)}$ is a symmetric traceless tensor of second rank describing the electric-field gradient at the position of the ion. It should be noted that even for states with $J = 0, 1/2$, a small quadrupole moment from mixing of other electronic states and nuclear quadrupole moments exists, which is usually negligible at a frequency uncertainty level above 10^{-19} (Beloy, Leibrandt, and Itano, 2017). The quadrupole shift depends on the total angular momentum F and its projection m_F along the quantization axis (Itano, 2000), according to

$$\Delta f_Q h \propto \frac{3m_F^2 - F(F+1)}{\sqrt{(2F+3)(2F+2)(2F+1)[2F(2F-1)]}}. \tag{14}$$

Furthermore, it depends on the orientation of the quantization axis with respect to the electric-field gradient.

An electric-field gradient is inherent to the axial trapping mechanism in linear ion traps and can become larger if more than one ion is trapped. Even in spherical ion traps, that can in principle be free of electric-field gradients, spurious electric fields typically result in gradients of up to a few $\mathrm{V/mm^2}$, resulting in shifts of a few Hz for a typical atomic quadrupole moment of ea_0^2, where e and a_0 are the electric charge and the Bohr radius, respectively. Quadrupole shift reduction or cancellation schemes are based on minimizing Eq. (14) or averaging frequency shifts of different transitions to zero. For example, selecting suitable hyperfine components F for the clock transition, the quadrupole shift can be made small. The dependence of the shift on the quantum number m_F^2 and the orientation of the gradient with respect to the quantization axis is identical to other tensorial shifts, such as the tensor component of the ac Stark effect. Therefore, averaging suitable pairs of Zeeman transitions cancels these shifts together with the linear Zeeman shift. Using such schemes, a suppression of the quadrupole shift by more than 4 orders of magnitude has been achieved in a singly charged ion (Dubé *et al*, 2005, 2013). Alternatively, the quadrupole shift can be canceled by averaging the same transition over three mutually orthogonal magnetic field directions. The level of suppression using this technique can reach a factor of 100 if the magnetic field direction is determined to better than $\pm 1°$. Since the electric-quadrupole moment scales with the square of the size of the electron orbitals, the quadrupole shift in HCI is suppressed by $1/Z_a^2$, resulting in a reduction between one and several orders of magnitude compared to singly charged ions.

3. Motion-induced shifts

An atom in motion experiences special relativistic frequency shifts with respect to an atom in the laboratory frame. Consider the case of an atom moving with velocity $v_\parallel$ along the direction of the clock laser with frequency f in the laboratory system probing the reference transition. According to special relativity, the atom observes the clock laser with a first-order Doppler shift of $\Delta f_{D1}/f = \langle v_\parallel\rangle/c$, where the average is taken over typical time scales required for stabilizing the probe laser frequency to the atomic transition frequency. For an ion oscillating in an ion trap that is fixed to the laboratory frame, this shift averages to zero. However, thermal drifts in the relative position of the trap with respect to the probe laser phase or probe-synchronous shifts in the ion's position in the trap can result in fractional frequency drifts of

10^{-17} for a relative velocity of only 3 nm/s. Therefore it may be required to phase stabilize the laser to the position of the trap using interferometric schemes (Ye *et al*, 2003; Falke *et al*, 2012). Since HCI are particularly sensitive to electric fields, displacements synchronous to the clock interrogation that may arise through charging of the ion trap structure via the clock laser need to be avoided or measured using counterpropagating probe laser beams (Rosenband *et al*, 2008).

In addition to the linear Doppler shift, the atom also experiences a second-order Doppler or time-dilation shift

$$\frac{\Delta f_{D2}}{f} = -\frac{\langle v^2 \rangle}{2c^2} = -\frac{E_{\mathrm{kin}}}{mc^2}$$

from motion in all directions, which is directly related to the total kinetic energy E_{kin} of the ion in the trap. This shift can be difficult to quantify, since one has to make assumptions about the velocity distribution (Chen *et al*, 2017). Heating of the ion during interrogation can increase the shift and result in additional uncertainty, making this shift one of the largest contributions to the uncertainty budget, e.g., of the Al^+ and Yb^+ clocks (Rosenband *et al*, 2008; Chou *et al*, 2010; Huntemann *et al*, 2016). Assuming a constant thermal distribution over the probe time, characterized by a mean occupation of motional levels $\bar{n}$, the kinetic energy in a linear Paul trap is given by the sum over all modes with frequencies ω_j:

$$E_{\mathrm{kin}} \approx \left(\frac{1}{2}+\frac{1}{2}\right) \sum_{j \in \mathrm{radial}} \hbar\omega_j \left(\bar{n}_j + \frac{1}{2}\right) \tag{15}$$

$$+\frac{1}{2} \sum_{j \in \mathrm{axial}} \hbar\omega_j \left(\bar{n}_j + \frac{1}{2}\right). \tag{16}$$

The first sum is over all radial modes. One of the $1/2$ prefactors reflects the fact that kinetic energy makes up only half the total energy in a harmonic oscillator, and the second $\approx 1/2$ is from intrinsic micromotion of the ion in the trap (Berkeland *et al*, 1998). It will be discussed in more detail in Sec. VII.D.4. The second sum is over axial modes that ideally are not affected by micromotion. It is interesting to note that the zero point energy contributes to the time-dilation effect and can be on the order of 10^{-19} for typical trap frequencies of a few MHz and light ion species, such as Al^+. For HCI, motional shifts will depend crucially on the performance of sympathetic cooling with the singly charged cooling ion as discussed in Sec. VII.B, which in turn will depend on the rate of collisions with background gas (discussed in Sec. VII.D.5) and the anomalous motional heating rate in the trap. Since HCI will be trapped in a cryogenic environment, we expect that both effects can be made small to not be a limiting factor in clock accuracy.

4. Micromotion shifts

The trapping mechanism of Paul traps is based on a periodically oscillating electric-quadrupole field with angular frequency Ω_{rf}. This field vanishes in a spherical trap at a single point and in a linear trap along the (axial) nodal line, on which ideally the ion is located (see Sec. VII.A). Since an ion in the trap has a minimal size along each direction corresponding to the zero point wave function extent $x_0 = \sqrt{\hbar/2m\omega_x}$, it is always subject to an oscillating force leading to intrinsic (and unavoidable) micromotion in the radial (x, y) direction in addition to any secular motion around its equilibrium position at the much lower frequency $\omega_{x,y}$ (Berkeland *et al*, 1998). This intrinsic micromotion grows with the oscillation amplitude and thus the temperature of the ion. Electric dc fields displace the ion from its equilibrium position and result in additional, so-called excess micromotion. Similarly, a phase difference between the rf applied to a pair of electrodes results in excess micromotion. The amplitude of excess micromotion scales in both cases with the charge Q of the ion. Therefore, HCI are particularly sensitive to micromotion and excess micromotion needs to be avoided. This is typically achieved by probing micromotion using one of several techniques (Berkeland *et al*, 1998; Keller *et al*, 2015) and applying compensation voltages to steer the ion back to the position of vanishing rf field. Since HCI experience Q times stronger micromotion, the corresponding signal is also Q times stronger, allowing micromotion compensation to a level comparable to singly charged ions. Therefore, excess micromotion will not pose a limitation to optical frequency standards based on HCI as long as the stray electric fields in the cryogenic environment remain sufficiently constant between micromotion probe cycles, which will be subject to future investigations.

Micromotion contributes to the second-order Doppler shift in the radial direction as discussed in Sec. VII.D.3, Eq. (15). In thermal equilibrium with the sympathetic cooling ion, the second-order Doppler shift of HCI from secular motion and intrinsic micromotion is identical to singly charged ions. However, the oscillating electric field also leads to an ac Stark shift of the clock states as discussed in Sec. VII.D.2. This shift depends on the differential polarizability $\Delta\alpha_S$ between the two clock states. One can show that both shifts exhibit the same scaling with the oscillating field E_{rf} at the position of the ion. For some ion species, such as Ca^+ and Sr^+ with negative $\Delta\alpha_S$, a so-called "magic" rf drive frequency exists, for which both shifts cancel (Dubé *et al*, 2014; Huang *et al*, 2017). In the case of HCI, the polarizability of individual states and thus the differential polarizability is smaller compared to singly charged ions owing to the smaller size of electron orbitals. Therefore, the total micromotion-induced ac Stark shift in HCI-based optical clocks is typically smaller compared to singly charged ion clocks and could even be made to vanish in case a sufficiently large negative $\Delta\alpha_S$ is found.

5. Collisional shifts

Collisions with residual background gas atoms can result in a transient distortion of the electronic energy levels and thus to a shift in the clock transition frequency. An upper bound to this frequency shift $|\Delta\omega| \leq \sqrt{\gamma_g \gamma_e}$ is given by the total collision rates γ_g, γ_e for the ion in the ground and excited state, respectively (Vutha, Kirchner, and Dubé, 2017). These rates can be either calculated from scattering theory or measured experimentally by observing decrystallization and reordering of a two-ion crystal (Rosenband *et al*, 2008). Since HCI are operated at cryogenic temperatures, background gas pressure is significantly reduced compared to room-temperature setups, thus minimizing collisional shifts. Furthermore, collisions of neutral background gas atoms or molecules with a

HCI almost always result in charge-transfer reactions, with the HCI capturing one electron from its neutral collision partner at a relatively far distance of several atomic units. The sudden mutual repulsion of the ionized neutral and the HCI imparts a momentum kick to both particles, and this usually removes the downcharged HCI from the trap. In this case the systematic uncertainty from collisional shifts vanishes.

E. Evaluation of HCI clock candidates

In this section, we assess HCI candidates proposed for optical clocks and frequency references. Ideally, HCI clock candidates outperform their neutral and singly charged counterparts in the atomic properties that are responsible for systematic frequency shifts and the statistical uncertainty of the clock. Unfortunately, for many of the HCI candidates proposed as optical clock references not enough atomic data for a proper evaluation are available. This illustrates the strong demand for more detailed and more accurate atomic structure calculations and measurements. Therefore, we provide a list of primary clock ion selection criteria and order of magnitude values for the most important atomic parameters, inspired by Al^+ and Yb^+, two of the currently most advanced ion clock candidates:

- a clock transition in a range accessible by current laser technology, i.e., 200 nm − 2 μm;
- a transition with a large quality factor, i.e., high transition frequency and a long-lived excited state with a lifetime time $\gtrsim$1 s to provide high stability;
- a small linear Zeeman shift coefficient, i.e., $|C_{M1}| \lesssim 100$ kHz/mT;
- a small quadratic Zeeman shift coefficient, i.e., $|C_{M2}| \lesssim 100$ Hz/mT^2;
- a small electric-quadrupole moment Θ, i.e., $|\Theta| \lesssim 0.1 e a_0^2$;
- a small differential polarizability, i.e., $|\Delta\alpha_S| \lesssim 10^{-41}$ Jm^2/V^2;
- a sparse level structure to simplify initial state preparation and laser complexity; and
- long-lived isotopes with a lifetime of many days, or longer.

The second requirement is often neglected in the literature. Assuming a transition wavelength of 500 nm (transition frequency $\nu_0 = 600$ THz) and an excited state lifetime of $\tau = 1$ s, we get according to Eq. (10) an instability of $\sigma_y(T) \approx 7 \times 10^{-16}/\sqrt{t/\mathrm{s}}$. This already corresponds to an averaging time of 5.5 days to achieve a relative frequency uncertainty of 10^{-18} for the measurement. As a consequence, ions with an excited clock state lifetime exceeding 1 s are required to achieve uncertainties within practical averaging times. However, the linewidth of the clock transition should not be too small, since it would require significant laser intensities for excitation, possibly inducing ac Stark shifts similar to the Yb^+ octupole transition (Huntemann *et al*, 2012).

Despite the lack of atomic structure data, some general guidelines for suitable clock transitions are at hand and can be applied with caution, since exceptions may exist:

- a vanishing electronic spin or the availability of a $m = 0 \to m' = 0$ transition to eliminate the linear Zeeman shift,
- small total angular momentum to reduce the number of hyperfine levels and magnetic substructure which simplifies initial state preparation and minimizes second-order Zeeman and tensorial shifts, and
- large fine- and hyperfine-structure splittings to reduce second-order Zeeman and ac Stark shifts.

In addition to the primary criteria, one might apply secondary criteria such as the availability of a cooling transition, known level structure from experiment or accurate atomic structure calculations. Particularly important for possible applications is the sensitivity of the clock transition to a change in fundamental constants, QED tests, or other physics beyond the standard model. This results in a trade-off between achievable accuracy and the sensitivity to such effects.

In the following, we discuss some selected species representative of a whole class of HCI with slightly different properties. In this assessment, we took into account the atomic properties where available and discuss possible cancellation techniques that will further reduce systematic frequency shifts. When referring to classes of HCI, in particular, for which no atomic data are available, we apply the scaling laws previously discussed. Qualifiers for the magnitude of the shifts are relative to typical atomic parameters for singly charged ions, which are considered to be "large" in this comparison.

1. Hyperfine transitions

Optical clocks based on $M1$ hyperfine transitions in selected HCI have been discussed by Schiller (2007) and Yudin, Taichenachev, and Derevianko (2014). All of the investigated species with transitions between the $F = 0 \leftrightarrow F = 1$ hyperfine components of the $^2S_{1/2}$ electronic ground state with nuclear spin $I = 1/2$ have very favorable atomic properties concerning systematic frequency shifts. They have no electric-quadrupole moment, feature a vanishing first-order Zeeman shift by employing a $m = 0 \to m' = 0$ transition and have a very small second-order Zeeman coefficient C_{M2}, since the hyperfine splitting is large compared to any Zeeman shift (see Sec. VII.D.1). Since all dipole-allowed transitions are in the XUV wavelength regime, only a small differential polarizability arises from $M1$ couplings between hyperfine components (Itano, Lewis, and Wineland, 1982). As a consequence, all electric and magnetic field shifts are extremely small with a fractional frequency uncertainty below 10^{-20}, rendering HCI based on hyperfine transitions ideal candidates for high-accuracy clocks. The only drawback in these systems is the achievable statistical uncertainty, since either the transition frequency is low with a long excited state lifetime or vice versa. The longest investigated excited state lifetime for a transition near the optical regime is that of $^{171}Yb^{69+}$ with a transition wavelength of 2160 nm and an excited state lifetime of 0.37 s (Yudin, Taichenachev, and Derevianko, 2014). The achievable instability of $\sigma_y(\tau) \approx 4.9 \times 10^{-15}/\sqrt{t/\mathrm{s}}$ (Peik, Schneider, and Tamm, 2006) is better by more than an order of magnitude compared to the best Cs fountain clocks. Given the high sensitivity of hyperfine transitions to changes in μ, X_q, and α, as discussed in Sec. II, HCI clocks based on these transitions could help to significantly improve bounds on a possible variation of these

quantities compared to what is currently possible with measurements involving Cs clocks. Since only motional and collisional frequency shifts have to be evaluated, they represent a promising starting point for HCI-based clocks.

2. Fine-structure transitions

At more moderate charge states, fine-structure transitions in the optical regime can be found and optical clocks based on one-valence electron (OVE) $^2P_{1/2} \leftrightarrow {}^2P_{3/2}$ $(I = 3/2)$ and two-valence electrons (TVE) $^3P_0 \leftrightarrow {}^3P_1$ $(I = 1/2)$ transitions have been investigated by Yudin, Taichenachev, and Derevianko (2014). The sensitivity to frequency shifting effects is typically an order of magnitude larger compared to the hyperfine clocks discussed in the previous section. The electric-quadrupole shift is nonzero for the excited clock state of the OVE systems. However, it can be made small by a proper choice of hyperfine components [see Eq. (14)]. Currently no estimates on the actual value of the quadrupole moment exist that would allow a proper evaluation of this shift. While for the OVE species $m_F = 0 \to m_F' = 0$ transitions are available, the large electronic linear Zeeman shift needs to be canceled by averaging suitable combinations of m_F transitions for the TVE systems. As a consequence of the smaller hyperfine splitting, the second-order Zeeman effect and $M1$ transition-induced differential polarizability are larger compared to the hyperfine transition clocks, but still significantly smaller compared to clocks based on neutral or singly charged atoms. Transitions between the $^2F_{5/2} \leftrightarrow {}^2F_{7/2}$ fine structure in $^{184}W^{13+}$ $(I = 1/2)$ and $^{191}Ir^{16+}$ $(I = 3/2)$ have been investigated by Nandy and Sahoo (2016). These transitions share the properties of the OVE systems discussed and exhibit nonzero electric-quadrupole moments on the order of $0.015ea_0^2$ that are smaller by a factor of 4 compared to the Yb^+ excited clock state due to common mode suppression between ground and excited state.

While the accuracy of clocks based on fine-structure transitions is very promising, their achievable statistical uncertainty is a limiting factor. The best instability of $\sigma_y(t) \approx 3.2 \times 10^{-15}/\sqrt{t/\mathrm{s}}$ for the OVE species is found for $^{79,81}Br^{4+}$ with an excited state lifetime of $\tau \approx 0.5$ s and a transition wavelength of $\lambda \approx 1642$ nm. A similar instability of $\sigma_y(t) \approx 4 \times 10^{-15}/\sqrt{t/\mathrm{s}}$ is achieved by the TVE system $^{123,125}Te^{2+}$ with an excited state lifetime of $\tau \approx 0.51$ s and a transition wavelength of $\lambda \approx 2105$ nm.

3. Level-crossing transitions

The largest investigated group of HCI optical clock candidates is based on level-crossing transitions (Berengut *et al*, 2012a). Many of them feature a large sensitivity to a change in the fine-structure constant (Berengut, Dzuba, and Flambaum, 2010; Berengut *et al*, 2011, 2012b), which was the original motivation to study them and is discussed in more detail in Sec. II. This group can be divided into one-valence electron systems for which atomic structure calculations can provide estimates of the atomic properties required for a proper evaluation of the clock candidates, and systems with a more complicated electronic structure for which accurate data are currently unavailable. HCI clock candidates belonging to the former group include Nd^{13+} and Sm^{15+} (Ag-like isoelectronic sequence) that have optical transitions between the $5s_{1/2} \leftrightarrow 4f_{7/2}$ electronic states at wavelengths of 170 and 180 nm, respectively, and excited state lifetimes of several days with zero nuclear spin $(I = 0)$ (Dzuba, Derevianko, and Flambaum, 2012b); see also Fig. 2. A partial systematic frequency shift evaluation reveals (Dzuba, Derevianko, and Flambaum, 2012b) that the differential polarizability is with $\Delta\alpha_S \sim 10^{-41}$ $\mathrm{Jm^2/V^2}$ comparable to the Al^+ polarizability, the large linear electronic Zeeman shift needs to be canceled by averaging suitable transitions, whereas the second-order Zeeman shift is extremely small with $C_{M2} \sim 10$ $\mathrm{mHz/mT^2}$. The electric-quadrupole moments of the $4f_{5/2}$ states have not been calculated, thus cancellation techniques as discussed in Sec. VII.D.2 need to be applied. While the transition itself has only a mild sensitivity to a change in the fine-structure constant, the $4f_{5/2}$ ground state in Sm^{15+} may exhibit a large sensitivity to a violation of local Lorentz invariance (LLI) as discussed in Sec. VIII.A. Nandy and Sahoo (2016) investigated the same transition in $^{195}Pt^{17+}$ $(I = 1/2)$ at a wavelength of around 400 nm. This transition exhibits a long lifetime of 128 years, a strong linear Zeeman effect, which can be eliminated by probing $m_F = 0 \to m_F' = 0$ states, an electric-quadrupole moment of $-0.081ea_0^2$, which is comparable to the Yb^+ octupole transition, and small second-order Zeeman $(\Delta f/f \sim 1.6 \times 10^{-24})$ and polarizability $(\Delta f/f \sim 2 \times 10^{-18})$ shifts.

The larger group of HCI clocks based on level crossings contains HCI for which estimates of the atomic properties are missing. Therefore, only a qualitative assessment for selected cases is possible. All investigated species have a transition in the optical with a sufficiently long excited state lifetime, typically well exceeding 1 s. HCI with an optical level-crossing transition for the isoelectronic sequences of Ag-like, Cd-like, In-like, and Sn-like ions have been identified (Safronova *et al*, 2014a, 2014b, 2014c). The Cd-like sequence such as Nd^{12+} with $I = 0$ offers no transitions satisfying either the specified wavelength range nor excited state lifetime. Examples of the Ag-like sequence with $I = 0$ have already been discussed earlier in this section. Optical clocks based on the In-like sequence with $I = 0$ use level crossings between similar states, such as $s_{1/2}/p_{1/2}$ and $f_{5/2}/f_{7/2}$, and therefore will share similar properties: a large linear and a small quadratic Zeeman shift, a nonzero electric-quadrupole moment, and small polarizabilities. Species with hyperfine structure will in general have worse properties, such as larger tensorial shifts and an increased quadratic Zeeman effect, while featuring an $m_F = 0 \to m_F' = 0$ transition free of the linear Zeeman shift. A representative of the Sn-like sequence is $^{141}Pr^{9+}$ with $I = 5/2$ shown in Fig. 6. It features several long-lived excited states at laser-accessible wavelengths. The $^3P_0$ ground state is free of a first-order electric-quadrupole shift, and exhibits only small linear and quadratic Zeeman shifts. However, the $^3G_3$ and $^3F_2$ excited clock states have nonvanishing electric-quadrupole moments, and strong linear $(J > 0)$ and medium quadratic (hyperfine splitting) Zeeman shifts.

Electron-hole transitions at the $4f - 5s$ level crossing have been proposed (Berengut *et al*, 2011) and experimentally investigated (Windberger *et al*, 2015; Bekker, 2017) for the

case of Ir^{17+}. The single-hole system Ir^{16+} has a transition of unknown linewidth at 267 nm between the $^2F_{7/2} \leftrightarrow {}^2S_{1/2}$ states (Bekker, 2017) with a nonvanishing electric-quadrupole moment. Hyperfine structure ($I = 3/2$) results in a linear Zeeman-free $m_F = 0 \rightarrow m_F' = 0$ transition with second-order Zeeman shift. The double-hole system Ir^{17+} features several transitions of unknown linewidth in the optical, the lowest being at 1415.6 nm between the $^3F_4^0 \leftrightarrow {}^3H_6$ states (Bekker, 2017) with nonvanishing electric-quadrupole moment. All transitions exhibit an electronic linear Zeeman shift and a hyperfine-induced second-order Zeeman shift. However, of all considered stable atomic systems, the transitions in Ir^{17+} feature the largest sensitivity to a change in the fine-structure constant.

A HCI with even more complex electronic structure investigated as an optical clock candidate is Ho^{14+} (Dzuba, Flambaum, and Katori, 2015). A transition at around 400 nm connects the $^8F_{1/2} \leftrightarrow {}^6H_{5/2}$ states with nonvanishing electric-quadrupole moment. The excited state has an estimated lifetime of around 37 s, mostly from $E1$ decay into other states. While the nuclear spin of $I = 7/2$ enables a $m_F = 0 \rightarrow m_F' = 0$ transition free of the linear Zeeman effect, the large number of hyperfine levels and small hyperfine splitting will result in a large second-order Zeeman shift and complicates state initialization.

4. Intraconfiguration transitions

Another category of HCI for optical clocks is based on optical intraconfiguration transitions in the $4f^{12}$ shell that have been investigated with (Derevianko, Dzuba, and Flambaum, 2012) and without (Dzuba, Derevianko, and Flambaum, 2012a) hyperfine structure. One example with hyperfine structure is $^{209}Bi^{25+}$ with $I = 9/2$ and a transition between the $^3H_6 \leftrightarrow {}^3F_4$ states with an excited state lifetime of about 3 h. This transition features a very small differential polarizability, large linear and quadratic Zeeman shifts, and a quadrupole moment up to 4 times larger compared to the Yb^+ F state. Through a proper choice of transition, the effective quadrupole moment can be reduced by 2 orders of magnitude, at the expense of complicated state initialization. While the transition is not particularly sensitive to a change in fundamental constants, the large angular momentum may exhibit a high sensitivity to a violation of LLI as discussed in Sec. VIII.A. HCI species of this kind without hyperfine structure ($I = 0$) have a much simpler level structure and consequently smaller quadratic Zeeman shift (Dzuba, Derevianko, and Flambaum, 2012a). All other properties are similar compared to the case with hyperfine structure, except that a more conventional electric-quadrupole suppression technique (see Sec. VII.D.2) has to be employed.

F. Evaluation summary

All discussed HCI clock candidates have rich features and partially fulfill the primary criteria previously listed. However, it remains an open challenge to obtain sufficient information about the atomic properties of most of the species that would allow a full assessment of their systematic frequency shifts and enable identification of a superior candidate. By employing systematic shift cancellation schemes, such as magic-drive frequency operation and averaging the frequencies of all Zeeman components, all linear magnetic- and tensorial electric-field shifts can be significantly suppressed and likely brought to a level below the current best singly charged ion optical clocks. This opens up exciting prospects for testing fundamental physics with HCI. As an example, transitions in Ir^{17+} (Berengut *et al*, 2011) and Cf^{15+}/Cf^{17+} have more than a factor of 20 higher sensitivity to a change in the fine-structure constant α compared to the Yb^+ $E3$ transition, which is the most sensitive system currently employed. Similarly, HCI clocks based on hyperfine transitions are sensitive to a change in the electron-to-proton mass ratio, providing more than an order of magnitude better statistical uncertainty compared to the currently employed Cs clocks. Other optical transitions in HCI may not be well suited for clocks with ultimate performance, but rather are sensitive to other new physics effects as discussed in the next section. Improving the bounds on such effects using HCI with their high sensitivity might turn out to be a much more efficient approach compared to improving the systematic uncertainty of conventional neutral or singly charged atom clocks and performing frequency comparisons at a challenging level of below 10^{-18}.

VIII. OTHER APPLICATIONS AND FUTURE DEVELOPMENTS

A. Tests of local Lorentz invariance

LLI is one of the cornerstones of modern physics: the outcome of any local nongravitational experiment is independent of the velocity and the orientation of the freely falling apparatus. The recent interest in tests of Lorentz symmetry is motivated by theoretical developments in quantum gravity suggesting that Lorentz symmetry may be violated at some energies, tremendous progress in experimental precision, and development of a theoretical framework to analyze different classes of experiments. Separate violations of LLI are possible for each type of particle, and the experiments include searches for Lorentz violation (LV) in the matter, photon, neutrino, and gravity sectors. In this section, we limit the discussion to specific LLI tests relevant to HCI applications.

Lorentz violation tests are analyzed in the context of an effective field theory known as the standard model extension (SME). The *Data Tables for Lorentz and CPT Violation* by Kostelecký and Russell (2011, 2017) gave tables of the measured and derived values of coefficients for Lorentz and *CPT* violation in the SME. In minimal SME, the standard model Lagrangian is augmented with every possible combination of the SM fields that are not term-by-term Lorentz invariant, while maintaining gauge invariance, energy-momentum conservation, and Lorentz invariance of the total action (Colladay and Kostelecký, 1998). A general expression for the quadratic Hermitian Lagrangian density describing a single spin-1/2 Dirac fermion of mass m (electron, proton, or neutron) in the presence of Lorentz violation is given by (Kostelecký and Lane, 1999)

$$\mathcal{L} = \tfrac{1}{2} ic\bar{\psi}\Gamma_\nu \overleftrightarrow{\partial^\nu}\psi - Mc^2\bar{\psi}\psi, \tag{17}$$

where ψ is a four-component Dirac spinor, c is the speed of light in a vacuum, $f\overleftrightarrow{\partial^\nu}g = f\partial^\nu g - g\partial^\nu f$,

$$M = m + a_\mu\gamma^\mu + b_\mu\gamma_5\gamma^\mu + \tfrac{1}{2}H_{\mu\nu}\sigma^{\mu\nu}, \tag{18}$$

and

$$\Gamma_\nu = \gamma_\nu + c_{\mu\nu}\gamma_\nu + d_{\mu\nu}\gamma_5\gamma_\nu + e_\nu + i\gamma_5 f_\nu + \tfrac{1}{2}g_{\lambda\mu\nu}\sigma_{\lambda\mu}. \tag{19}$$

The γ_μ are Dirac matrices, $\mu = 0, 1, 2, 3$, γ_5 is a Dirac matrix associated with pseudoscalars, and $\sigma^{\mu\nu} = (i/2)(\gamma^\mu\gamma^\nu - \gamma^\nu\gamma^\mu)$. The first terms in the expressions for M and Γ_ν give the usual SM Lagrangian. Lorentz violation is quantified by the parameters a_μ, b_μ, $c_{\mu\nu}$, $d_{\mu\nu}$, e_μ, f_μ, $g_{\lambda\mu\nu}$, and $H_{\mu\nu}$. The coefficients in Eq. (18) have dimensions of mass; the coefficients in Eq. (19) are dimensionless. The framework of interpreting the laboratory experiments involving monitoring atomic or nuclear frequencies in terms of the SME coefficients has been described in detail by Kostelecký and Lane (1999) and Kostelecký and Mewes (2002).

Violations of Lorentz invariance in bound electronic states result in a perturbation of the Hamiltonian that can be described by (Kostelecký and Lane, 1999; Hohensee *et al*, 2013)

$$\delta H = -\left(C_0^{(0)} - \frac{2U}{3c^2}c_{00}\right)\frac{\mathbf{p}^2}{2m_e} - \frac{1}{6m_e}C_0^{(2)}T_0^{(2)}, \tag{20}$$

where $\mathbf{p}$ is the momentum of a bound electron. The second term in the parentheses gives the leading order gravitational redshift anomaly in terms of the Newtonian potential U. The parameters $C_0^{(0)}$ and $C_0^{(2)}$ are elements of the $c_{\mu\nu}$ tensor in the laboratory frame introduced by Eq. (19):

$$C_0^{(0)} = c_{00} + (2/3)c_{jj}, \tag{21}$$

$$C_0^{(2)} = c_{jj} + (2/3)c_{33}, \tag{22}$$

where $j = 1, 2$, and 3.

The nonrelativistic form of the $T_0^{(2)}$ operator is $T_0^{(2)} = \mathbf{p}^2 - 3p_z^2$. Predicting the energy shift due to LV involves the calculation of the expectation value of the Hamiltonian (20) for the atomic states of interest. The larger the matrix elements, the more sensitive is this atomic state. In atomic experiments aimed at the LLI tests in the electron-photon sector (Hohensee *et al*, 2013; Pruttivarasin *et al*, 2015), one searches for variations of the atomic energy levels when the orientation of the electronic wave function rotates with respect to a standard reference frame, such as the Sun centered celestial-equatorial frame. The rotation is simply supplied by Earth's daily and annual periodic motion.

Pruttivarasin *et al* (2015) performed a test of Lorentz symmetry using an electronic analog of a Michelson-Morley experiment using the $^2D_{5/2}$ atomic states of $^{40}Ca^+$ ion with anisotropic electron momentum distributions. A pair of $^{40}Ca^+$ ions was trapped in a linear Paul trap, with a static magnetic field applied, defining the eigenstates of the system. The direction of this magnetic field changes with respect to the Sun as the Earth rotates. The Lorentz violation effects depend on the magnetic quantum number m_J. A test of LLI can be performed by monitoring the frequency difference between the LV shifts of the $m_J = 5/2$ and $1/2$ substates of the $3d^2D_{5/2}$ manifold

$$\frac{1}{h}(E_{m_J=5/2} - E_{m_J=1/2}) = [-4.45(9)\times 10^{15}\ \text{Hz}]\times C_0^{(2)} \tag{23}$$

as the Earth rotates. The Ca^+ experiment improved the limits to the c_{JK} coefficients (J, $K = 1$, 2, and 3) of the LV violation in the electron-photon sector to the 10^{-18} level.

Further significant improvement of the LV constraints with such experiments requires another system with a long-lived or ground state that has a large $\langle j|T_0^{(2)}|j\rangle$ matrix element. Dzuba *et al* (2016) and Shaniv *et al* (2018) calculated this matrix element in a variety of systems and identified the $4f^{13}6s^2\,^2F_{7/2}$ state of Yb^+ and HCI as systems with large sensitivities to violation of LLI. HCI ions of interest are among those already proposed for the tests of the α variation. The advantage of HCI for LLI tests is the possibility to use a ground rather than an excited state as the LLI probe state. The matrix elements $\langle j|T_0^{(2)}|j\rangle$ for some HCI listed in Shaniv *et al* (2018) are more than a factor of 50 larger than for Ca^+ and exceed those for the Yb^+ $^2F_{7/2}$ state. An experimental scheme for a search of Lorentz violation with HCI is described by Shaniv *et al* (2018).

B. Probing for new forces

Motivated by the failure of the standard model to describe dark matter or dark energy, searches for possible candidate fields or other, yet unidentified fields and their nongravitational effects on atoms and molecules have commenced (Safronova *et al*, 2018). Precision spectroscopy measurements allow searches for new light scalar fields and constraining their couplings to ordinary matter (Ficek *et al*, 2017). Recently, a technique based on isotope shift spectroscopy has been proposed to probe for such fields that mediate forces, e.g., between electrons and neutrons (Delaunay and Soreq, 2016; Frugiuele *et al*, 2016; Delaunay, Frugiuele *et al*, 2017; Delaunay, Ozeri *et al*, 2017; Berengut *et al*, 2018; Flambaum, Geddes, and Viatkina, 2018). The idea is based on the observation of King (1963) that appropriately scaled isotope shifts of two transitions exhibit a linear dependence. An additional force between neutrons and electrons would break this linearity. Two major effects result in a change of the transition frequency of a selected transition with the neutron number: the field and mass shifts. The field shift arises from a difference in the nuclear charge radius for the two isotopes. This results in a change in the overlap of the wave functions of the involved electronic states with the nuclear charge distribution and thus a change in their binding energy. The mass shift takes into account the change in recoil upon photon absorption by the electrons bound to the nucleus. Neglecting higher-order effects, the isotope shift of transition i between isotopes A and A' can thus be written as (Heilig and Steudel, 1974)

$$\delta\nu_i^{A,A'} = F_i\delta\langle r^2\rangle_{A,A'} + k_i\frac{A - A'}{AA'}, \tag{24}$$

where F_i and k_i are the field and mass shift constants, respectively, and $\delta\langle r^2\rangle$ is the change in the nuclear charge

radius. While optical spectroscopy can achieve very high fractional resolutions of better than 10^{-17}, the change in nuclear charge radius is much less well known. By measuring at least two transitions i, i' and introducing the modified isotope shift $m\delta\nu_i = \delta\nu_i^{A,A'}[AA'/(A+A')]$, the dependence on $\delta\langle r^2\rangle$ can be eliminated:

$$m\delta\nu_i = \frac{F_i}{F_i'} m\delta\nu_i' + k_i k_i' \frac{F_i}{F_i'}. \tag{25}$$

Plotting the two modified isotope shifts in one graph has become known as a King plot (King, 1963). A hypothetical new force carrier represented by a scalar field ϕ mediated by an unknown particle with mass m_ϕ that couples to neutrons and electrons adds an additional term to Eq. (24) (Berengut *et al*, 2018):

$$\delta\nu_i^{A,A'} = F_i \delta\langle r^2\rangle_{A,A'} + k_i \frac{A-A'}{AA'} + \alpha_{\mathrm{NP}} X_i \gamma_{AA'}. \tag{26}$$

In this equation, α_{NP} is the new physics coupling constant, X_i depends on the form of the potential of the scalar field ϕ, while $\gamma_{AA'}$ depends only on nuclear properties. The additional frequency shift for a single transition will in general result in nonlinearity in Eq. (25) that could be bounded experimentally by measuring at least two transitions on at least four even isotopes (without hyperfine structure). The highest sensitivity is obtained when comparing transitions for which two of the electronic states have very different orbitals to maximize the differential effect. To be able to distinguish between higher-order nuclear effects and α_{NP}, the range of the scalar field should be larger than the size of the nucleus. The sensitivity for massive fields is enhanced for electron orbitals that are concentrated just outside the nucleus. As a consequence, narrow optical transitions between electronic state of different character in HCI are ideal for this purpose. However, even fine or hyperfine transitions can serve as narrow reference lines when combined with transitions in neutral or singly charged atoms. Possible candidates for which narrow lines and at least four stable isotopes exist are Yb and, in particular, Ca, since experimental data for Ca^+ are already available (Gebert *et al*, 2015; Shi *et al*, 2017; Solaro *et al*, 2017). Once nonlinearities in the King plot have been observed, the challenge remains to isolate α_{NP} from all other standard physics higher-order effects neglected in Eq. (24) (Flambaum, Geddes, and Viatkina, 2018).

C. Toward higher transition frequencies

Science based on frequency metrology experienced a tremendous boost with the development of optical frequency combs which enabled the counting and comparison of optical frequencies (Hall, 2006; Hänsch, 2006). Moving from microwave to optical frequencies implies a 4 order of magnitude gain in statistical uncertainty according to Eq. (9) for the same probe time. One may ask if a similar jump can be envisioned by again going higher in photon energy, say into the VUV or soft x-ray range. The main obstacle for this in the realm of atoms and singly charged ions (Rosenband *et al*, 2008; Wolf *et al*, 2009; Wübbena *et al*, 2012) as x-ray clocks is the ionization of such systems under irradiation. Ions in higher charge states overcome this limitation and offer both allowed and forbidden transitions, the latter with suitably long lifetimes. Recent developments of VUV frequency combs based on high-harmonic sources (Gohle *et al*, 2005; Jones *et al*, 2005; Yost, Schibli, and Ye, 2008) have paved the way for the extension of the current photon-metrology methods by at least 1 order of magnitude. In view of the very rapid developments in this field, one can expect that within a few years the same quality of combs becomes available at wavelengths of a few nm. By then, the methods of trapping and cooling of HCI have to be sufficiently improved to take full advantage of the exquisite frequency control at the 10^{18} Hz range.

The main advantage of x-ray clocks is their improved statistical uncertainty according to Eq. (9) for the same probe times. However, this will put stringent requirements to the phase coherence of the probe laser and its delivery all the way to the ion. To take full advantage of the improved statistical uncertainty, systematic shifts need to be suppressed using advanced schemes developed in the context of quantum-information processing. Examples are decoherence-free subspaces (Kielpinski *et al*, 2001; Roos *et al*, 2006; Pruttivarasin *et al*, 2015) or other correlation-based measurement schemes (Chwalla *et al*, 2007).

A long-term perspective for the development of the field can be drawn along the following lines: The development of VUV and soft x-ray frequency combs will enable HCI frequency standards as well as HCI probes for fundamental physics in this wavelength regime, supported by quantum-computing-based control schemes for systematic shift suppression and advanced sensing schemes.

IX. CONCLUSION

Stimulating the further development of ideas for new applications of highly charged ions enabled by rapidly improving control of these systems is the central aim of this work. We hope that this review will assist in promoting further rapid experimental progress, and that it will also serve to bring together the HCI and laser-cooled trapped ion communities, which have been previously somewhat disjoint due to very distinct experimental approaches. On the background of earlier theoretical and experimental work, we discussed novel developments and their implications for the future. Based on recent developments, exciting new avenues of research are opened by the use of cold HCI in such diverse applications as tests of fundamental physics, metrology, development of frequency combs, and quantum information.

ACKNOWLEDGMENTS

We thank Steven King, Peter Micke, Andrei Nefiodov, Natalia Oreshkina, Sergey Porsev, and John Webb for helpful comments on the manuscript. M. G. K. acknowledges support from the Russian Foundation for Basic Research under Grant No. 17-02-00216. M. S. S. acknowledges support of the Office of Naval Research, USA, under Award No. N00014-17-1-2252. J. R. C. L.-U. acknowledges support by the DFG Collaborative Research Centre SFB 1225 (ISOQUANT). P. O. S. acknowledges support from PTB and DFG through SCHM2678/5-1 and the Collaborative Research Centre

(Sonderforschungsbereich) SFB 1227 DQ-*mat*, project B03. This project has received funding from the European Metrology Programme for Innovation and Research (EMPIR) co-financed by the Participating States and from the European Union's Horizon 2020 research and innovation programme (Project No. 17FUN07 CC4C and No. 15SIB03 OC18).

REFERENCES

Akhiezer, A. I., and V. B. Berestetskii, 1965, *Quantum Electrodynamics* (Interscience Publishers, New York).

Ali, R., C. P. Bhalla, C. L. Cocke, M. Schulz, and M. Stockli, 1991, "Dielectronic recombination on and electron-impact excitation of heliumlike argon," Phys. Rev. A **44**, 223.

Ali, R., C. P. Bhalla, C. L. Cocke, and M. Stockli, 1990, "Dielectronic recombination on heliumlike argon," Phys. Rev. Lett. **64**, 633.

Allan, D. W., 1966, "Statistics of atomic frequency standards," Proc. IEEE **54**, 221.

Allen, F. I., C. Biedermann, R. Radtke, and G. Fussmann, 2007, "Charge exchange of highly charged argon ions as a function of projectile energy," J. Phys. Conf. Ser. **58**, 188.

Amaro, P., S. Schlesser, M. Guerra, E.-O. Le Bigot, J.-M. Isac, P. Travers, J. P. Santos, C. I. Szabo, A. Gumberidze, and P. Indelicato, 2012, "Absolute measurement of the relativistic magnetic dipole transition energy in heliumlike argon," Phys. Rev. Lett. **109**, 043005.

Amaro, Pedro, Chintan Shah, Rene Steinbrügge, Christian Beilmann, Sven Bernitt, José R. Crespo López-Urrutia, and Stanislav Tashenov, 2017, "State-selective influence of the Breit interaction on the angular distribution of emitted photons following dielectronic recombination," Phys. Rev. A **95**, 022712.

Andreev, O. V., D. A. Glazov, A. V. Volotka, V. M. Shabaev, and G. Plunien, 2012, "Evaluation of the screened vacuum-polarization corrections to the hyperfine splitting of Li-like bismuth," Phys. Rev. A **85**, 022510.

Andreev, O. Yu, L. N. Labzowsky, G. Plunien, and G. Soff, 2001, "QED calculation of the interelectron interaction in two- and three-electron ions," Phys. Rev. A **64**, 042513.

Arianer, J., E. Baron, M. Brient, A. Cabrespine, A. Liebe, A. Sérafini, and T. Ton That, 1975, "Multiply charged ion source," Nucl. Instrum. Methods **124**, 157.

Arianer, J., and C. Goldstein, 1976, "The Orsay electron beam ion source," IEEE Trans. Nucl. Sci. **23**, 979.

Artemyev, A. N., T. Beier, G. Plunien, V. M. Shabaev, G. Soff, and V. A. Yerokhin, 1999, "Vacuum-polarization screening corrections to the energy levels of lithiumlike ions," Phys. Rev. A **60**, 45.

Artemyev, A. N., V. M. Shabaev, M. M. Sysak, V. A. Yerokhin, T. Beierand, G. Plunien, and G. Soff 2003, "Evaluation of the two-photon exchange diagrams for the $1s^2 2p_{3/2}$ electron configuration in Li-like ions," Phys. Rev. A **67**, 062506.

Artemyev, A. N., V. M. Shabaev, I. I. Tupitsyn, G. Plunien, and V. A. Yerokhin, 2007, "QED calculation of the $2p_{3/2} - 2p_{1/2}$ transition energy in boronlike argon," Phys. Rev. Lett. **98**, 173004.

Artemyev, A. N., V. M. Shabaev, and V. A. Yerokhin, 1995a, "Nuclear recoil corrections to the $2p_{3/2}$ state energy of hydrogen-like and high-Z lithium-like atoms in all orders in αZ," J. Phys. B **28**, 5201.

Artemyev, A. N., V. M. Shabaev, and V. A. Yerokhin, 1995b, "Relativistic nuclear recoil corrections to the energy levels of hydrogenlike and high-Z lithiumlike atoms in all orders in αZ," Phys. Rev. A **52**, 1884.

Artemyev, A. N., V. M. Shabaev, V. A. Yerokhin, G. Plunien, and G. Soff, 2005, "QED calculation of the $n = 1$ and $n = 2$ energy levels in He-like ions," Phys. Rev. A **71**, 062104.

Arvanitaki, Asimina, Junwu Huang, and Ken Van Tilburg, 2015, "Searching for dilaton dark matter with atomic clocks," Phys. Rev. D **91**, 015015.

Ashkin, A., 1978, "Trapping of atoms by resonance radiation pressure," Phys. Rev. Lett. **40**, 729.

Aspect, A., J. Dalibard, A. Heidmann, C. Salomon, and C. Cohen-Tannoudji, 1986, "Cooling atoms with stimulated emission," Phys. Rev. Lett. **57**, 1688.

Aumayr, F., H. Kurz, D. Schneider, M. A. Briere, J. W. McDonald, C. E. Cunningham, and H. P. Winter, 1993, "Emission of electrons from a clean gold surface induced by slow, very highly charged ions at the image charge acceleration limit," Phys. Rev. Lett. **71**, 1943.

Back, T. V., H. S. Margolis, P. K. Oxley, J. D. Silver, and E. G. Myers, 1998, "Laser spectroscopy of the $1s^2 2s2p\ ^3P_2 - ^3P_1$ transition in beryllium-like argon using the Oxford EBIT," Hyperfine Interact. **114**, 203.

Barcons, X., *et al.*, 2017, "Athena: Esa's x-ray observatory for the late 2020s," Astron. Nachr. **338**, 153.

Barrett, M., *et al.*, 2003, "Sympathetic cooling of $^9Be^+$ and $^{24}Mg^+$ for quantum logic," Phys. Rev. A **68**, 042302.

Bashkin, S., 1968, "Beam foil spectroscopy," Appl. Opt. **7**, 2341.

Bechtold, V., N. Chan-Tung, S. Dousson, R. Geller, B. Jacquot, and Y. Jongen, 1980, "ECR ion source for multiply-charged oxygen beams," Nucl. Instrum. Methods **178**, 305.

Beier, T., L. Dahl, H.-J. Kluge, C. Kozhuharov, W. Quint, and HITRAP Collaboration, 2005, "Trapping ions of hydrogen-like uranium: The HITRAP project at GSI," Nucl. Instrum. Methods Phys. Res., Sect. B **235**, 473.

Beier, T., P. J. Mohr, H. Persson, and G. Soff, 1998, "Influence of nuclear size on QED corrections in hydrogenlike heavy ions," Phys. Rev. A **58**, 954.

Beiersdorfer, P., 2003, "Laboratory X-ray astrophysics," Annu. Rev. Astron. Astrophys. **41**, 343.

Beiersdorfer, P., 2010, "Testing QED and atomic-nuclear interactions with high-Z ions," J. Phys. B **43**, 074032.

Beiersdorfer, P., 2015, "Highly charged ions in magnetic fusion plasmas: research opportunities and diagnostic necessities," J. Phys. B **48**, 144017.

Beiersdorfer, P., H. Chen, D. B. Thorn, and E. Träbert, 2005, "Measurement of the two-loop Lamb shift in lithiumlike U^{89+}," Phys. Rev. Lett. **95**, 233003.

Beiersdorfer, P., J. Crespo López-Urrutia, V. Decaux, K. Widmann, and P. Neill, 1997, "Polarization spectroscopy of x-ray transitions from beam-excited highly charged ions," Rev. Sci. Instrum. **68**, 1073.

Beiersdorfer, P., S. R. Elliott, J. Crespo López-Urrutia, and K. Widmann, 1997, "Measurements of nuclear parameters of high-Z isotopes performed on a high-energy electron beam ion trap," Nucl. Phys. A **626**, 357.

Beiersdorfer, P., R. E. Olson, G. V. Brown, H. Chen, C. L. Harris, P. A. Neill, L. Schweikhard, S. B. Utter, and K. Widmann, 2000, "X-ray emission following low-energy charge exchange collisions of highly charged ions," Phys. Rev. Lett. **85**, 5090.

Beiersdorfer, P., A. Osterheld, S. R. Elliott, M. H. Chen, D. Knapp, and K. Reed, 1995, "Structure and Lamb shift of $2s_{1/2} - 2p_{3/2}$ levels in lithiumlike Th^{87+} through neonlike Th^{80+}," Phys. Rev. A **52**, 2693.

Beiersdorfer, P., A. L. Osterheld, V. Decaux, and K. Widmann, 1996, "Observation of lifetime-limited X-ray linewidths in cold highly charged ions," Phys. Rev. Lett. **77**, 5353.

Beiersdorfer, P., A. L. Osterheld, J. H. Scofield, J. R. Crespo López-Urrutia, and K. Widmann, 1998, "Measurement of QED and hyperfine splitting in the $2s_{1/2} - 2p_{3/2}$ x-ray transition in Li-like $^{209}Bi^{80+}$," Phys. Rev. Lett. **80**, 3022.

Beiersdorfer, P., T. Phillips, V. L. Jacobs, K. W. Hill, M. Bitter, S. von Goeler, and S. M. Kahn, 1993, "High-resolution measurements, line identification, and spectral modeling of K-alpha transitions in Fe XVIII-Fe XXV," Astrophys. J. **409**, 846.

Beiersdorfer, P., T. W. Phillips, K. L. Wong, R. E. Marrs, and D. A. Vogel, 1992, "Measurement of level-specific dielectronic-recombination cross sections of heliumlike Fe XXV," Phys. Rev. A **46**, 3812.

Beiersdorfer, P., L. Schweikhard, J. Crespo López-Urrutia, and K. Widmann, 1996, "The magnetic trapping mode of an electron beam ion trap: New opportunities for highly charged ion research," Rev. Sci. Instrum. **67**, 3818.

Beiersdorfer, P., E. Träbert, G. V. Brown, J. Clementson, D. B. Thorn, M. H. Chen, K. T. Cheng, and J. Sapirstein, 2014, "Hyperfine splitting of the $2s_{1/2}$ and $2p_{1/2}$ levels in Li- and Be-like ions of $^{141}_{59}Pr$," Phys. Rev. Lett. **112**, 233003.

Beiersdorfer, P., *et al.*, 2001, "Hyperfine structure of hydrogenlike thallium isotopes," Phys. Rev. A **64**, 032506.

Beiersdorfer, P., *et al.*, 2003, "Laboratory simulation of charge exchange-produced X-ray emission from comets," Science **300**, 1558.

Beiersdorfer, Peter, and Gregory V. Brown, 2015, "Experimental study of the x-ray transitions in the heliumlike isoelectronic sequence: Updated results," Phys. Rev. A **91**, 032514.

Bekker, H., 2017, private communication.

Beloy, K., D. R. Leibrandt, and W. M. Itano, 2017, "Hyperfine-mediated electric quadrupole shifts in Al^+ and In^+ ion clocks," arXiv:1701.09146.

Berengut, J. C., V. A. Dzuba, and V. V. Flambaum, 2010, "Enhanced laboratory sensitivity to variation of the fine-structure constant using highly-charged ions," Phys. Rev. Lett. **105**, 120801.

Berengut, J. C., V. A. Dzuba, and V. V. Flambaum, 2011, "Transitions in Zr, Hf, Ta, W, Re, Hg, Ac, and U ions with high sensitivity to variation of the fine-structure constant," Phys. Rev. A **84**, 054501.

Berengut, J. C., V. A. Dzuba, V. V. Flambaum, and A. Ong, 2011, "Electron-hole transitions in multiply charged ions for precision laser spectroscopy and searching for variations in α," Phys. Rev. Lett. **106**, 210802.

Berengut, J. C., V. A. Dzuba, V. V. Flambaum, and A. Ong, 2012a, "Highly charged ions with E1, M1, and E2 transitions within laser range," Phys. Rev. A **86**, 022517.

Berengut, J. C., V. A. Dzuba, V. V. Flambaum, and A. Ong, 2012b, "Optical transitions in highly charged californium ions with high sensitivity to variation of the fine-structure constant," Phys. Rev. Lett. **109**, 070802.

Berengut, Julian C., *et al.*, 2018, "Probing New Long-Range Interactions by Isotope Shift Spectroscopy," Phys. Rev. Lett. **120**, 091801.

Berkeland, D. J., J. D. Miller, J. C. Bergquist, W. M. Itano, and D. J. Wineland, 1998, "Minimization of ion micromotion in a Paul trap," J. Appl. Phys. **83**, 5025.

Bernitt, S., *et al.*, 2012, "An unexpectedly low oscillator strength as the origin of the Fe XVII emission problem," Nature (London) **492**, 225.

Berry, H. G., 1977, "Beam-foil spectroscopy," Rep. Prog. Phys. **40**, 155.

Beyer, A., *et al.*, 2017, "The Rydberg constant and proton size from atomic hydrogen," Science **358**, 79.

Beyer, H. F., R. D. Deslattes, F. Folkmann, and R. E. LaVilla, 1985, "Determination of the 1*s* Lamb shift in one-electron argon recoil ions," J. Phys. B **18**, 207.

Beyer, H. F., P. Indelicato, K. D. Finlayson, D. Liesen, and R. D. Deslattes, 1991, "Measurement of the 1*s* Lamb shift in hydrogen-like nickel," Phys. Rev. A **43**, 223.

Beyer, H. F., *et al.*, 1995, "Measurement of the ground-state Lamb shift of hydrogenlike uranium at the electron cooler of the ESR," Z. Phys. D **35**, 169.

Beyer, Heinrich, H.-J. Kluge, and Viatcheslav Shevelko, 1997, *X-Ray Radiation of Highly Charged Ions* (Springer, Berlin/Heidelberg).

Bieber, D. J., H. S. Margolis, P. K. Oxley, and J. D. Silver, 1997, "Studies of magnetic dipole transitions in highly charged argon and barium using an electron beam ion trap," Phys. Scr. **T73**, 64.

Biedermann, Christoph, Andreas Förster, Gerd Fußmann, and Rainer Radtke, 1997, "First results from the Berlin EBIT," Phys. Scr. **T73**, 360.

Bjorken, James D., and S. D. Drell, 1964, *Relativistic Quantum Mechanics* (McGraw-Hill, New York).

Blatt, S., *et al.*, 2008, "New limits on coupling of fundamental constants to gravity using ^{87}Sr optical lattice clocks," Phys. Rev. Lett. **100**, 140801.

Blessenohl, M. A., *et al.*, 2018, "An electron beam ion trap and source for re-acceleration of rare-isotope ion beams at triumf," Rev. Sci. Instrum. **89**, 052401.

Blundell, S. A., 1992, "Accurate screened QED calculations in high-Z many-electron ions," Phys. Rev. A **46**, 3762.

Böhm, S, A. Enulescu, T. Fritio, I. Orban, S. Tashenov, and R. Schuch, 2007, "First results from the stockholm electron beam ion trap," J. Phys. Conf. Ser. **58**, 303.

Bollinger, J. J., J. D. Prestage, Wayne M. Itano, and D. J. Wineland, 1985, "Laser-cooled-atomic frequency standard," Phys. Rev. Lett. **54**, 1000.

Bosselmann, Ph., U. Staude, D. Horn, K.-H. Schartner, F. Folkmann, A. E. Livingston, and P. H. Mokler, 1999, "Measurements of $2s^2S_{1/2} - 2p^2P_{1/2,3/2}$ transition energies in lithiumlike heavy ions. II. Experimental results for Ag and discussion along the isoelectronic series," Phys. Rev. A **59**, 1874.

Bouchendira, R., P. Cladé, S. Guellati-Khélifa, F. Nez, and F. Biraben, 2011, "New determination of the fine structure constant and test of the quantum electrodynamics," Phys. Rev. Lett. **106**, 080801.

Brandau, C., *et al.*, 2002, "High Rydberg resonances in dielectronic recombination of Pb^{79+}," Phys. Rev. Lett. **89**, 053201.

Brandau, C., *et al.*, 2003, "Precise determination of the $2s_{1/2} - 2p_{1/2}$ splitting in very heavy lithiumlike ions utilizing dielectronic recombination," Phys. Rev. Lett. **91**, 073202.

Brenner, G., J. R. Crespo López-Urrutia, S. Bernitt, D. Fischer, R. Ginzel, K. Kubiček, V. Mäckel, P. H. Mokler, M. C. Simon, and J. Ullrich, 2009, "On the transition rate of the Fe X red coronal line," Astrophys. J. **703**, 68.

Brenner, G., J. R. Crespo López-Urrutia, Z. Harman, P. H. Mokler, and J. Ullrich, 2007, "Lifetime determination of the Fe XIV $3s^23p^2P^o_{3/2}$ metastable level," Phys. Rev. A **75**, 032504.

Brewer, Samuel M., Nicholas D. Guise, and Joseph N. Tan, 2013, "Capture and isolation of highly charged ions in a unitary Penning trap," Phys. Rev. A **88**, 063403.

Briand, J. P., P. Chevallier, P. Indelicato, K. P. Ziock, and D. D. Dietrich, 1990, "Observation and measurement of $n = 2 \rightarrow n = 1$ transitions of hydrogenlike and heliumlike uranium," Phys. Rev. Lett. **65**, 2761.

Briand, J. P., J. P. Mossé, P. Indelicato, P. Chevallier, D. Girard-Vernhet, A. Chetioui, M. T. Ramos, and J. P. Desclaux, 1983, "Spectroscopy of hydrogenlike and heliumlike argon," Phys. Rev. A **28**, 1413.

Briand, J. P., M. Tavernier, P. Indelicato, R. Marrus, and H. Gould, 1983, "High-precision spectroscopic studies of Lyman α lines of hydrogenlike iron: A measurement of the 1s Lamb shift," Phys. Rev. Lett. **50**, 832.

Briand, J. P., M. Tavernier, R. Marrus, and J. P. Desclaux, 1984, "High-precision spectroscopic study of heliumlike iron," Phys. Rev. A **29**, 3143.

Briand, P., R. Geller, B. Jacquot, and C. Jacquot, 1975, "Nouvelle source d'ions multicharges a hautes performances," Nucl. Instrum. Methods **131**, 407.

Britton, J., *et al.*, 2006, "A microfabricated surface-electrode ion trap in silicon," arXiv:quant-ph/0605170.

Brown, I. G., J. E. Galvin, R. A. MacGill, and R. T. Wright, 1986, "Miniature high current metal ion source," Appl. Phys. Lett. **49**, 1019.

Brownnutt, M., M. Kumph, P. Rabl, and R. Blatt, 2015, "Ion-trap measurements of electric-field noise near surfaces," Rev. Mod. Phys. **87**, 1419.

Bruhns, H., J. Braun, K. Kubiček, J. R. Crespo López-Urrutia, and J. Ullrich, 2007, "Testing QED screening and two-loop contributions with He-like ions," Phys. Rev. Lett. **99**, 113001.

Cadoret, M., E. de Mirandes, P. Cladé, S. Guellati-Khélifa, C. Schwob, F. Nez, L. Julien, and F. Biraben, 2008, "Combination of Bloch oscillations with a Ramsey-Bordé interferometer: New determination of the fine structure constant," Phys. Rev. Lett. **101**, 230801.

Calmet, Xavier, and Matthias Keller, 2015, "Cosmological evolution of fundamental constants: From theory to experiment," Mod. Phys. Lett. A **30**, 1540028.

Chantler, C. T., *et al.*, 2012, "Testing three-body quantum electrodynamics with trapped Ti^{20+} ions: Evidence for a Z-dependent divergence between experiment and calculation," Phys. Rev. Lett. **109**, 153001.

Chantler, C. T., *et al.*, 2013, "Chantler et al. Reply," Phys. Rev. Lett. **110**, 159302.

Chen, J.-S., S. M. Brewer, C. W. Chou, D. J. Wineland, D. R. Leibrandt, and D. B. Hume, 2017, "Sympathetic ground state cooling and time-dilation shifts in an $^{27}Al^{+}$ optical clock," Phys. Rev. Lett. **118**, 053002.

Chen, M. H., K. T. Cheng, and W. R. Johnson, 1993, "Relativistic configuration-interaction calculations of $n = 2$ triplet states of heliumlike ions," Phys. Rev. A **47**, 3692.

Cheng, K. T., and M. H. Chen, 2000, "Energy levels of the low-lying states of mid-Z heliumlike ions," Phys. Rev. A **61**, 044503.

Cheng, K. T., M. H. Chen, W. R. Johnson, and J. Sapirstein, 1994, "Relativistic configuration-interaction calculations for the ground stateand $n = 2$ singlet states in heliumlike ions," Phys. Rev. A **50**, 247.

Cheng, K. T., M. H. Chen, and J. Sapirstein, 2000, "Quantum electrodynamic corrections in high-Z Li-like and Be-like ions," Phys. Rev. A **62**, 054501.

Cheng, K. T., W. R. Johnson, and J. Sapirstein, 1993, "Lamb-shift calculations for non-Coulomb potentials," Phys. Rev. A **47**, 1817.

Chiaverini, J., R. B. Blakestad, J. Britton, J. D. Jost, C. Langer, D. Leibfried, R. Ozeri, and D. J. Wineland, 2005, "Surface-electrode architecture for ion-trap quantum information processing," arXiv:quant-ph/0501147.

Chin, Cheng, V. V. Flambaum, and M. G. Kozlov, 2009, "Ultracold molecules: new probes on the variation of fundamental constants," New J. Phys. **11**, 055048.

Chou, C. W., D. B. Hume, J. C. J. Koelemeij, D. J. Wineland, and T. Rosenband, 2010, "Frequency comparison of two high-accuracy Al^{+} optical clocks," Phys. Rev. Lett. **104**, 070802.

Chou, Chin-wen, Christoph Kurz, David B. Hume, Philipp N. Plessow, David R. Leibrandt, and Dietrich Leibfried, 2017, "Preparation and coherent manipulation of pure quantum states of a single molecular ion," Nature (London) **545**, 203.

Chu, S., 1998, "The manipulation of neutral particles," Rev. Mod. Phys. **70**, 685.

Church, D. A., J. Steiger, B. R. Beck, L. Gruber, and J. P. Holder, 1999, "RETRAP: An ion trap for laser spectroscopy of highly-charged ions," in *Trapped charged particles and fundamental physics*, AIP Conference Proceedings, Vol. 457 (AIP, Melville) p. 235.

Chwalla, M., K. Kim, T. Monz, P. Schindler, M. Riebe, C. F. Roos, and R. Blatt, 2007, "Precision spectroscopy with two correlated atoms," Appl. Phys. B **89**, 483.

Clos, G., M. Enderlein, U. Warring, T. Schaetz, and D. Leibfried, 2014, "Decoherence-Assisted Spectroscopy of a Single Mg^{+} Ion," Phys. Rev. Lett. **112**, 113003.

Cohen-Tannoudji, Claude N, 1998, "Nobel Lecture: Manipulating atoms with photons," Rev. Mod. Phys. **70**, 707.

Colladay, D., and V. A. Kostelecký, 1998, "Lorentz-violating extension of the standard model," Phys. Rev. D **58**, 116002.

Crespo López-Urrutia, J. R., 2008, "The visible spectrum of highly charged ions: A window to fundamental physics," Can. J. Phys. **86**, 111.

Crespo López-Urrutia, J. R., P. Beiersdorfer, D. W. Savin, and K. Widmann, 1996, "Direct observation of the spontaneous emission of the hyperfine transition $F = 4$ to $F = 3$ in ground state hydrogenlike $^{165}Ho^{66+}$ in an electron beam ion trap," Phys. Rev. Lett. **77**, 826.

Crespo López-Urrutia, J. R., P. Beiersdorfer, D. W. Savin, and K. Widmann, 1998, "Precision measurement of the lifetime of the $1s2s\ ^3S_1$ metastable level in heliumlike O^{6+}," Phys. Rev. A **58**, 238.

Crespo López-Urrutia, J. R., P. Beiersdorfer, and K. Widmann, 2006, "Lifetime of the $1s2s\ ^3S_1$ metastable level in He-like S^{14+} measured with an electron beam ion trap," Phys. Rev. A **74**, 012507.

Crespo López-Urrutia, J. R., P. Beiersdorfer, K. Widmann, B. B. Birkett, A.-M. Mårtensson-Pendrill, and M. G. H. Gustavsson, 1998, "Nuclear magnetization distribution radii determined by hyperfine transitions in the 1s level of H-like ions $^{185}Re^{74+}$ and $^{187}Re^{74+}$," Phys. Rev. A **57**, 879.

Crespo López-Urrutia, J. R., A. Dorn, R. Moshammer, and J. Ullrich, 1999, "The Freiburg electron beam ion trap/source project FreEBIT," Phys. Scr. **T80B**, 502.

Currell, F., and G. Fussmann, 2005, "Physics of electron beam ion traps and sources," IEEE Trans. Plasma Sci. **33**, 1763.

Currell, Frederick John, *et al.*, 1996, "A new versatile electron-beam ion trap," J. Phys. Soc. Jpn. **65**, 3186.

Currell, Fred J., 2003, Ed., *The Physics of Multiply and Highly Charged Ions*, Sources, Applications and Fundamental Processes, Vol. 1 (Springer, New York).

Czarnecki, Andrzej, and Robert Szafron, 2016, "Light-by-light scattering in the Lamb shift and the bound electron g factor," Phys. Rev. A **94**, 060501(R)..

Dehmelt, H. G., 1968, "Radiofrequency spectroscopy of stored ions I: Storage," Adv. At. Mol. Phys. **3**, 53.

Delaunay, Cédric, Claudia Frugiuele, Elina Fuchs, and Yotam Soreq, 2017, "Probing new spin-independent interactions through precision spectroscopy in atoms with few electrons," Phys. Rev. D **96**, 115002.

Delaunay, Cédric, Roee Ozeri, Gilad Perez, and Yotam Soreq, 2017, "Probing atomic Higgs-like forces at the precision frontier," Phys. Rev. D **96**, 093001.

Delaunay, Cédric, and Yotam Soreq, 2016, "Probing new physics with isotope shift spectroscopy," arXiv:1602.04838.

Dent, T., S. Stern, and C. Wetterich, 2008, "Unifying cosmological and recent time variations of fundamental couplings," Phys. Rev. D **78**, 103518.

Derevianko, A., 2016, "Atomic clocks and dark-matter signatures," J. Phys. Conf. Ser. **723**, 012043.

Derevianko, A., V. A. Dzuba, and V. V. Flambaum, 2012, "Highly charged ions as a basis of optical atomic clockwork of exceptional accuracy," Phys. Rev. Lett. **109**, 180801.

Derevianko, A., and M. Pospelov, 2014, "Hunting for topological dark matter with atomic clocks," Nat. Phys. **10**, 933.

Deslattes, R. D., H. F. Beyer, and F. Folkmann, 1984, "Precision x-ray wavelength measurements in helium-like argon recoil ions," J. Phys. B **17**, L689.

Dicke, R. H., 1953, "The Effect of Collisions upon the Doppler Width of Spectral Lines," Phys. Rev. **89**, 472.

Dilling, J., *et al.*, 2006, "Mass measurements on highly charged radioactive ions, a new approach to high precision with TITAN," Int. J. Mass Spectrom. **251**, 198.

Doležal, M., *et al.*, 2015, "Analysis of thermal radiation in ion traps for optical frequency standards," Metrologia **52**, 842.

Donets, E. D., 1967, "Avtorskoe svidetelstvo USSR, N248860 from 16.03.1967," Bull. OIPOTZ **N24**, 65 (in Russian).

Donets, E. D., 1985, "Electron beam ion sources and associated physics at JINR," Nucl. Instrum. Methods Phys. Res., Sect. B **9**, 522.

Donets, E. D., 1990, "Electron beam ion sources and their development at JINR (invited)," Rev. Sci. Instrum. **61**, 225.

Donets, E. D., and A. I. Pikin, 1975, J. Tech. Phys. **45**, 2373 (in Russian).

Draganič, I., J. R. Crespo López-Urrutia, R. DuBois, S. Fritzsche, V. M. Shabaev, R. Soria Orts, I. I. Tupitsyn, Y. Zou, and J. Ullrich, 2003, "High precision wavelength measurements of QED-sensitive forbidden transitions in highly charged argon ions," Phys. Rev. Lett. **91**, 183001.

Drake, G. W. F., 1979, "Unified relativistic theory for $1s2p\,^3P_1 - 1s^2\,^1S_0$ and $1s2p\,^1P_1 - 1s^2\,^1S_0$ frequencies and transition rates in heliumlike ions," Phys. Rev. A **19**, 1387..

Drake, G. W. F., 1988, "Theoretical energies for the $n = 1$ and 2 states of the helium isoelectronic sequence up to $Z = 100$," Can. J. Phys. **66**, 586.

Drake, G. W. F., 2002, "Progress in helium fine-structure calculations and the fine-structure constant," Can. J. Phys. **80**, 1195.

Drake, G. W. F., and Z.-C. Yan, 2008, "High-precision spectroscopy as a test of quantum electrodynamics in light atomic systems," Can. J. Phys. **86**, 45.

Drakoudis, A., M. Söllner, and G. Werth, 2006, "Instabilities of ion motion in a linear Paul trap," Int. J. Mass Spectrom. **252**, 61.

Drullinger, R. E., D. J. Wineland, and J. C. Bergquist, 1980, "High-resolution optical spectra of laser cooled ions," Appl. Phys. **22**, 365.

Dubé, P., A. Madej, J. Bernard, L. Marmet, J.-S. Boulanger, and S. Cundy, 2005, "Electric quadrupole shift cancellation in single-ion optical frequency standards," Phys. Rev. Lett. **95**, 033001.

Dubé, Pierre, Alan A. Madej, Maria Tibbo, and John E. Bernard, 2014, "High-accuracy measurement of the differential scalar polarizability of a $^{88}Sr^+$ clock using the time-dilation effect," Phys. Rev. Lett. **112**, 173002.

Dubé, Pierre, Alan A. Madej, Zichao Zhou, and John E. Bernard, 2013, "Evaluation of systematic shifts of the $^{88}Sr^+$ single-ion optical frequency standard at the 10^{-17} level," Phys. Rev. A **87**, 023806.

Dumont, V., and J. K. Webb, 2017, "Modelling long-range wavelength distortions in quasar absorption echelle spectra," Mon. Not. R. Astron. Soc. **468**, 1568.

Dzuba, V., V. Flambaum, and M. Marchenko, 2003, "Relativistic effects in Sr, Dy, Yb II, and Yb III and search for variation of the fine-structure constant," Phys. Rev. A **68**, 022506..

Dzuba, V. A., A. Derevianko, and V. V. Flambaum, 2012a, "High-precision atomic clocks with highly charged ions: Nuclear-spin-zero f^{12}-shell ions," Phys. Rev. A **86**, 054501..

Dzuba, V. A., A. Derevianko, and V. V. Flambaum, 2012b, "Ion clock and search for the variation of the fine-structure constant using optical transitions in Nd^{13+} and Sm^{15+}," Phys. Rev. A **86**, 054502.

Dzuba, V. A., A. Derevianko, and V. V. Flambaum, 2012, "High-precision atomic clocks with highly charged ions: Nuclear-spin-zero f^{12}-shell ions," Phys. Rev. A **86**, 054501; **87**, 029906(E) (2013).

Dzuba, V. A., and V. V. Flambaum, 2009, "Atomic calculations and search for variation of the fine-structure constant in quasar absorption spectra," Can. J. Phys. **87**, 15.

Dzuba, V. A., and V. V. Flambaum, 2015, "Highly charged ions for atomic clocks and search for variation of the fine structure constant," Hyperfine Interact. **236**, 79.

Dzuba, V. A., and V. V. Flambaum, 2016, "Hyperfine-induced electric dipole contributions to the electric octupole and magnetic quadrupole atomic clock transitions," Phys. Rev. A **93**, 052517.

Dzuba, V. A., V. V. Flambaum, M. G. Kozlov, and M. Marchenko, 2002, "α dependence of transition frequencies for ions Si II, Cr II, Fe II, Ni II and Zn II," Phys. Rev. A **66**, 022501.

Dzuba, V. A., V. V. Flambaum, and Hidetoshi Katori, 2015, "Optical clock sensitive to variation of the fine structure constant based on the Ho^{14+} ion," Phys. Rev. A **91**, 022119.

Dzuba, V. A., V. V. Flambaum, and M. G. Kozlov, 1996, "Combination of the many body perturbation theory with configuration interaction method," Phys. Rev. A **54**, 3948.

Dzuba, V. A., V. V. Flambaum, M. S. Safronova, S. G. Porsev, T. Pruttivarasin, M. A. Hohensee, and H. Häffner, 2016, "Strongly enhanced effects of Lorentz symmetry violation in entangled Yb^+ ions," Nat. Phys. **12**, 465.

Dzuba, V. A., M. S. Safronova, U. I. Safronova, and V. V. Flambaum, 2015, "Actinide ions for testing the spatial α-variation hypothesis," Phys. Rev. A **92**, 060502.

Dzuba, V. A., V. V. Flambaum, and J. K. Webb, 1999, "Calculations of the relativistic effects in many-electron atoms and space-time variation of fundamental constants," Phys. Rev. A **59**, 230.

Edlén, B., 1943, "Die Deutung der Emissionslinien im Spektrum der Sonnenkorona," Z. Astrophys. **22**, 30 [http://adsabs.harvard.edu/abs/1943ZA.....22...30E].

Edlén, Bengt, 1947, "Spectra of highly ionized atoms," Physica (Utrecht) **13**, 545.

Edlén, Bengt, 1984, "Forbidden lines in hot plasmas," Phys. Scr. **T8**, 5.

Eides, Michael I., Howard Grotch, and Valery A. Shelyuto, 2001, "Theory of light hydrogenlike atoms," Phys. Rep. **342**, 63.

Eliav, E., U. Kaldor, and Y. Ishikawa, 1994, "Relativistic coupled cluster method based on Dirac-Coulomb-Breit wavefunctions. Ground state energies of atoms with two to five electrons," Chem. Phys. Lett. **222**, 82.

Elliott, S. R., P. Beiersdorfer, and M. H. Chen, 1996, "Trapped-ion technique for measuring the nuclear charge radii of highly charged radioactive isotopes," Phys. Rev. Lett. **76**, 1031.

Elliott, S. R., and R. E. Marrs, 1995, "A wire probe as an ion-source for an electron-beam ion-trap," Nucl. Instrum. Methods Phys. Res., Sect. B **100**, 529.

Epp, S. W., 2013, "Comment on "Testing three-body quantum electrodynamics with trapped Ti^{20+} ions: Evidence for a Z-dependent divergence between experiment and calculation"," Phys. Rev. Lett. **110**, 159301.

Epp, S. W., *et al.*, 2007, "Soft x-ray laser spectroscopy on trapped highly charged ions at flash," Phys. Rev. Lett. **98**, 183001.

Epp, S. W., *et al.*, 2010, "X-ray laser spectroscopy of highly charged ions at FLASH," J. Phys. B **43**, 194008.

Epp, S. W., *et al.* 2015, "Single-photon excitation of Kα in heliumlike Kr^{34+}: Results supporting quantum electrodynamics predictions," Phys. Rev. A **92**, 020502.

Ettenauer, S., *et al.*, 2011, "First use of high charge states for mass measurements of short-lived nuclides in a Penning trap," Phys. Rev. Lett. **107**, 272501.

Falke, S., M. Misera, U. Sterr, and C. Lisdat, 2012, "Delivering pulsed and phase stable light to atoms of an optical clock," Appl. Phys. B **107**, 301.

Feili, D., Ph. Bosselmann, K.-H. Schartner, F. Folkmann, A. E. Livingston, E. Träbert, X. Ma, and P. H. Mokler, 2000, "Measurements of $2s\,^2S_{1/2} - 2p\,^2P_{1/2}$ transition energies in lithiumlike heavy ions. III. Experimental results for Sn^{47+} and Xe^{51+}," Phys. Rev. A **62**, 022501.

Feldman, U., J. F. Seely, and A. K. Bhatia, 1985, "Spectral line intensities for the O I, N I, C I, B I, and Be I isoelectronic sequences, $Z = 26$–36," At. Data Nucl. Data Tables **32**, 305.

Feldman, Uri, Marvin Swartz, and Leonard Cohen, 1967, "Vacuum ultraviolet source," Rev. Sci. Instrum. **38**, 1372.

Ficek, Filip, Derek F. Jackson Kimball, Mikhail G. Kozlov, Nathan Leefer, Szymon Pustelny, and Dmitry Budker, 2017, "Constraints on exotic spin-dependent interactions between electrons from helium fine-structure spectroscopy," Phys. Rev. A **95**, 032505.

Finkenthal, M., R. E. Bell, H. W. Moos, and TFR Group, 1984, "Forbidden (M1) lines in the spectra of titanium, vanadium, chromium, iron, and nickel observed in a tokamak plasma," J. Appl. Phys. **56**, 2012.

Fischer, Charlotte Froese, Georgio Tachiev, Gediminas Gaigalas, and Michel R. Godefroid, 2007, "An MCHF atomic-structure package for large-scale calculations," Comput. Phys. Commun. **176**, 559.

Flambaum, V. V., A. J. Geddes, and A. V. Viatkina, 2018, "Isotope shift, nonlinearity of king plots, and the search for new particles," Phys. Rev. A **97**, 032510.

Flambaum, V. V., and J. S. Ginges, 2005, "Radiative potential and calculations of QED radiative corrections to energy levels and electromagnetic amplitudes in many-electron atoms," Phys. Rev. A **72**, 052115.

Flowers, J. L., H. A. Klein, D. J. E. Knight, and H. S. Margolis, 2001, "Hydrogenic Systems for Calculable Frequency Standards: Status and Options," NPL Report No. CBTLM 11.

Fritzsche, S., C. Froese Fischer, and G. Gaigalas, 2002, "RELCI: A program for relativistic configuration interaction calculations," Comput. Phys. Commun. **148**, 103.

Frugiuele, Claudia, Elina Fuchs, Gilad Perez, and Matthias Schlaffer, 2016, "Atomic probes of new physics," arXiv:1602.04822.

Fu, Y., K. Yao, B. Wei, D. Lu, R. Hutton, and Y. Zou, 2010, "Overview of the Shanghai EBIT," J. Instrum. **5**, C08011.

Gebert, Florian, Yong Wan, Fabian Wolf, Christopher N. Angstmann, Julian C. Berengut, and Piet O. Schmidt, 2015, "Precision isotope shift measurements in calcium ions using quantum logic detection schemes," Phys. Rev. Lett. **115**, 053003.

Geller, R., 1970, "New high intensity ion source with very low extraction voltage," Appl. Phys. Lett. **16**, 401.

Ghosh, Pradip K, 1996, *Ion Traps* (Clarendon Press, Oxford/New York), 1st ed.

Gillaspy, J. D., 2001, "Highly charged ions," J. Phys. B **34**, R39.

Gillaspy, J. D., 2014, "Precision spectroscopy of trapped highly charged heavy elements: pushing the limits of theory and experiment," Phys. Scr. **89**, 114004.

Gillaspy, J. D., *et al.*, 1995, "Overview of the electron beam ion trap program at NIST," Phys. Scr. **T59**, 392.

Ginges, J. S. M., and J. C. Berengut, 2016, "QED radiative corrections and many-body effects in atoms: the Uehling potential and shifts in alkali metals," J. Phys. B **49**, 095001.

Godun, R. M., P. B. R. Nisbet-Jones, J. M. Jones, S. A. King, L. A. M. Johnson, H. S. Margolis, K. Szymaniec, S. N. Lea, K. Bongs, and P. Gill, 2014, "Frequency ratio of two optical clock transitions in $^{171}Yb^+$ and constraints on the time variation of fundamental constants," Phys. Rev. Lett. **113**, 210801.

Gohle, Christoph, Thomas Udem, Maximilian Herrmann, Jens Rauschenberger, Ronald Holzwarth, Hans Schuessler, Ferenc Krausz, and Theodor Hänsch, 2005, "A frequency comb in the extreme ultraviolet," Nature (London) **436**, 234.

González Martínez, A. J., *et al.*, 2005, "State-selective quantum interference observed in the recombination of highly charged $Hg^{75+\cdots 78+}$ mercury ions in an electron beam ion trap," Phys. Rev. Lett. **94**, 203201.

Grotrian, W., 1939, "Zur frage der deutung der linien im spektrum der sonnenkorona," Naturwissenschaften **27**, 214.

Gruber, L., J. Steiger, J. P. Holder, B. R. Beck, H. E. DeWitt, J. Glassman, J. W. McDonald, D. A. Church, and D. Schneider, 2001, "Evidence for highly charged ion Coulomb crystallization in multicomponent strongly coupled plasmas," Phys. Rev. Lett. **86**, 636.

Guéna, J., *et al.*, 2017, "First international comparison of fountain primary frequency standards via a long distance optical fiber link," Metrologia **54**, 348.

Guise, Nicholas D., Joseph N. Tan, Samuel M. Brewer, Charlotte F. Fischer, and Per Jönsson, 2014, "Measurement of the Kr XVIII $3d\,^2D_{5/2}$ lifetime at low energy in a unitary Penning trap," Phys. Rev. A **89**, 040502..

Gumberidze, A., *et al.*, 2004, "Electron-electron interaction in strong electromagnetic fields: The two-electron contribution to the ground-state energy in He-like uranium," Phys. Rev. Lett. **92**, 203004.

Gumberidze, A., *et al.*, 2005, "Quantum electrodynamics in strong electric fields: The ground-state Lamb shift in hydrogenlike uranium," Phys. Rev. Lett. **94**, 223001.

Gustavsson, Martin G. H., 1999, "Hyperfine Structure in Highly Charged Hydrogen-Like Ions—Investigations of the nuclear charge and magnetization distributions," Ph.D. thesis (Göteborg University).

Gustavsson, Martin G. H., and Ann-Marie Mårtensson-Pendrill, 1998, "Need for remeasurements of nuclear magnetic dipole moments," Phys. Rev. A **58**, 3611.

Hall, John, 2006, "Nobel Lecture: Defining and measuring optical frequencies," Rev. Mod. Phys. **78**, 1279.

Hanneke, D., S. Fogwell, and G. Gabrielse, 2008, "New measurement of the electron magnetic moment and the fine structure constant," Phys. Rev. Lett. **100**, 120801.

Hänsch, T. W., and A. L. Schawlow, 1975, "Cooling of gases by laser radiation," Opt. Commun. **13**, 68.

Hänsch, Theodor, 2006, "Nobel Lecture: Passion for precision," Rev. Mod. Phys. **78**, 1297.

Harilal, S. S., B. O'Shay, M. S. Tillack, Y. Tao, R. Paguio, A. Nikroo, and C. A. Back, 2006, "Spectral control of emissions from tin doped targets for extreme ultraviolet lithography," J. Phys. D **39**, 484.

Heilig, K., and A. Steudel, 1974, "Changes in mean-square nuclear charge radii from optical isotope shifts," At. Data Nucl. Data Tables **14**, 613.

Hempel, C., B. P. Lanyon, P. Jurcevic, R. Gerritsma, R. Blatt, and C. F. Roos, 2013, "Entanglement-enhanced detection of single-photon scattering events," Nat. Photonics **7**, 630.

Herschbach, N., K. Pyka, J. Keller, and T. E. Mehlstäubler, 2012, "Linear Paul trap design for an optical clock with Coulomb crystals," Appl. Phys. B **107**, 891.

Hite, D. A., *et al.*, 2012, "100-Fold Reduction of Electric-Field Noise in an Ion Trap Cleaned with In Situ Argon-Ion-Beam Bombardment," Phys. Rev. Lett. **109**, 103001.

Hitomi Collaboration, 2016, "The quiescent intracluster medium in the core of the perseus cluster," Nature (London) **535**, 117.

Hitomi Collaboration, 2017, "Solar abundance ratios of the iron-peak elements in the Perseus cluster," Nature (London) **551**, 478.

Hobein, M., A. Solders, M. Suhonen, Y. Liu, and R. Schuch, 2011, "Evaporative cooling and coherent axial oscillations of highly charged ions in a penning trap," Phys. Rev. Lett. **106**, 013002.

Hohensee, M. A., N. Leefer, D. Budker, C. Harabati, V. A. Dzuba, and V. V. Flambaum, 2013, "Limits on violations of Lorentz symmetry and the Einstein equivalence principle using radio-frequency spectroscopy of atomic dysprosium," Phys. Rev. Lett. **111**, 050401.

Hoogerheide, S. Fogwell, and J. N. Tan, 2015, "A miniature EBIT with ion extraction for isolating highly charged ions," J. Phys. Conf. Ser. **583**, 012044.

Hosaka, K., D. N. Crosby, K. Gaarde-Widdowson, C. J. Smith, J. D. Silver, T. Kinugawa, S. Ohtani, and E. G. Myers, 2004, "Laser spectroscopy of hydrogenlike nitrogen in an electron beam ion trap," Phys. Rev. A **69**, 011802.

Hu, Zhimin, Xiaoying Han, Yueming Li, Daiji Kato, Xiaomin Tong, and Nobuyuki Nakamura, 2012, "Experimental demonstration of the Breit interaction which dominates the angular distribution of x-ray emission in dielectronic recombination," Phys. Rev. Lett. **108**, 073002.

Huang, Y., H. Guan, W. Bian, L. Ma, K. Liang, T. Li, and K. Gao, 2017, "A comparison of two $^{40}Ca^{+}$ single-ion optical frequency standards at the 5×10^{-17} level and an evaluation of systematic shifts," Appl. Phys. B **123**, 166.

Hubac, I., and P. Neogrady, 1994, "Size-consistent Brillowin-Wigner perturbation theory with exponentially parametrized wave function: Brillowin-Wigner coupled-cluster theory," Phys. Rev. A **50**, 4558.

Hume, D., T. Rosenband, and D. Wineland, 2007, "High-fidelity adaptive qubit detection through repetitive quantum nondemolition measurements," Phys. Rev. Lett. **99**, 120502.

Huntemann, N., B. Lipphardt, M. Okhapkin, Chr. Tamm, E. Peik, A. V. Taichenachev, and V. I. Yudin, 2012, "Generalized Ramsey Excitation Scheme with Suppressed Light Shift," Phys. Rev. Lett. **109**, 213002.

Huntemann, N., B. Lipphardt, C. Tamm, V. Gerginov, S. Weyers, and E. Peik, 2014, "Improved limit on a temporal variation of m_p/m_e from comparisons of Yb^{+} and Cs atomic clocks," Phys. Rev. Lett. **113**, 210802.

Huntemann, N., C. Sanner, B. Lipphardt, Chr. Tamm, and E. Peik, 2016, "Single-ion atomic clock with 3×10^{-18} systematic uncertainty," Phys. Rev. Lett. **116**, 063001.

Indelicato, P., J. P. Briand, M. Tavernier, and D. Liesen, 1986, "Experimental study of relativistic correlations and QED effects in heliumlike krypton ions," Z. Phys. D **2**, 249.

Indelicato, P., and J. P. Desclaux, 1990, "Multiconfiguration Dirac-Fock calculations of transition energies with QED corrections in three-electron ions," Phys. Rev. A **42**, 5139.

Indelicato, P., O. Gorveix, and J. P. Desclaux, 1987, "Multiconfigurational Dirac-Fock studies of two-electron ions. II. Radiative corrections and comparison with experiment," J. Phys. B **20**, 651.

Indelicato, Paul, and Peter J. Mohr, 2017, "Introduction to bound-state quantum electrodynamics," in *Handbook of Relativistic Quantum Chemistry*, edited by Wenjian Liu (Springer, Berlin/Heidelberg), p. 131.

Itano, W. M., 2000, "External-field shifts of the $^{199}Hg^{+}$ optical frequency standard," J. Res. Natl. Inst. Stand. Technol. **105**, 829.

Itano, W. M., J. C. Bergquist, J. J. Bollinger, J. M. Gilligan, D. J. Heinzen, F. L. Moore, M. G. Raizen, and D. J. Wineland, 1993, "Quantum projection noise: Population fluctuations in two-level systems," Phys. Rev. A **47**, 3554.

Itano, Wayne M., L. L. Lewis, and D. J. Wineland, 1982, "Shift of $^2S_{1/2}$ hyperfine splittings due to blackbody radiation," Phys. Rev. A **25**, 1233.

Iwamae, A., M. Atake, A. Sakaue, R. Katai, M. Goto, and S. Morita, 2007, "Polarization separated Zeeman spectra from magnetic dipole transitions in highly charged argon in the large helical device," Phys. Plasmas **14**, 042504.

James, D. F. V., 1998, "Quantum dynamics of cold trapped ions with application to quantum computation," Appl. Phys. B **66**, 181.

Johnson, W. R., 2007, *Atomic Structure Theory. Lectures on Atomic Physics* (Springer, Berlin/Heidelberg).

Johnson, W. R., K. T. Cheng, and M. H. Chen, 2004, "Chapter 3: Accurate relativistic calculations including QED contributions for few-electron systems," Theor. Comput. Chem. **14**, 120.

Johnson, W. R., D. R. Plante, and J. Sapirstein, 1995, "Relativistic calculations of transition amplitudes in the helium isoelectronic sequence," Adv. At. Mol. Opt. Phys. **35**, 255.

Johnson, W. R., and G. Soff, 1985, "The Lamb shift in hydrogen-like atoms, $1 < Z < 110$," At. Data Nucl. Data Tables **33**, 405.

Jones, R. J., Kevin Moll, Michael Thorpe, and Jun Ye, 2005, "Phase-coherent frequency combs in the vacuum ultraviolet via high-harmonic generation inside a femtosecond enhancement cavity," Phys. Rev. Lett. **94**, 193201.

Joshi, Y. N., A. N. Ryabtsev, and S. S. Churilov, 2001, "Nine-times ionized cerium spectrum: Ce X," Phys. Scr. **64**, 326.

Karpeshin, F. F., and M. B. Trzhaskovskaya, 2015, "The theory of the Bohr-Weisskopf effect in the hyperfine structure," Nucl. Phys. A **941**, 66.

Karshenboim, S. G., 2005, "Precision physics of simple atoms: QED tests, nuclear structure and fundamental constants," Phys. Rep. **422**, 1.

Kaufman, J. R., V. Kaufman, J. Sugar, T. L. Pittman, and W. L. Rowan, 1983, "Magnetic-dipole transitions observed in highly ionized Ga, Ge, As, and Kr," Phys. Rev. A **27**, 1721.

Keller, J., T. Burgermeister, D. Kalincev, J. Kiethe, and T. E. Mehlstäubler, 2016, "Evaluation of trap-induced systematic frequency shifts for a multi-ion optical clock at the 10^{-19} level," J. Phys. Conf. Ser. **723**, 012027.

Keller, J., D. Kalincev, T. Burgermeister, A. Kulosa, A. Didier, T. Nordmann, J. Kiethe, and T. E. Mehlstäubler, 2017, "Optical clocks based on linear ion chains with high stability and accuracy," arXiv:1712.02335.

Keller, J., H. L. Partner, T. Burgermeister, and T. E. Mehlstäubler, 2015, "Precise determination of micromotion for trapped-ion optical clocks," J. Appl. Phys. **118**, 104501.

Kentsch, U., G. Zschornack, F. Grossmann, V. P. Ovsyannikov, F. Ullmann, S. Fritzsche, and A. Surzhykov, 2002, "Production of bare argon, manganese, iron and nickel nuclei in the Dresden EBIT," Nucl. Instrum. Methods Phys. Res., Sect. B **187**, 238.

Khodja, H., and J. P. Briand, 1997, "A warm electron beam ion trap: The micro-EBIT," Phys. Scr. **T71**, 113.

Kielpinski, D., B. E. King, C. J. Myatt, C. A. Sackett, Q. A. Turchette, W. M. Itano, C. Monroe, D. J. Wineland, and W. H. Zurek, 2000,

"Sympathetic cooling of trapped ions for quantum logic," Phys. Rev. A **61**, 032310.

Kielpinski, D., V. Meyer, M. A. Rowe, C. A. Sackett, W. M. Itano, C. Monroe, and D. J. Wineland, 2001, "A Decoherence-Free Quantum Memory Using Trapped Ions," Science **291**, 1013.

Kim, Y.-K., D. H. Baik, P. Indelicato, and J. P. Desclaux, 1991, "Resonance transition energies of Li-, Na-, and Cu-like ions," Phys. Rev. A **44**, 148.

King, W. H., 1963, "Comments on the article "Peculiarities of the isotope shift in the samarium spectrum"," J. Opt. Soc. Am. **53**, 638.

Klaft, I., *et al.*, 1994, "Precision laser spectroscopy of the ground state hyperfine splitting of hydrogenlike $^{209}Bi^{82+}$," Phys. Rev. Lett. **73**, 2425.

Kluge, H. J., T. Beier, K. Blaum, L. Dahl, S. Eliseev, John R. Sabin, Erkki J. Brandas, Ingvar Lindgren, Eva Lindroth, and Sten Salomonson, 2008, "HITRAP: A facility at GSI for highly charged ions," Adv. Quantum Chem. **53**, 83.

Knapp, D. A., P. Beiersdorfer, M. H. Chen, J. H. Scofield, and D. Schneider, 1995, "Observation of interference between dielectronic recombination and radiative recombination in highly charged uranium ions," Phys. Rev. Lett. **74**, 54.

Knapp, D. A., R. E. Marrs, M. A. Levine, C. L. Bennett, M. H. Chen, J. R. Henderson, M. B. Schneider, and J. H. Scofield, 1989, "Dielectronic recombination of heliumlike nickel," Phys. Rev. Lett. **62**, 2104.

Köhler, F., S. Sturm, A. Kracke, G. Werth, W. Quint, and K. Blaum, 2015, "The electron mass from *g*-factor measurements on hydrogen-like carbon $^{12}C^{5+}$," J. Phys. B **48**, 144032.

Köhler, F., *et al.*, 2016, "Isotope dependence of the Zeeman effect in lithium-like calcium," Nat. Commun. **7**, 10246.

Konovalova, E. A., and M. G. Kozlov, 2015, "Correlation, Breit, and QED effects in spectra of Mg-like ions," Phys. Rev. A **92**, 042508.

Kostelecký, V. A., and C. D. Lane, 1999, "Constraints on Lorentz violation from clock-comparison experiments," Phys. Rev. D **60**, 116010.

Kostelecký, V. A., and M. Mewes, 2002, "Signals for Lorentz violation in electrodynamics," Phys. Rev. D **66**, 056005.

Kostelecký, V. A., and N. Russell, 2011, "Data tables for Lorentz and CPT violation," Rev. Mod. Phys. **83**, 11.

Kostelecký, V. A., and N. Russell, 2017, "Data tables for Lorentz and CPT violation," arXiv:0801.0287v10.

Kotochigova, S. A., and I. I. Tupitsyn, 1987, "Theoretical investigation of rare-earth and barium spectra by the Hartree-Fock-Dirac method," J. Phys. B **20**, 4759.

Kozhedub, Y. S., O. V. Andreev, V. M. Shabaev, I. I. Tupitsyn, C. Brandau, C. Kozhuharov, G. Plunien, and T. Stöhlker, 2008, "Nuclear deformation effect on the binding energies in heavy ions," Phys. Rev. A **77**, 032501.

Kozlov, A., V. A. Dzuba, and V. V. Flambaum, 2013, "Transition amplitudes, polarizabilities, and energy levels within optical wavelength of highly charged ions Sm^{14+} and Sm^{13+}," Phys. Rev. A **88**, 062509.

Kozlov, M. G., 2004, "Precision calculations of atoms with few valence electrons," Int. J. Quantum Chem. **100**, 336.

Kozlov, M. G., I. I. Tupitsyn, and D. Reimers, 2009, "Sensitivity coefficients to alpha-variation for fine-structure transitions in Carbon-like ions," Phys. Rev. A **79**, 022117.

Kozlov, M. G., and S. A. Levshakov, 2013, "Microwave and submillimeter molecular transitions and their dependence on fundamental constants," Ann. Phys. (Berlin) **525**, 452.

Kozlov, M. G., S. G. Porsev, M. S. Safronova, and I. I. Tupitsyn, 2015, "CI-MBPT: A package of programs for relativistic atomic calculations based on a method combining configuration interaction and many-body perturbation theory," Comput. Phys. Commun. **195**, 199.

Kozlov, M. G., M. S. Safronova, S. G. Porsev, and I. I. Tupitsyn, 2016, "Effective three-particle forces in polyvalent atoms," Phys. Rev. A **94**, 032512.

Kubiček, K., J. Braun, H. Bruhns, J. R. Crespo López-Urrutia, P. H. Mokler, and J. Ullrich, 2012, "High-precision laser-assisted absolute determination of X-ray diffraction angles," Rev. Sci. Instrum. **83**, 013102.

Kubiček, K., P. H. Mokler, V. Mäckel, J. Ullrich, and J. R. Crespo López-Urrutia, 2014, "Transition energy measurements in hydrogenlike and heliumlike ions strongly supporting bound-state QED calculations," Phys. Rev. A **90**, 032508.

Labaziewicz, Jaroslaw, Yufei Ge, Paul Antohi, David Leibrandt, Kenneth Brown, and Isaac Chuang, 2008, "Suppression of heating rates in cryogenic surface-electrode ion traps," Phys. Rev. Lett. **100**, 013001.

Labzowsky, Leonti, Andrei Nefiodov, Günter Plunien, Gerhard Soff, and Pekka Pyykkö, 1997, "Vacuum-polarization corrections to the hyperfine-structure splitting of highly charged $^{209}_{83}$Bi ions," Phys. Rev. A **56**, 4508.

Lapierre, A., J. R. Crespo López-Urrutia, J. Braun, G. Brenner, H. Bruhns, D. Fischer, A. J. González Martínez, V. Mironov, C. Osborne, and G. Sikler, 2006, "Lifetime measurement of the Ar XIV $1s^22s^22p\ ^2P^o_{3/2}$ metastable level at the Heidelberg electron-beam ion trap," Phys. Rev. A **73**, 052507.

Lapierre, A., *et al.*, 2005, "Relativistic electron correlation, quantum electrodynamics, and the lifetime of the $1s^22s^22p\ ^2P^o_{3/2}$ level in boronlike argon," Phys. Rev. Lett. **95**, 183001.

Larson, D. J., J. C. Bergquist, J. J. Bollinger, Wayne M. Itano, and D. J. Wineland, 1986, "Sympathetic cooling of trapped ions: A laser-cooled two-species nonneutral ion plasma," Phys. Rev. Lett. **57**, 70.

Lechner, Regina, Christine Maier, Cornelius Hempel, Petar Jurcevic, Ben P. Lanyon, Thomas Monz, Michael Brownnutt, Rainer Blatt, and Christian F. Roos, 2016, "Electromagnetically-induced-transparency ground-state cooling of long ion strings," Phys. Rev. A **93**, 053401.

Leefer, N., C. T. M. Weber, A. Cingöz, J. R. Torgerson, and D. Budker, 2013, "New limits on variation of the fine-structure constant using atomic dysprosium," Phys. Rev. Lett. **111**, 060801.

Lennarz, A., *et al.*, 2014, "In-trap spectroscopy of charge-bred radioactive ions," Phys. Rev. Lett. **113**, 082502.

Leopold, T., L. Schmöger, S. Feuchtenbeiner, C. Grebing, P. Micke, N. Scharnhorst, I. D. Leroux, J. R. Crespo López-Urrutia, and P. O. Schmidt, 2016, "A tunable low-drift laser stabilized to an atomic reference," Appl. Phys. B **122**, 236.

Leroux, Ian D., Nils Scharnhorst, Stephan Hannig, Johannes Kramer, Lennart Pelzer, Mariia Stepanova, and Piet O. Schmidt, 2017, "On-line estimation of local oscillator noise and optimisation of servo parameters in atomic clocks," Metrologia **54**, 307.

Lett, Paul D., Richard N. Watts, Christoph I. Westbrook, William D. Phillips, Phillip L. Gould, and Harold J. Metcalf, 1988, "Observation of atoms laser cooled below the doppler limit," Phys. Rev. Lett. **61**, 169.

Levine, M. A., R. E. Marrs, J. R. Henderson, D. A. Knapp, and M. B. Schneider, 1988, "The electron beam ion trap: A new instrument for atomic physics measurements," Phys. Scr. **T22**, 157.

Levine, M. A., *et al.*, 1989, "The use of an electron beam ion trap in the study of highly charged ions," Nucl. Instrum. Methods Phys. Res., Sect. B **43**, 431.

Levine, Morton A., R. E. Marrs, and Robert W. Schmieder, 1985, "Measurement of instabilities and ion heating in an electron beam ion source," Nucl. Instrum. Methods Phys. Res., Sect. A **237**, 429.

Liang, G. Y., *et al.*, 2009, "Experimental investigations of ion charge distributions, effective electron densities, and electron-ion cloud overlap in electron beam ion trap plasma using extreme-ultraviolet spectroscopy," Astrophys. J. **702**, 838.

Lin, Y., J. P. Gaebler, T. R. Tan, R. Bowler, J. D. Jost, D. Leibfried, and D. J. Wineland, 2013, "Sympathetic electromagnetically-induced-transparency laser cooling of motional modes in an ion chain," Phys. Rev. Lett. **110**, 153002.

Lindgren, I., B. Asen, S. Salomonson, and A. M. Mårtensson-Pendrill, 2001, "QED procedure applied to the quasidegenerate fine-structrue levels of He-like ions," Phys. Rev. A **64**, 062505.

Lindgren, I., H. Persson, and S. Salomonson, 1995, "Full QED calculations of two-photon exchange for heliumlike-systems: Analysis in the Coulomb and Feynman gauges," Phys. Rev. A **51**, 1167.

Lochmann, Matthias, *et al.*, 2014, "Observation of the hyperfine transition in lithium-like bismuth $^{209}Bi^{80+}$: Towards a test of QED in strong magnetic fields," Phys. Rev. A **90**, 030501.

Ludlow, Andrew, Martin Boyd, Jun Ye, E. Peik, and P. O. Schmidt, 2015, "Optical atomic clocks," Rev. Mod. Phys. **87**, 637.

Machado, J., C. I. Szabo, J. P. Santos, P. Amaro, M. Guerra, A. Gumberidze, G. Bian, J. M. Isac, and P. Indelicato, 2018, "High-precision measurements of $n = 2 \rightarrow n = 1$ transition energies and level widths in He- and Be-like argon ions," arXiv:1802.05970.

Mäckel, V., R. Klawitter, G. Brenner, J. R. Crespo López-Urrutia, and J. Ullrich, 2011, "Laser spectroscopy on forbidden transitions in trapped highly charged Ar^{13+} ions," Phys. Rev. Lett. **107**, 143002.

Major, Fouad G., Viorica N. Gheorghe, and Günther Werth, 2006, *Charged Particle Traps: Physics and Techniques of Charged Particle Field Confinement* (Springer-Verlag, Berlin/Heidelberg).

Marciano, W. J., 1984, Phys. Rev. Lett. **52**, 489.

Marmar, E. S., J. E. Rice, E. Källne, J. Källne, and R. E. LaVilla, 1986, "Precision measurement of the 1*s* Lamb shift in hydrogenlike argon," Phys. Rev. A **33**, 774.

Marrs, R. E., 1999, "Self-cooling of highly charged ions during extraction from electron beam ion sources and traps," Nucl. Instrum. Methods Phys. Res., Sect. B **149**, 182.

Marrs, R. E., P. Beiersdorfer, and D. Schneider, 1994, "The electron-beam ion trap," Phys. Today **47**, 27.

Marrs, R. E., S. R. Elliott, and D. A. Knapp, 1994, "Production and trapping of hydrogenlike and bare uranium ions in an electron beam ion trap," Phys. Rev. Lett. **72**, 4082.

Martinson, I., 1989, "The spectroscopy of highly ionised atoms," Rep. Prog. Phys. **52**, 157.

Matei, D. G., *et al.*, 2017, "1.5 μm lasers with sub 10 mHz linewidth," arXiv:1702.04669.

McDonald, J. W., D. Schneider, M. W. Clark, and D. Dewitt, 1992, "Observation of high electron emission yields following highly charged ion impact (up to Th^{75+}) on surfaces," Phys. Rev. Lett. **68**, 2297.

Meierfrankenfeld, D., A. Bury, and M. Thoennessen, 2011, "Discovery of scandium, titanium, mercury, and einsteinium isotopes," At. Data Nucl. Data Tables **97**, 134.

Metcalf, Harold J, and Peter van der Straten, 2007, "Laser cooling and trapping of neutral atoms," in *The Optics Encyclopedia* (Wiley-VCH Verlag GmbH & Co. KGaA, Berlin).

Micke, P., *et al.*, 2018, "The heidelberg compact electron beam ion traps," Rev. Sci. Instrum. **89**, 063109.

Micke, Peter, Maria Schwarz, Steven A. King, Tobias Leopold, Lisa Schmöger, Julian Stark, Thomas Pfeifer, Piet O. Schmidt, and José R. Crespo López-Urrutia, 2018, "A maintenance-free ultra-low vibration cryogenic system for ion traps and other applications," to be submitted.

Mohr, P. J., 1974, "Self-energy radiative corrections in hydrogen-like systems," Ann. Phys. (N.Y.) **88**, 26.

Mohr, P. J., 1985, "Quantum electrodynamics of high-Z few-electron atoms," Phys. Rev. A **32**, 1949.

Mohr, P. J., 1992, "Self-energy correction to one-electron energy levels in a strong coulomb field," Phys. Rev. A **46**, 4421.

Mohr, P. J., D. B. Newell, and B. N. Taylor, 2016, "CODATA recommended values of the fundamental physical constants: 2014," Rev. Mod. Phys. **88**, 035009.

Mohr, P. J., G. Plunien, and G. Soff, 1998, "QED corrections in heavy atoms," Phys. Rep. **293**, 227.

Mohr, P. J., and G. Soff, 1993, "Nuclear size correction to the electron self-energy," Phys. Rev. Lett. **70**, 158.

Mohr, P. J., B. N. Taylor, and D. B. Newell, 2012, "CODATA recommended values of the fundamental physical constants: 2010," Rev. Mod. Phys. **84**, 1527.

Mokler, P. H., D. H. H. Hoffmann, W. A. Schöfeldt, Z. Stachura, A. Warczak, H. Schmidt-Böcking, and R. Schuch, 1985, "Highly ionized, decelerated heavy ions," Nucl. Instrum. Methods Phys. Res., Sect. B **10–11**, 58.

Morgan, C. A., F. G. Serpa, E. Takcs, E. S. Meyer, J. D. Gillaspy, J. Sugar, J. R. Roberts, C. M. Brown, and U. Feldman, 1995, "Observation of visible and uv magnetic dipole transitions in highly charged xenon and barium," Phys. Rev. Lett. **74**, 1716.

Morigi, G., and H. Walther, 2001, "Two-species Coulomb chains for quantum information," Eur. Phys. J. D **13**, 261.

Motohashi, Kenji, Akihiko Moriya, Hiroyuki Yamada, and Seiji Tsurubuchi, 2000, "Compact electron-beam ion trap using NdFeB permanent magnets," Rev. Sci. Instrum. **71**, 890.

Nakamura, N., Y. Nakai, Y. Kanai, K. Komaki, and A. Endo, 2004, "Compact electron beam ion source with high-Tc bulk superconductors," Rev. Sci. Instrum. **75**, 3034.

Nakamura, N., *et al.*, 1997, "An overview of the Tokyo electron beam ion trap," Phys. Scr. **T73**, 362.

Nakamura, Nobuyuki, Daiji Kato, Nozomu Miura, Tetsuro Nakahara, and Shunsuke Ohtani, 2001, "Intensity ratio between Lyman-α_1 and -α_2 lines of hydrogenlike titanium observed in an electron-beam ion trap," Phys. Rev. A **63**, 024501.

Nakamura, Nobuyuki, Anthony P. Kavanagh, Hirofumi Watanabe, Hiroyuki A. Sakaue, Yueming Li, Daiji Kato, Fred J. Currell, Xiao-Min Tong, Tsutomu Watanabe, and Shunsuke Ohtani, 2009, "Asymmetric profiles observed in the recombination of Bi^{79+}: A benchmark for relativistic theories involving interference," Phys. Rev. A **80**, 014503.

Nakamura, Nobuyuki, Hiroyuki Kikuchi, Hiroyuki Sakaue, and Tetsuya Watanabe, 2008, "Compact electron beam ion trap for spectroscopy of moderate charge state ions," Rev. Sci. Instrum. **79**, 063104.

Nandy, D. K., and B. K. Sahoo, 2016, "Highly charged W^{13+}, Ir^{16+}, and Pt^{17+} ions as promising optical clock candidates for probing variations of the fine-structure constant," Phys. Rev. A **94**, 032504.

Neuhauser, W., M. Hohenstatt, P. Toschek, and H. Dehmelt, 1978, "Optical-sideband cooling of visible atom cloud confined in parabolic well," Phys. Rev. Lett. **41**, 233.

Niles, A. M., E. W. Magee, D. B. Thorn, G. V. Brown, H. Chen, and P. Beiersdorfer, 2006, "Laser ablation system for the injection of neutral materials into an electron beam ion trap," Rev. Sci. Instrum. **77**, 10F106.

Okada, K., M. Ichikawa, and M. Wada, 2015, "Characterization of ion Coulomb crystals for fundamental sciences," Hyperfine Interact. **236**, 87.

Ong, A., J. C. Berengut, and V. V. Flambaum, 2014, "Optical transitions in highly charged ions for detection of variations in

the fine-structure constant," in *Fundamental Physics in Particle Traps*, Springer Tracts in Modern Physics, edited by W. Quint and M. Vogel (Springer-Verlag, Berlin/Heidelberg), Vol. 256, p. 293.

Oreshkina, Natalia S., Stefano M. Cavaletto, Niklas Michel, Zoltán Harman, and Christoph H. Keitel, 2017, "Hyperfine splitting in simple ions for the search of the variation of fundamental constants," Phys. Rev. A **96**, 030501.

O'Sullivan, Gerry, *et al.*, 2015, "Spectroscopy of highly charged ions and its relevance to EUV and soft x-ray source development," J. Phys. B **48**, 144025.

Otranto, S., R. E. Olson, and P. Beiersdorfer, 2006, "X-ray emission cross sections following charge exchange by multiply charged ions of astrophysical interest," Phys. Rev. A **73**, 022723.

Ovsyannikov, V. P., and A. V. Nefiodov, 2016a, "Main magnetic focus ion source: Basic principles, theoretical predictions and experimental confirmations," Nucl. Instrum. Methods Phys. Res., Sect. B **370**, 32.

Ovsyannikov, V. P., and A. V. Nefiodov, 2016b, "Main magnetic focus ion source with the radial extraction of ions," Nucl. Instrum. Methods Phys. Res., Sect. B **367**, 1.

Ovsyannikov, V. P., and G. Zschornack, 1999, "First investigations of a warm electron beam ion trap for the production of highly charged ions," Rev. Sci. Instrum. **70**, 2646.

Pachucki, K., A. Czarnecki, U. D. Jentschura, and V. A. Yerokhin, 2005, "Complete two-loop correction to the bound-electron g factor," Phys. Rev. A **72**, 022108.

Palmer, C. W. P., 1987, "Reformulation of the theory of the mass shift," J. Phys. B **20**, 5987.

Pedregosa, J., 2017, "Molecular dynamics simulations," personal communication.

Peik, Ekkehard, Tobias Schneider, and Christian Tamm, 2006, "Laser frequency stabilization to a single ion," J. Phys. B **39**, 145.

Penetrante, B. M., J. N. Bardsley, D. DeWitt, M. Clark, and D. Schneider, 1991, "Evolution of ion-charge-state distributions in an electron-beam ion trap," Phys. Rev. A **43**, 4861.

Penetrante, B. M., J. N. Bardsley, M. A. Levine, D. A. Knapp, and R. E. Marrs, 1991, "Evaporative cooling of highly charged dysprosium ions in an enhanced electron-beam ion trap," Phys. Rev. A **43**, 4873.

Penetrante, B. M., D. Schneider, R. E. Marrs, and J. N. Bardsley, 1992, "Modeling the ion-source performance of an electron-beam ion trap (invited)," Rev. Sci. Instrum. **63**, 2806.

Persson, H., S. Salomonson, P. Sunnergren, I. Lindgren, and M. G. H. Gustavsson, 1997, "A theoretical survey of QED tests in highly charged ions," Hyperfine Interact. **108**, 3.

Persson, H., S. M. Schneider, W. Greiner, G. Soff, and I. Lindgren, 1996, "Self-energy correction to the hyperfine structure splitting of hydrogenlike atoms," Phys. Rev. Lett. **76**, 1433.

Peskin, Michael E, and Daniel V. Schroeder, 1995, *An introduction to Quantum Field Theory* (Perseus Books, Reading, MA).

Phillips, William D., 1998, "Nobel lecture: Laser cooling and trapping of neutral atoms," Rev. Mod. Phys. **70**, 721.

Phillips, William D., John V. Prodan, and Harold J. Metcalf, 1985, "Laser cooling and electromagnetic trapping of neutral atoms," J. Opt. Soc. Am. B **2**, 1751.

Plante, D. R., W. R. Johnson, and J. Sapirstein, 1994, "Relativistic all-order many-body calculations of the $n = 1$ and $n = 2$ states of heliumlike ions," Phys. Rev. A **49**, 3519.

Plunien, G., B. Müller, W. Greiner, and G. Soff, 1989, "Nuclear polarization contribution to the Lamb shift in heavy atoms," Phys. Rev. A **39**, 5428.

Pohl, Randolf, 2016, "Laser spectroscopy of muonic hydrogen and the puzzling proton," J. Phys. Soc. Jpn. **85**, 091003.

Pohl, Randolf, Ronald Gilman, Gerald A. Miller, and Krzysztof Pachucki, 2013, "Muonic Hydrogen and the Proton Radius Puzzle," Annu. Rev. Nucl. Part. Sci. **63**, 175.

Pohl, Randolf, *et al.*, 2010, "The size of the proton," Nature (London) **466**, 213.

Pohl, Randolf, *et al.*, 2016, "Laser spectroscopy of muonic deuterium," Science **353**, 669.

Poli, N., C. W. Oates, P. Gill, and G. M. Tino, 2013, "Optical atomic clocks," Riv. Nuovo Cimento **36**, 555.

Porto, J. V., I. Kink, and J. D. Gillaspy, 2000, "UV light from the ground term of Ti-like ytterbium, tungsten, and bismuth," Phys. Rev. A **61**, 054501.

Poth, H., R. W. Hasse, T. Katayama, and A. Noda, 1991, "The HITRAP project at GSI—A facility for experimentation with trapped highly-charged ions," in *Cooler Rings and their Applications* (World Scientific Publishing Company, Singapore), p. 108.

Prior, M. H., 1987, "Forbidden lines from highly charged, metastable ion beams," J. Opt. Soc. Am. B **4**, 144.

Pruttivarasin, T., M. Ramm, S. G. Porsev, I. I. Tupitsyn, M. S. Safronova, M. A. Hohensee, and H. Häffner, 2015, "Michelson-Morley analogue for electrons using trapped ions to test Lorentz symmetry," Nature (London) **517**, 592.

Pyka, Karsten, Norbert Herschbach, Jonas Keller, and Tanja E. Mehlstäubler, 2014, "A high-precision segmented Paul trap with minimized micromotion for an optical multiple-ion clock," Appl. Phys. B **114**, 231.

Quint, W., *et al.*, 2001, "HITRAP: A facility for experiments with trapped highly charged ions," Hyperfine Interact. **132**, 453.

Ramsey, N., 1985, *Molecular Beams* (Oxford University Press, New York).

Reimers, D., 2002, "Baryons in the diffuse intergalactic medium," Space Sci. Rev. **100**, 89.

Richard, P., M. Stöckli, R. D. Deslattes, P. Cowan, R. E. LaVilla, B. Johnson, K. Jones, M. Meron, R. Mann, and K. Schartner, 1984, "Measurement of the 1s Lamb shift in hydrogenlike chlorine," Phys. Rev. A **29**, 2939.

Riehle, Fritz, 2004, *Frequency Standards: Basics and Applications* (Wiley-VCH, Weinheim).

Riis, Erling, and Alastair G. Sinclair, 2004, "Optimum measurement strategies for trapped ion optical frequency standards," J. Phys. B **37**, 4719.

Riley, William J., 2008, *Handbook of Frequency Stability Analysis*, NIST Special Publications, Vol. 1065, U.S. Department of Commerce (National Institute of Standards and Technology, Boulder, CO).

Roberts, B. M., V. A. Dzuba, and V. V. Flambaum, 2013, "Quantum electrodynamics corrections to energies, transition amplitudes, and parity nonconservation in Rb, Cs, Ba^+, Tl, Fr, and Ra^+," Phys. Rev. A **87**, 054502.

Rodríguez, D., *et al.*, 2010, "MATS and LaSpec: High-precision experiments using ion traps and lasers at FAIR," Eur. Phys. J. Spec. Top. **183**, 1.

Roos, C. F., M. Chwalla, K. Kim, M. Riebe, and R. Blatt, 2006, "Designer atoms' for quantum metrology," Nature (London) **443**, 316.

Roos, C. F., D. Leibfried, A. Mundt, F. Schmidt-Kaler, J. Eschner, and R. Blatt, 2000, "Experimental demonstration of ground state laser cooling with electromagnetically induced transparency," Phys. Rev. Lett. **85**, 5547.

Rosenband, T., *et al.*, 2008, "Frequency ratio of Al^+ and Hg^+ single-ion optical clocks; metrology at the 17th decimal place," Science **319**, 1808.

Rudolph, J. K., *et al.*, 2013, "X-ray resonant photoexcitation: Linewidths and energies of Kα transitions in highly charged Fe ions," Phys. Rev. Lett. **111**, 103002.

Runke, J., *et al.*, 2014, "Preparation of actinide targets for the synthesis of the heaviest elements," J. Radioanal. Nucl. Chem. **299**, 1081.

Safronova, M. S., D. Budker, D. DeMille, Derek F. Jackson Kimball, A. Derevianko, and C. W. Clark, 2018, "Search for new physics with atoms and molecules,"arXiv:1710.01833.

Safronova, M. S., V. A. Dzuba, V. V. Flambaum, U. I. Safronova, S. G. Porsev, and M. G. Kozlov, 2014a, "Atomic properties of Cd-like and Sn-like ions for the development of frequency standards and search for the variation of the fine-structure constant," Phys. Rev. A **90**, 052509.

Safronova, M. S., V. A. Dzuba, V. V. Flambaum, U. I. Safronova, S. G. Porsev, and M. G. Kozlov, 2014b, "Highly charged Ag-like and In-like ions for the development of atomic clocks and the search for alpha variation," Phys. Rev. A **90**, 042513.

Safronova, M. S., V. A. Dzuba, V. V. Flambaum, U. I. Safronova, S. G. Porsev, and M. G. Kozlov, 2014c, "Highly-charged ions for atomic clocks, quantum information, and search for α-variation," Phys. Rev. Lett. **113**, 030801.

Safronova, M. S., M. G. Kozlov, W. R. Johnson, and D. Jiang, 2009, "Development of a configuration-interaction + all-order method for atomic calculations," Phys. Rev. A **80**, 012516.

Safronova, U. I., V. V. Flambaum, and M. S. Safronova, 2015, "Transitions between the 4 f -core-excited states in Ir^{16+}, Ir^{17+}, and Ir^{18+} ions for clock applications," Phys. Rev. A **92**, 022501.

Sakaue, H. A., D. Kato, N. Nakamura, E. Watanabe, and N. Yamamoto, 2009, "EUV spectroscopy of highly charged iron ions with a low energy compact EBIT," J. Phys. Conf. Ser. **163**, 012020.

Sapirstein, J., and K. T. Cheng, 2011, "S-matrix calculations of energy levels of the lithium isoelectronic sequence," Phys. Rev. A **83**, 012504.

Savukov, I. M., and W. R. Johnson, 2002, "Combined CI + MBPT calculations of energy levels and transition amplitudes in Be, Mg, Ca, and Sr," Phys. Rev. A **65**, 042503.

Schabinger, B., S. Sturm, A. Wagner, J. Alonso, and W. Quint, 2012, "Experimental g factor of hydrogenlike silicon-28," Eur. Phys. J. D **66**, 71.

Scharnhorst, Nils, Javier Cerrillo, Johannes Kramer, Ian D. Leroux, Jannes B. Wübbena, Alex Retzker, and Piet O. Schmidt, 2017, "Multi-mode double-bright EIT cooling," arXiv:1711.00738.

Schiller, S., 2007, "Hydrogenlike highly charged ions for tests of the time independence of fundamental constants," Phys. Rev. Lett. **98**, 180801.

Schmidt, P. O., T. Rosenband, C. Langer, W. M. Itano, J. C. Bergquist, and D. J. Wineland, 2005, "Spectroscopy using quantum logic," Science **309**, 749.

Schmidt, Piet O., and Ian D. Leroux, 2015, "Trapped-ion optical frequency standards," in *Trapped Charged Particles*, Advanced Textbooks in Physics (World Scientific, Singapore), p. 377.

Schmöger, L., M. Schwarz, T. M. Baumann, O. O. Versolato, B. Piest, T. Pfeifer, J. Ullrich, P. O. Schmidt, and J. R. Crespo López-Urrutia 2015, "Deceleration, precooling, and multi-pass stopping of highly charged ions in Be^+ Coulomb crystals," Rev. Sci. Instrum. **86**, 103111.

Schmöger, L., *et al.*, 2015, "Coulomb crystallization of highly charged ions," Science **347**, 1233.

Schmöger, Lisa, 2017, Kalte hochgeladene Ionen für Frequenzmetrologie, dissertation (Heidelberg University, Germany).

Schneider, D., D. A. Church, G. Weinberg, J. Steiger, B. Beck, J. McDonald, E. Magee, and D. Knapp, 1994, "Confinement in a cryogenic penning trap of highest charge state ions from EBIT," Rev. Sci. Instrum. **65**, 3472.

Schneider, D., M. W. Clark, B. M. Penetrante, J. McDonald, D. Dewitt, and J. N. Bardsley, 1991, "Production of high-charge-state thorium and uranium ions in an electron-beam ion trap," Phys. Rev. A **44**, 3119.

Schnorr, K., V. Mäckel, N. S. Oreshkina, S. Augustin, F. Brunner, Z. Harman, C. H. Keitel, J. Ullrich, and J. R. Crespo López-Urrutia, 2013, "Coronium in the laboratory: Measuring the Fe XIV green coronal line by laser spectroscopy," Astrophys. J. **776**, 121.

Schulte, M., N. Lörch, I. D. Leroux, P. O. Schmidt, and K. Hammerer, 2016, "Quantum Algorithmic Readout in Multi-Ion Clocks," Phys. Rev. Lett. **116**, 013002.

Schwarz, M., *et al.*, 2012, "Cryogenic linear Paul trap for cold highly charged ion experiments," Rev. Sci. Instrum. **83**, 083115.

Schweppe, J., *et al.*, 1991, "Measurement of the Lamb shift in lithiumlike uranium U^{89+}," Phys. Rev. Lett. **66**, 1434.

Schwerdtfeger, P., L. F. Paśteka, A. Punnett, and P. O. Bowman, 2015, "Relativistic and quantum electrodynamic effects in superheavy elements," Nucl. Phys. A **944**, 551.

Seelig, P., *et al.*, 1998, "Ground state hyperfine splitting of hydrogenlike $^{207}Pb^{81+}$ by laser excitation of a bunched ion beam in the GSI experimental storage ring," Phys. Rev. Lett. **81**, 4824.

Seidelin, S., *et al.*, 2006, "Microfabricated surface-electrode ion trap for scalable quantum information processing," Phys. Rev. Lett. **96**, 253003.

Serpa, F. G., E. W. Bell, E. S. Meyer, J. D. Gillaspy, and J. R. Roberts, 1997, "Kr spectra from an electron-beam ion trap: 300 nm to 460 nm," Phys. Rev. A **55**, 1832.

Serpa, F. G., C. A. Morgan, E. S. Meyer, J. D. Gillaspy, E. Träautbert, D. A. Church, and E. Takács, 1997, "Measurement of a magnetic-dipole transition probability in Xe^{32+} using an electron-beam ion trap," Phys. Rev. A **55**, 4196.

Shabaev, V. M., 1985, "Mass corrections in a strong nuclear field," Theor. Math. Phys. **63**, 588.

Shabaev, V. M., 1993, "Finite nuclear size corrections to the energy levels of the multicharged ions," J. Phys. B **26**, 1103.

Shabaev, V. M., 1994, "Hyperfine structure of hydrogen-like ions," J. Phys. B **27**, 5825.

Shabaev, V. M., 1998, "QED theory of the nuclear recoil effect in atoms," Phys. Rev. A **57**, 59.

Shabaev, V. M., 2002, "Two-time Green's function method in quantum electrodynamics of high-Z few-electron atoms," Phys. Rep. **356**, 119.

Shabaev, V. M., A. N. Artemyev, T. Beier, G. Plunien, V. A. Yerokhin, and G. Soff, 1998, "Recoil correction to the ground-state energy of hydrogenlike atoms," Phys. Rev. A **57**, 4235.

Shabaev, V. M., A. N. Artemyev, and V. A. Yerokhin, 2000, "QED and nuclear effects in high-Z few-electron atoms," Phys. Scr. **T86**, 7.

Shabaev, V. M., A. N. Artemyev, V. A. Yerokhin, O. M. Zherebtsov, and G. Soff, 2001, "Towards a test of QED in investigations of the hyperfine splitting in heavy ions," Phys. Rev. Lett. **86**, 3959.

Shabaev, V. M., D. A. Glazov, N. S. Oreshkina, A. V. Volotka, G. Plunien, H.-J. Kluge, and W. Quint, 2006, "g-factor of heavy ions: A new access to the fine structure constant," Phys. Rev. Lett. **96**, 253002.

Shabaev, V. M., D. A. Glazov, G. Plunien, and A. V. Volotka, 2015, "Theory of bound-electron g factor in highly charged ions," J. Phys. Chem. Ref. Data **44**, 031205.

Shabaev, V. M., D. A. Glazov, M. B. Shabaeva, V. A. Yerokhin, G. Plunien, and G. Soff, 2002, "g factor of high-Z lithiumlike ions," Phys. Rev. A **65**, 062104.

Shabaev, V. M., M. Tomaselli, T. Kühl, A. N. Artemyev, and V. A. Yerokhin, 1997, "Ground-state hyperfine splitting of high-Z hydrogenlike ions," Phys. Rev. A **56**, 252.

Shabaev, V. M., I. I. Tupitsyn, and V. A. Yerokhin, 2013, "Model operator approach to the Lamb shift calculations in relativistic many-electron atoms," Phys. Rev. A **88**, 012513.

Shabaev, V. M., I. I. Tupitsyn, and V. A. Yerokhin, 2015, "QEDMOD: Fortran program for calculating the model Lamb-shift operator," Comput. Phys. Commun. **189**, 175.

Shah, C., P. Amaro, R. Steinbrügge, S. Bernitt, J. R. Crespo López-Urrutia, and S. Tashenov, 2018, "Polarization of K-shell dielectronic recombination satellite lines of Fe XIX—XXV and its application for diagnostics of anisotropies of hot plasmas," Astrophys. J. Suppl. Ser. **234**, 27.

Shaniv, R., R. Ozeri, M. S. Safronova, S. G. Porsev, V. A. Dzuba, V. V. Flambaum, and H. Häffner, 2018, "New Methods for Testing Lorentz Invariance with Atomic Systems," Phys. Rev. Lett. **120**, 103202.

Shi, C., *et al.*, 2017, "Unexpectedly large difference of the electron density at the nucleus in the $4p\ ^2P_{1/2,3/2}$ fine-structure doublet of Ca^+," Appl. Phys. B **123**, 2.

Shlyaptseva, A. S., R. C. Mancini, P. Neill, and P. Beiersdorfer, 1997, "Polarization of x-ray Li- and Be-like Fe satellite lines excited by an electron beam," Rev. Sci. Instrum. **68**, 1095.

Shlyaptseva, A. S., R. C. Mancini, P. Neill, P. Beiersdorfer, J. R. Crespo López-Urrutia, and K. Widmann, 1998, "Polarization-dependent spectra of x-ray dielectronic satellite lines of Be-like Fe," Phys. Rev. A **57**, 888.

Shull, J. Michael, Britton D. Smith, and Charles W. Danforth, 2012, "The baryon census in a multiphase intergalactic medium: 30% of the baryons may still be missing," Astrophys. J. **759**, 23.

Silver, J. D., *et al.*, 1994, "The Oxford electron-beam ion trap: A device for spectroscopy of highly charged ions," Rev. Sci. Instrum. **65**, 1072.

Simon, M. C., *et al.*, 2010a, "Resonant and near-threshold photoionization cross sections of Fe^{14+}," Phys. Rev. Lett. **105**, 183001.

Simon, M. C., *et al.*, 2010b, "Photoionization of N^{3+} and Ar^{8+} in an electron beam ion trap by synchrotron radiation," J. Phys. B **43**, 065003.

Skripnikov, Leonid V., *et al.*, 2018, "New nuclear magnetic moment of ^{209}Bi: Resolving the bismuth hyperfine puzzle," Phys. Rev. Lett. **120**, 093001.

Solaro, Cyrille, Steffen Meyer, Karin Fisher, Michael V. DePalatis, and Michael Drewsen, 2017, "Direct frequency-comb-driven Raman transitions in the terahertz range," arXiv:1712.07429.

Soria Orts, R., *et al.*, 2007, "Zeeman splitting and g factor of the $1s^22s^22p\ ^2P_{3/2}$ and $^2P_{1/2}$ levels in Ar^{13+}," Phys. Rev. A **76**, 052501.

Soria Orts, R. S., *et al.*, 2006, "Exploring relativistic many-body recoil effects in highly charged ions," Phys. Rev. Lett. **97**, 103002.

Stadnik, Y. V., and V. V. Flambaum, 2015, "Can dark matter induce cosmological evolution of the fundamental constants of nature?" Phys. Rev. Lett. **115**, 201301.

Stadnik, Y. V., and V. V. Flambaum, 2016, "Improved limits on interactions of low-mass spin-0 dark matter from atomic clock spectroscopy," Phys. Rev. A **94**, 022111.

Staude, U., Ph. Bosselmann, R. Büttner, D. Horn, K.-H. Schartner, F. Folkmann, A. E. Livingston, T. Ludziejewski, and P. H. Mokler, 1998, "Measurements of $2s\ ^2S_{1/2} - 2p\ ^2P_{3/2,1/2}$ transition energies in lithiumlike heavy ions: Experiments and results for Ni^{25+} and Zn^{27+}," Phys. Rev. A **58**, 3516.

Stenholm, Stig, 1986, "The semiclassical theory of laser cooling," Rev. Mod. Phys. **58**, 699.

Sturm, S., F. Köhler, J. Zatorski, A. Wagner, Z. Harman, G. Werth, W. Quint, C. H. Keitel, and K. Blaum, 2014, "High-precision measurement of the atomic mass of the electron," Nature (London) **506**, 467.

Sturm, S., M. Vogel, F. Köhler-Langes, W. Quint, K. Blaum, and G. Werth, 2017, "High-precision measurements of the bound electron's magnetic moment," Atoms **5**, 4.

Sturm, S., A. Wagner, M. Kretzschmar, W. Quint, G. Werth, and K. Blaum, 2013, "g-factor measurement of hydrogenlike $^{28}Si^{13+}$ as a challenge to QED calculations," Phys. Rev. A **87**, 030501.

Sturm, S., A. Wagner, B. Schabinger, J. Zatorski, Z. Harman, W. Quint, G. Werth, C. H. Keitel, and K. Blaum, 2011, "g factor of hydrogenlike $^{28}Si^{13+}$," Phys. Rev. Lett. **107**, 023002.

Sturm, S., G. Werth, and K. Blaum, 2013, "Electron g-factor determinations in Penning traps," Ann. Phys. (Berlin) **525**, 620.

Suckewer, S., E. Hinnov, S. Cohen, M. Finkenthal, and K. Sato, 1982, "Identification of magnetic dipole lines above 2000 Å in several highly ionized Mo and Zr ions on the PLT tokamak," Phys. Rev. A **26**, 1161.

Sugar, J., and V. Kaufman, 1981, "Ag I isoelectronic sequence: Wavelengths and energy levels for Ce XII through Ho XXI and for W XXVIII," Phys. Scr. **24**, 742.

Sunnergren, P., H. Persson, S. Salomonson, S. M. Schneider, I. Lindgren, and G. Soff, 1998, "Radiative corrections to the hyperfine-structure splitting of hydrogenlike systems," Phys. Rev. A **58**, 1055.

Takacs, E., T. D. Kimmel, K. H. Brandenburg, R. K. Wilson, A. C. Gall, J. E. Harriss, and C. E. Sosolik, 2015, "Diagnostic measurements of CUEBIT based on the dielectronic resonance process," AIP Conf. Proc. **1640**, 154.

Tavernier, M., J. P. Briand, P. Indelicato, D. Liesen, and P. Richard, 1985, "Measurement of the $1s$ Lamb shift of hydrogen-like krypton," J. Phys. B **18**, L327.

Torretti, F., *et al.*, 2017, "Optical spectroscopy of complex open-4d-shell ions $Sn^{7+} - Sn^{10+}$," Phys. Rev. A **95**, 042503.

Träbert, E., 2002, "Precise atomic lifetime measurements with stored ion beams and ion traps," Can. J. Phys. **80**, 1481.

Träbert, E., 2008, "Atomic lifetime measurements employing an electron beam ion trap," Can. J. Phys. **86**, 73.

Trinczek, M., A. Werdich, V. Mironov, P. Guo, A. J. González Martínez, J. Braun, J. R. Crespo López-Urrutia, and J. Ullrich, 2006, "A laser ion source for an electron beam ion trap," Nucl. Instrum. Methods Phys. Res., Sect. B **251**, 289.

Tupitsyn, I. I., and E. V. Berseneva, 2013, "A single-particle nonlocal potential for taking into account quantum-electrodynamic corrections in calculations of the electronic structure of atoms," Opt. Spectrosc. **114**, 682.

Tupitsyn, I. I., M. G. Kozlov, M. S. Safronova, V. M. Shabaev, and V. A. Dzuba, 2016, "Quantum electrodynamical shifts in multivalent heavy ions," Phys. Rev. Lett. **117**, 253001.

Tupitsyn, I. I., V. M. Shabaev, J. R. Crespo López-Urrutia, I. Draganić, R. Soria Orts, and J. Ullrich, 2003, "Relativistic calculations of isotope shifts in highly charged ions," Phys. Rev. A **68**, 022511.

Ullmann, Johannes, *et al.*, 2017, "High precision hyperfine measurements in bismuth challenge bound-state strong-field QED," Nat. Commun. **8**, 15484.

Utter, S. B., P. Beiersdorfer, and G. V. Brown, 2000, "Measurement of an unusual M1 transition in the ground state of Ti-like W^{52+}," Phys. Rev. A **61**, 030503(R).

Uzan, Jean-Philippe, 2011, "Varying constants, gravitation and cosmology," Living Rev. Relativity **14**, 2.

Versolato, O. O., M. Schwarz, A. Windberger, J. Ullrich, P. O. Schmidt, M. Drewsen, and J. R. Crespo López-Urrutia, 2013,

"Cold highly charged ions in a cryogenic Paul trap," Hyperfine Interact. **214**, 189.

Volotka, A. V., D. A. Glazov, O. V. Andreev, V. M. Shabaev, I. I. Tupitsyn, and G. Plunien, 2012, "Test of many-electron QED effects in the hyperfine splitting of heavy high-Z ions," Phys. Rev. Lett. **108**, 073001.

Volotka, A. V., D. A. Glazov, G. Plunien, and V. M. Shabaev, 2013, "Progress in quantum electrodynamics theory of highly charged ions," Ann. Phys. (Berlin) **525**, 636.

Volotka, A. V., D. A. Glazov, V. M. Shabaev, I. I. Tupitsyn, and G. Plunien, 2014, "Many-electron QED corrections to the g factor of lithiumlike ions," Phys. Rev. Lett. **112**, 253004.

Volotka, A. V., and G. Plunien, 2014, "Nuclear polarization study: New frontiers for tests of QED in heavy highly charged ions," Phys. Rev. Lett. **113**, 023002.

Volotka, Andrey V., Dmitry A. Glazov, Günter Plunien, and Vladimir M. Shabaev, 2013, "Progress in quantum electrodynamics theory of highly charged ions," Ann. Phys. (Berlin) **525**, 636.

von Lindenfels, D., *et al.*, 2013, "Experimental access to higher-order Zeeman effects by precision spectroscopy of highly charged ions in a Penning trap," Phys. Rev. A **87**, 023412.

Vutha, Amar C, Tom Kirchner, and Pierre Dubé, 2017, "The collisional frequency shift of a trapped-ion optical clock," Phys. Rev. A **96**, 022704.

Wagner, A., S. Sturm, F. Köhler, D. A. Glazov, A. V. Volotka, G. Plunien, W. Quint, G. Werth, V. M. Shabaev, and K. Blaum, 2013, "g factor of lithiumlike silicon $^{28}Si^{11+}$," Phys. Rev. Lett. **110**, 033003.

Wan, Yong, Florian Gebert, Fabian Wolf, and Piet O. Schmidt, 2015, "Efficient sympathetic motional-ground-state cooling of a molecular ion," Phys. Rev. A **91**, 043425.

Wan, Yong, Florian Gebert, Jannes B. Wübbena, Nils Scharnhorst, Sana Amairi, Ian D. Leroux, Börge Hemmerling, Niels Lörch, Klemens Hammerer, and Piet O. Schmidt, 2014, "Precision spectroscopy by photon-recoil signal amplification," Nat. Commun. **5**, 4096.

Wargelin, B. J., P. Beiersdorfer, and S. M. Kahn, 1993, "Radiative lifetime of the long-lived $1s2s\ ^3S_1$ state in heliumlike neon by electron-beam excitation of trapped ions," Phys. Rev. Lett. **71**, 2196.

Wargelin, B. J., P. Beiersdorfer, P. A. Neill, R. E. Olson, and J. H. Scofield, 2005, "Charge-exchange spectra of hydrogenic and He-like iron," Astrophys. J. **634**, 687.

Watanabe, H., D. Crosby, F. J. Currell, T. Fukami, D. Kato, S. Ohtani, J. D. Silver, and C. Yamada, 2001, "Magnetic dipole transitions in titaniumlike ions," Phys. Rev. A **63**, 042513.

Watanabe, H., H. Tobiyama, A. P. Kavanagh, Y. M. Li, N. Nakamura, H. A. Sakaue, F. J. Currell, and S. Ohtani, 2007, "Dielectronic recombination of He-like to C-like iodine ions," Phys. Rev. A **75**, 012702.

Watanabe, Hirofumi, and Fred Currell, 2004, "The Belfast EBIT," J. Phys. Conf. Ser. **2**, 182.

Webb, J. K., J. A. King, M. T. Murphy, V. V. Flambaum, R. F. Carswell, and M. B. Bainbridge, 2011, "Indications of a spatial variation of the fine structure constant," Phys. Rev. Lett. **107**, 191101.

Whitmore, J. B., and M. T. Murphy, 2015, "Impact of instrumental systematic errors on fine-structure constant measurements with quasar spectra," Mon. Not. R. Astron. Soc. **447**, 446.

Wicht, A., J. M. Hensley, E. Sarajlic, and S. Chu, 2002, "A preliminary measurement of the fine structure constant based on atom interferometry," Phys. Scr. **T102**, 82.

Widmann, K., P. Beiersdorfer, V. Decaux, and M. Bitter, 1996, "Measurements of the Kα transition energies of heliumlike krypton," Phys. Rev. A **53**, 2200.

Wilhelm, Richard A, Elisabeth Gruber, Janine Schwestka, Roland Kozubek, Teresa I. Madeira, José P. Marques, Jacek Kobus, Arkady V. Krasheninnikov, Marika Schleberger, and Friedrich Aumayr, 2017, "Interatomic coulombic decay: The mechanism for rapid deexcitation of hollow atoms," Phys. Rev. Lett. **119**, 103401.

Wilson, A. C., C. Ospelkaus, A. P. VanDevender, J. A. Mlynek, K. R. Brown, D. Leibfried, and D. J. Wineland, 2011, "A 750-mW, continuous-wave, solid-state laser source at 313 nm for cooling and manipulating trapped $^9Be^+$ ions," Appl. Phys. B **105**, 741.

Windberger, A., *et al.*, 2015, "Identification of the predicted $5s - 4f$ level crossing optical lines with applications to metrology and searches for the variation of fundamental constants," Phys. Rev. Lett. **114**, 150801.

Windberger, A., *et al.*, 2016, "Analysis of the fine structure of Sn^{11+}-Sn^{14+} ions by optical spectroscopy in an electron-beam ion trap," Phys. Rev. A **94**, 012506.

Wineland, D. J., R. E. Drullinger, and F. L. Walls, 1978, "Radiation-pressure cooling of bound resonant absorbers," Phys. Rev. Lett. **40**, 1639.

Wineland, D. J., and Wayne M. Itano, 1979, "Laser cooling of atoms," Phys. Rev. A **20**, 1521.

Wineland, D. J., C. Monroe, W. M. Itano, D. Leibfried, B. E. King, and D. M. Meekhof, 1998, "Experimental issues in coherent quantum-state manipulation of trapped atomic ions," J. Res. Natl. Inst. Stand. Technol. **103**, 259.

Winter, Hannspeter, and Friedrich Aumayr, 1999, "Hollow atoms," J. Phys. B **32**, R39.

Winters, D. F. A., A. M. Abdulla, J. R. Castrejón Pita, A. de Lange, D. M. Segal, and R. C. Thompson, 2005, "Plans for laser spectroscopy of trapped cold hydrogen-like HCI," Nucl. Instrum. Methods Phys. Res., Sect. B **235**, 201.

Wolf, A. L., S. A. Van Den Berg, W. Ubachs, and K. S. E. Eikema, 2009, "Direct frequency comb spectroscopy of trapped ions," Phys. Rev. Lett. **102**, 223901.

Wolf, Fabian, Yong Wan, Jan C. Heip, Florian Gebert, Chunyan Shi, and Piet O. Schmidt, 2016, "Non-destructive state detection for quantum logic spectroscopy of molecular ions," Nature (London) **530**, 457.

Wübbena, Jannes B., Sana Amairi, Olaf Mandel, and Piet O. Schmidt, 2012, "Sympathetic cooling of mixed-species two-ion crystals for precision spectroscopy," Phys. Rev. A **85**, 043412.

Xiao, J., Z. Fei, Y. Yang, X. Jin, D. Lu, Y. Shen, L. Liljeby, R. Hutton, and Y. Zou, 2012, "A very low energy compact electron beam ion trap for spectroscopic research in Shanghai," Rev. Sci. Instrum. **83**, 013303.

Xue, Y., *et al.*, 2014, "Kinematically complete study of electron transfer and rearrangement processes in slow Ar^{16+}-Ne collisions," Phys. Rev. A **90**, 052720.

Yamada, C., *et al.*, 2007, "Injection of refractory metals into EBIT using a Knudsen cell," J. Phys. Conf. Ser. **58**, 403.

Yan, Zong-Chao, and G. W. F. Drake, 1995, "High precision calculation of fine structure splittings in helium and He-like ions," Phys. Rev. Lett. **74**, 4791.

Ye, Jun, *et al.*, 2003, "Delivery of high-stability optical and microwave frequency standards over an optical fiber network," J. Opt. Soc. Am. B **20**, 1459.

Yerokhin, V. A., A. N. Artemyev, and V. M. Shabaev, 2007, "QED treatment of electron correlation in Li-like ions," Phys. Rev. A **75**, 062501.

Yerokhin, V. A., and Z. Harman, 2013, "Two-loop QED corrections with closed fermion loops for the bound-electron g factor," Phys. Rev. A **88**, 042502.

Yerokhin, V. A., P. Indelicato, and V. M. Shabaev, 2003a, "Evaluation of the two-loop self-energy correction to the ground state energy of H-like ions to all orders in $Z\alpha$," Eur. Phys. J. D **25**, 203.

Yerokhin, V. A., P. Indelicato, and V. M. Shabaev, 2003b, "Two-loop self-energy correction in high-Z hydrogenlike ions," Phys. Rev. Lett. **91**, 073001.

Yerokhin, V. A., K. Pachucki, Z. Harman, and C. H. Keitel, 2011, "QED theory of the nuclear magnetic shielding in hydrogenlike ions," Phys. Rev. Lett. **107**, 043004.

Yerokhin, V. A., and V. M. Shabaev, 2015, "Lamb shift of $n = 1$ and $n = 2$ states of hydrogen-like atoms, $1 \leq Z \leq 110$," J. Phys. Chem. Ref. Data **44**, 033103.

Yerokhin, V. A., and A. Surzhykov, 2012, "Relativistic configuration-interaction calculation of energy levels of core-excited states in lithiumlike ions: Argon through krypton," Phys. Rev. A **86**, 042507.

Yost, D. C., T. R. Schibli, and Jun Ye, 2008, "Efficient output coupling of intracavity high-harmonic generation," Opt. Lett. **33**, 1099.

Yu, Y.-M., and B. K. Sahoo 2016, "Scrutinizing Al-like $^{51}V^{10+}$, $^{53}Cr^{11+}$, $^{55}Mn^{12+}$, $^{57}Fe^{13+}$, $^{59}Co^{14+}$, $^{61}Ni^{15+}$, and $^{63}Cu^{16+}$ ions for atomic clocks with uncertainties below the 10^{-19} level," Phys. Rev. A **94**, 062502.

Yudin, V. I., A. V. Taichenachev, and A. Derevianko 2014, "Magnetic-dipole transitions in highly-charged ions as a basis of ultra-precise optical clocks," Phys. Rev. Lett. **113**, 233003.

Zatorski, J., B. Sikora, S. G. Karshenboim, S. Sturm, F. Köhler-Langes, K. Blaum, C. H. Keitel, and Z. Harman 2017, "Extraction of the electron mass from g-factor measurements on light hydrogenlike ions," Phys. Rev. A **96**, 012502.

Zhang, X., N. Nakamura, Ch. Chen, M. Andersson, Y. Liu, and Sh. Ohtani, 2008, "Measurement of the QED energy shift in the $1s^2 2p_{3/2} - 1s^2 2s_{1/2}$ x-ray transition in Li-like $^{208}Pb^{79+}$," Phys. Rev. A **78**, 032504.

Zimmerer, P., N. Grün, and W. Scheid, 1991, "Scaling of relativistic Auger rates with Z for ions with two electrons," J. Phys. B **24**, 2633.

Zou, Y., R. Hutton, F. Currell, I. Martinson, and S. Hagmann, 2016, *Handbook for Highly Charged Ion Spectroscopic Research* (CRC Press, Boca Raton, FL).